Autonomous Mooring and Unmooring

with use of a Model Predictive Control Strategy

ME54035 MSc Thesis

R. W. Jagernath

Delft University of Technology

TU Delft

Autonomous Mooring and Unmooring

with use of a Model Predictive Control Strategy

by

R. W. Jagernath

to obtain the degree of
Master of Science
in Mechanical Engineering
at the Department of Maritime and Transport Technology of Faculty of Mechanical Engineering of Delft University of Technology
to be defended publicly on Wednesday October 9, 2024 at 09:00 AM.

Student number:	4713842	
MSc track:	Multi-Machine Engineering	
Report number:	2024.MME.8960	
Project duration:	September 2023 – September 2024	
Thesis committee:	Dr.ir. Y. Pang	TU Delft, Committee chair
	ir. V. Garofano	TU Delft, Daily supervisor
	Dr. J. Jovanova	TU Delft, Committee member
	J. García Martín	TU Delft, Committee member

An electronic version of this thesis is available at http://repository.tudelft.nl/.

Cover Image: How Marinas and Ports Are Going Green
https://www.seagoinggreen.org/blog/how-marinas-and-ports-are-going-green

TU Delft

“It’s beauty in the struggle, ugliness in the success”
— Jermaine Lamarr Cole

Preface

Dear reader,

This report has been written to obtain the Master's degree in Mechanical Engineering at the Delft University of Technology with a specialization in Multi-Machine Engineering. In this report, I present the findings of the potential for autonomous mooring and unmooring with a Model Predictive Control Strategy.

I would like to express my gratitude to my daily supervisor, ir. V. Garofano for mentoring me through this entire project. I am truly grateful for the regular guidance and motivation he provided. I am also grateful for all the constructive criticism and feedback he gave me in order to continuously improve the shortcomings in my work.

I would like to thank Dr.ir. Y. Pang for helping with the development of the research project. He guided me in structuring the report and provided invaluable insights in the academic field. He also consistently ensured I worked accurately towards the final goal of the project.

Throughout the past 7 years of my academic career, I experienced a lot of ups and down. During this period, I always felt supported by my friends and family. You all played a huge part in helping shape the person I am today. Without you, none of this would have been possible. Lastly, I would like to say that where one book closes, another one opens. I look forward towards the future, filled with new paths to explore and new memories to create.

R. W. Jagernath
Delft, September 2024

Summary

This thesis presents a thorough study into the development and implementation of a control method for autonomous unmooring, trajectory tracking and mooring on an autonomous model-scale vessel. Mooring and unmooring are vital processes in the operation of ships, as it is the system that secures and releases a ship to a terminal or multiple terminals. The process has remained relatively identical over the years, whereas autonomous shipping has been researched over time. This study addresses the lack of focus given to autonomous mooring and unmooring by offering a control strategy that leverages the vessel's thrusters to perform these tasks, along with trajectory tracking. The study begins by reviewing existing research on trajectory tracking and maritime vessel mooring/unmooring, revealing the gaps in the integration of both procedures within autonomous operations.

To overcome these challenges, the study selects an applicable mathematical model for the vessel which will be controlled. This model covers kinematic and kinetic elements, as well as actuation and thruster allocation. This sets the groundwork for the development of a control strategy capable of precisely predicting and tracking the vessel's position during unmooring, and trajectory tracking and mooring. Model Predictive Control (MPC) was chosen as an ideal control approach due to its ability to predict future states and effectively handle the complexities of marine operations. MPC makes it ideal for the difficulties of mooring and unmooring, where precise control is necessary to ensure safety and efficiency.

The control strategy was then developed and implemented in MATLAB/Simulink, with the approach modified to meet the model-scale vessel's specific dynamics and operational requirements. In addition, Key Performance Indicators (KPIs) to assess the effectiveness of the strategy were introduced. The strategy's performance was assessed in three operational phases: unmooring, trajectory tracking, and mooring. The results show that the MPC controls the vessel's trajectory well, with errors staying well below acceptable bounds. The largest deviation of the final trajectory during the mooring test was 9.8% of the length of the ship. A 1.0% deviation for the benchmark trajectories could also be observed. These results, in addition to others, validate the suggested strategy's accuracy and dependability in practical situations.

In summary, this thesis provides a comprehensive control approach for autonomous unmooring, trajectory tracking and mooring for an autonomous model-scale vessel, bridging the gap between theoretical study and implementation in simulation. While the research identifies several limitations that present the potential for additional study, it also lays a solid foundation for future developments in autonomous maritime technology.

Keywords: Autonomous Shipping, Mooring, Unmooring, Trajectory Tracking, Ship Dynamics, Model Predictive Control (MPC).

Contents

List of Figures

List of Tables

List of Abbreviations

CoA	Circle of Acceptance
CoG	Center of Gravity
DOF	Degree of Freedom
DP	Dynamic Positioning
ECR	Equality Cost Relaxation
FIR	Finite Impulse Response
GNC	Guidance Navigation Control
IIR	Infinite Impulse Response
KPI	Key Performance Indicator
LOS	Line-of-Sight
LQR	Linaer Quadratic Regulator
MIMO	Multiple-Input, Multiple-Output
MPC	Model Predictive Control
MV	Manipulated Variable
NED	North East Down
NN	Neural Network
PID	Proportional-Integral-Derivative
QP	Quadratic Programming
ROV	Remotely Operated Vehicle
SISO	Single-Input, Single-Output
SNAME	Society of Naval Architects and Marine Engineers
TA	Thruster Alllocation
USV	Unmanned Surface Vehicle
ZOH	Zero-Order Hold

List of Symbols

Sign	Description	Unit
A_{Fc}	Frontal projected area	m^2
A_{Lc}	Lateral projected area	m^2
C_N	Current coefficient about the z-axis	-
C_X	Current coefficient in x	-
C_Y	Current coefficient in y	-
I_z	Moment of inertia about z-axis	kg m^2
J	Cost function	-
K	Moment about the x axis	Nm
L_{oa}	Overall length of the vessel	m
M	Moment about the y axis	Nm
N_c	Control horizon	-
N_p	Prediction horizon	-
$N_{\dot{r}}$	Hydrodynamic derivative of force N w.r.t. $\dot{r}$	-
$N_{\dot{v}}$	Hydrodynamic derivative of force N w.r.t. $\dot{v}$	-
$N_{current}$	Surge damping force about the z-axis	N
N	Moment about the z axis	Nm
T_s	Sample time	s
$V_{current}$	Speed of the current	m/s
$X_{\dot{u}}$	Hydrodynamic derivative of force X w.r.t. $\dot{u}$	-
$X_{current}$	Surge damping force in the x-direction	N
X	Force in X direction	N
$Y_{\dot{r}}$	Hydrodynamic derivative of force Y w.r.t. $\dot{r}$	-
$Y_{current}$	Surge damping force in the y-direction	N
Y	Force in Y direction	N
Z	Force in Z direction	N
α	Thruster angle	rad
$\boldsymbol{C_A}$	Added mass Coriolis-centripetal matrix	-
$\boldsymbol{C_{RB}}$	Rigid-body Coriolis-centripetal matrix	-
$\boldsymbol{C}$	Coriolis-Centripetal Matrix	-
$\boldsymbol{D}$	Damping matrix	-
$\boldsymbol{F}$	Force vector	N
$\boldsymbol{I_b}$	Inertia matrix	-
$\boldsymbol{I}$	Identity matrix	-
$\boldsymbol{K}$	Diagonal force coefficient matrix	-
$\boldsymbol{M_A}$	Added mass matrix	-
$\boldsymbol{M_{RB}}$	Rigid-body mass matrix	-
$\boldsymbol{M}$	Mass matrix	-
$\boldsymbol{R}(\psi)$	Rotation matrix	-
$\boldsymbol{S}$	Vector cross product	-
$\boldsymbol{T}(\boldsymbol{\alpha})$	Thrust configuration matrix	-
$\boldsymbol{\alpha}$	Vector of thruster angles	-
$\boldsymbol{\nu_r}$	Relative velocity vector	-
$\boldsymbol{\nu}$	Linear velocity of the body fixed origin	-
$\boldsymbol{\omega}^{\boldsymbol{b}}_{\boldsymbol{b/n}}$	Linear velocity of b relative to n expressed in b	-
$\boldsymbol{\omega}$	Angular velocity of the body fixed origin	rad/s
$\boldsymbol{\tau_{RB}}$	Rigid body vector of external forces/moments	-
$\boldsymbol{\tau}$	Vector of forces and moments(control inputs)	-

Sign	Description	Unit
$\boldsymbol{f}$	Control forces and moments	-
$\boldsymbol{g(\eta)}$	Vector of gravitational/buoyancy forces and moments	-
$\boldsymbol{g_o}$	Ballast control vector	-
$\boldsymbol{r_g}$	The distance vector between CO and CoG	m
$\boldsymbol{u}(t)$	Input vector	-
$\boldsymbol{v^b_{b/n}}$	Linear velocity of b relative to n expressed in b	-
$\boldsymbol{x}(t)$	State vector	-
γ_c	Current angle of attack	rad
ϕ	Euler angle about the x axis	rad
ψ_{PS}	Portside thruster angle	rad
ψ_{SB}	Portside thruster angle	rad
ψ_{ref}	Reference angle	rad
ψ	Euler angle about the z axis	rad
ρ	Density	kg/m^3
θ	Euler angle about the y axis	rad
a	Acceleration	m/s^2
m	Mass of the vessel	kg
p	Angular velocity about the x axis	rad/s
q	Angular velocity about the y axis	rad/s
r	Angular velocity about the z axis	rad/s
s	Position	m
t	Time	s
u	Linear velocity in the x direction	m/s
v	Linear velocity in the y direction	m/s
w	Linear velocity in the z direction	m/s
x_g	Distance in x between CO and CoG	m
y_g	Distance in y between CO and CoG	m
z_g	Distance in z between CO and CoG	m

1 Introduction

1.1. Background

Autonomous systems have been a growing topic of interest within the maritime industry in recent years. This interest is driven by the increased efficiency, safety and sustainability benefits it provides [1, 2]. As the largest port in Europe, with a throughput volume of 469 million tonnes (2018), Rotterdam is an important hub for the worldwide flow of goods and an important gateway to the European market of 500 million consumers. The Port Of Rotterdam did €15 billion in 2017 and with an annual GDP growth rate of 2%, this amounts to €19 billion in 2030 [3]. Additionally, inland waterway shipping revenue in the Netherlands climbed by 43% in 2022. The country accounts for more than a third of total EU27 transport activity [4]. One area of particular importance in inland waterways is vessel mooring and unmooring, which is crucial for port operations and maritime logistics. The process of conventional mooring and unmooring has stayed relatively the same and requires ropes and windlasses as well as crew members [5]. The failures are often due to untrained and inexperienced staff, equipment failures, available weather conditions, poor communication, safety process errors, risk assessment failure, and fatigue [6]. Traditional mooring and unmooring processes are often labor-intensive, time-consuming, and subject to human error, making them solid candidates for automation. The development of autonomous mooring and unmooring capabilities has the potential to streamline port operations by reducing reliance on manual labor, increasing operational efficiency, and minimizing the risk of accidents and injuries [7].

Mooring and unmooring of vessels entail securing or releasing a ship to or from a berth with ropes, lines, and other equipment [8, 9]. Mooring and unmooring are the start and the finish in the process of a ship involving transit from point A to point B. This typically requires trained crew members to be able to maneuver the vessel safely and efficiently whilst taking into account external factors such as the wind, waves and current [7]. Advancements in the autonomous shipping industry (regarding control strategies, sensors and actuators) allow for this process to be developed into autonomous mooring and unmooring. Currently, two methods of automatic mooring are used: magnetic and vacuum. These methods involve high costs as well as other disadvantages regarding maintenance and electrical failures [7]. Another possible alternative to achieve autonomous mooring would be to use the thrusters of a vessel that are managed by a control strategy. Furthermore, these capabilities combined with other autonomous technologies can make ports operational day and night, resulting in increased throughput and quicker vessel turnaround times. By streamlining the mooring and unmooring procedures, it can help lower fuel consumption, emissions, and environmental impact [10].

Despite the potential benefits of autonomous mooring and unmooring, certain hurdles remain in creating robust and reliable control systems capable of efficiently managing the complexities of real-world marine situations. One such problem is the requirement to account for uncertainties and disturbances, such as changing weather conditions, vessel characteristics, and berth configurations. In addition, it also has to maintain safe and exact vessel location during the mooring and unmooring processes, which is also described as Dynamic Positioning (DP) [11].

Many studies have been conducted regarding autonomous shipping [12]. Autonomous shipping research with the use of a control strategy has mainly been focused on collision risk [13], trajectory tracking [14] and maneuvering with its focus on energy management [15]. Studies on autonomous mooring have focused mainly on offshore mooring and coastal observations [16, 17].

1.2. Research scope

The marine sector has been able to develop motion control systems. These are constructed from Guidance, Navigation and Control (GNC) systems that can operate vessels on a (semi-) autonomous level. Guidance is the action or system that continuously computes the relevant parameters used by the control system. The navigation system consists of directing the marine craft by taking the position, course and distance traveled into account. The control system uses a control loop that takes in outputs from the navigation and guidance system in order to compute the output [18]. The scope of this research can be defined using the GNC scheme which can be seen in figure 1.1. The guidance and control systems will be explored whilst the navigation stays out of the scope.

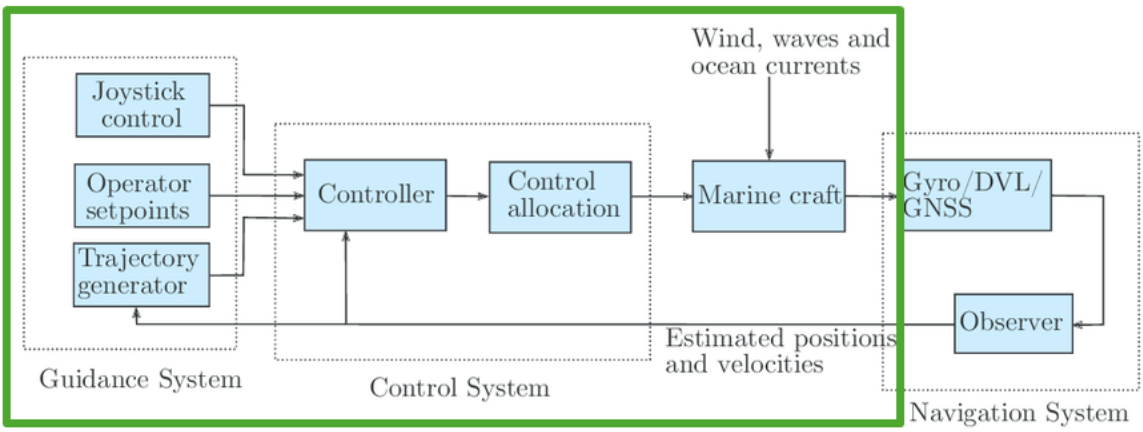

Figure 1.1: A typical GNC system for marine crafts [19]

The process will consist of three phases: unmooring, trajectory tracking and mooring. Each phase will include trajectory generation (based on a trapezoidal velocity profile) and control. Certain Key Performance Indicators (KPI) will be defined and used to assess the system. The scientific contribution of this research will entail the development of a control strategy for the autonomous unmooring and mooring in addition to trajectory tracking for an autonomous vessel. The specific application of autonomous mooring and unmooring combined with trajectory tracking remains unexplored in literature to date. This will increase efficiency and safety with use of autonomous operations for the current marine processes [1, 2].

1.3. Research objectives

The canals of Delft, which were traditionally utilized for trade and transportation, have the potential to be refreshed as modern transit channels by implementing autonomous vessels. These vessels could provide a sustainable and effective alternative to traditional road transportation. This aims to solve some of the most serious issues confronting cities today, such as traffic congestion, air pollution, and space efficiency. The objective is to create a controller for the goal of autonomous unmooring, trajectory tracking and autonomous mooring for the model scale vessel Tito Neri in the canals of Delft (inland waterway). The trajectory for the autonomous vessel will be from the station of Delft to “De Nieuwe Haven” in order to reach the campus of Delft University of Technology. The trajectory can be seen in figure 1.2. This trajectory will be generated using a trapezoidal velocity profile. This profile allows for the vessel to accelerate, maintain a certain speed and decelerate when the position has been reached [20].

The primary objective of this thesis is autonomous unmooring, trajectory tracking and autonomous

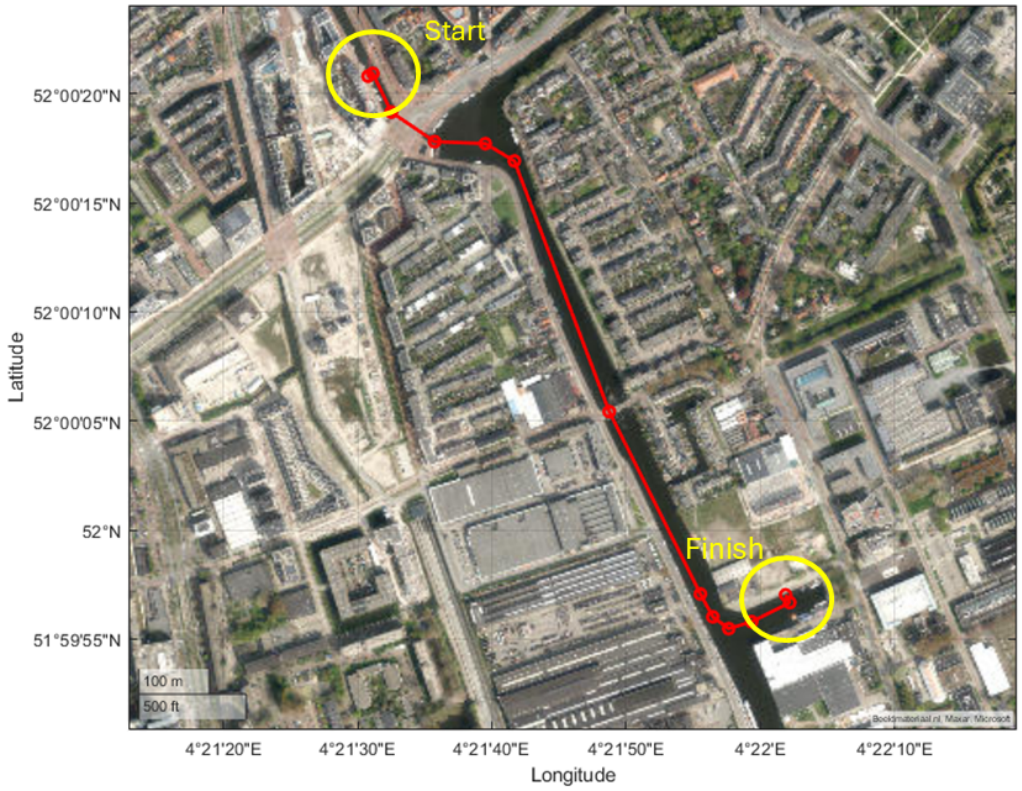

Figure 1.2: Delft trajectory to be followed by the vessel

mooring of an autonomous model scale vessel. More specifically, this research aims to develop a control strategy to control the actuator input of a small-scale vessel (Tito-Neri) in inland waterways in Delft for trajectory tracking and mooring and unmooring. The research question will thus be the following:

Research Question
How to realise trajectory tracking and autonomous mooring and unmooring capabilities of an autonomous model scale vessel?

From the research question, the following sub-questions can be derived and will be answered in this thesis.

1. *What are the research gaps and relevant theoretical concepts with respect to trajectory tracking and mooring and unmooring of autonomous marine vessels?*

   This sub-question focuses on the theoretical concepts regarding autonomous ships and guidance strategies, trajectory tracking and velocity profiles, mooring and unmooring, dynamic positioning and disturbances. This subquestion will be answered in Chapter 2.

2. *What is an applicable mathematical model for the model scale vessel?*

   This sub-question focuses on deriving and providing the mathematical model of the model scale vessel that will be controlled going forward. It will be answered in Chapter 3.

3. *What is the best control strategy to be selected for the application and how to design it?*

This sub-question has its focus on the selection of the control strategy that is best suited for the application of unmooring, trajectory tracking and mooring. It will also focus on how to design that control strategy and will be answered in Chapter 4.

4. *How to implement the proposed control strategy in simulation?*

   This sub-question will focuses on the implementation. This consists of generating the trajectories that will be used for the application and defining the relevant KPIs. It will also focus on the tuning of the control strategy as well as filtering of the results. This will be answered in Chapter 5.

5. *How to evaluate the performance of the control strategy for different trajectories under various operating conditions?*

   Lastly, the results and assessment of these results will be provided. This consists of the control strategy applied to all the benchmark trajectories and the Delft trajectory. The evaluation of the results with the KPIs to check the performance is also provided. This sub-question will be answered in Chapter 6.

Note: the title of this report indicates the selected method, but the decision to implement Model Predictive Control (MPC) will be explained.

1.4. Methodology

An overview of the methodology followed in this thesis can be seen in figure 1.3. The methodology serves as an approach to answering the research questions, as well as a guide for this report. First, a literature review is done in order to get helpful information about relevant theoretical concepts as well as define the need with regard to autonomous mooring and unmooring. After this is completed, the mathematical model of the model scale vessel will be provided based on an overview of the literature on mathematical vessel models. Then an appropriate control strategy will to be chosen and elaborated upon. After this, the main objective will be split into three phases that each make use of an MPC. With these phases in place, the trajectories can be generated which will later be used to assess the performance of the MPC. For this, the relevant KPIs have to be defined before moving on to the implementation. This implementation consists of two parts, namely the benchmark trajectories and the Delft trajectory, which serves as an amalgamation of the benchmark trajectories. The performance will be assessed using the defined KPIs. Lastly, a conclusion and recommendations for future studies will be provided.

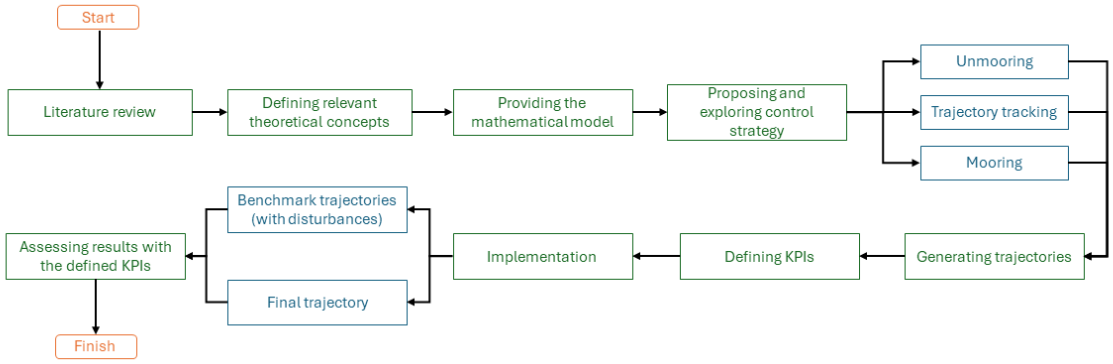

Figure 1.3: Overview of the methodology used

1.5. Research outline

The outline of this thesis is structured as follows. Chapter 2 provides a theoretical background that will dive into the relevant theoretical concepts regarding autonomous ships, trajectory tracking, mooring and unmooring, stationkeeping and the model scale vessel. Chapter 3 will introduce the mathematical model of the model scale vessel that will be controlled to achieve autonomous unmooring, trajectory tracking and mooring. First, the derivations of the relevant matrices will be shown, which will be followed by the thruster allocation. Then the parametrized Tito-Neri model will be shown that will be used by the control strategy. Chapter 4 will entail the selection of the control strategy to be used based on relevant requirements. It will dive into the chosen control strategy, its relevant concepts and parameters, as well as provide the algorithm to be used during the simulation. Chapter 5 will introduce the relevant KPIs and the reference trajectories that will be followed by the model-scale vessel in simulation. The results and assessment of those will be provided in chapter 6. These include the addition of disturbances induced by the current. Lastly, chapter 7 concludes this work and provides recommendations for future work.

2

Literature background

This chapter answers the sub-question: **What are the research gaps and relevant theoretical concepts with respect to trajectory tracking and mooring and unmooring of autonomous marine vessels?** To provide a solid theoretical background and identify the need for autonomous mooring and unmooring, this chapter is divided into sections. Section 2.1 focuses on the autonomous ship systems which includes GNC as well as current ship operations. Section 2.2 dives into trajectory tracking and focuses on velocity profiles for trajectory generation. It also includes the guidance strategies that will be used. Section 2.3 focuses on the mooring and unmooring operations. It shows the conventional methods used and focuses on its limitations in terms of safety to provide a gateway into autonomous operations. Lastly, section 2.4 introduces stationkeeping which involves the concept of DP and disturbances.

2.1. Autonomous ship systems

Autonomous vessels have been under investigation for a long time. World War II started the first experimentation with Unmanned Surface Vehicles (USV). The torpedo concept in 1944 to lay smoke and obscure vision is one from that period. During the period 1950-1980, the focus switched toward Remote Operating Vehicles (ROV) for underwater activities, rather than surface-based USVs. The focus here was on minesweeping drones, given the time period after World War II. The development of modern USVs in the following period (1990-2000) gained traction and was driven by advancements in technology. The focus of the Navy during this period was mainly on reconnaissance and surveillance missions. In figure 2.1 a small overview of the evolution from 1950-2000 can be seen. The image on the left shows an ROV, the middle one shows a Remote Minehunting System (RMS) and on the right a Reconnaissance Vehicle.

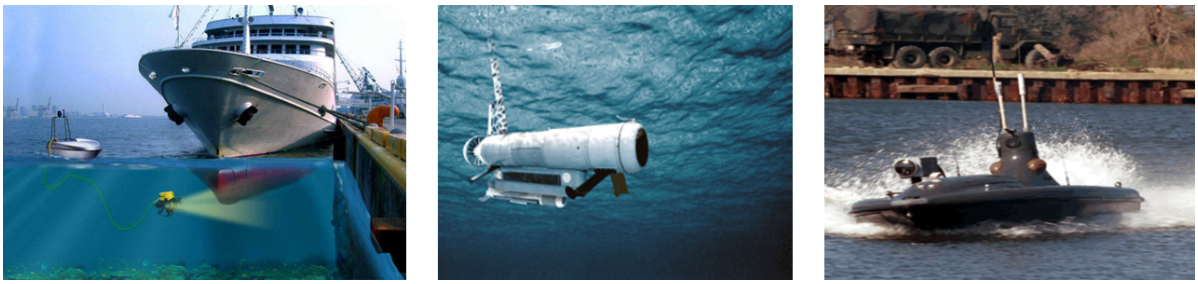

Figure 2.1: ROV, RMS and a Reconnaissance Vehicle [21]

In the past two decades, numerous institutions, universities, businesses and militaries have begun developing USVs for various applications. The development of completely autonomous USVs in highly dynamic maritime environments remains an open question for the near future. There are currently multiple research projects on this specific topic [21, 22]. USVs and autonomous ships both contribute to the expanding field of unmanned marine systems, but their size, autonomy degree, intended uses,

and regulatory issues differentiate the two. USVs are typically smaller, remotely controlled, or semi-autonomous vessels employed for specific purposes. Autonomous ships are larger, fully autonomous vessels meant for long-distance operations [23].

Significant progress in developing completely effective autonomous ship systems did not occur until around the start of the twenty-first century. The technological innovation in USVs led to the start of advancements in autonomous ship systems. Since a simple autonomous ship collision-free guidance system in 1999, a lot of progress has been made since then [24]. The first fully Autonomous cargo ship (MV Yara Birkeland) completed its maiden voyage only in 2022. This ship was built in Norway for the sake of transporting fertilizers between ports [25].

2.1.1. Guidance, Navigation and Control (GNC)

In addition to the developments of the ship systems, the marine sector has been able to develop motion control systems. These are constructed from GNC systems that can operate vessels on a (semi-)autonomous level. This happened due to the quick development of sensor technology, communication, computing software, and hardware. For instance, heading control was made possible by the gyrocompass and the introduction of the Global Positioning System (GPS) allowed for path following and trajectory tracking [18]. The GNC signal flow for a conventional ship autopilot can be seen in figure 2.2.

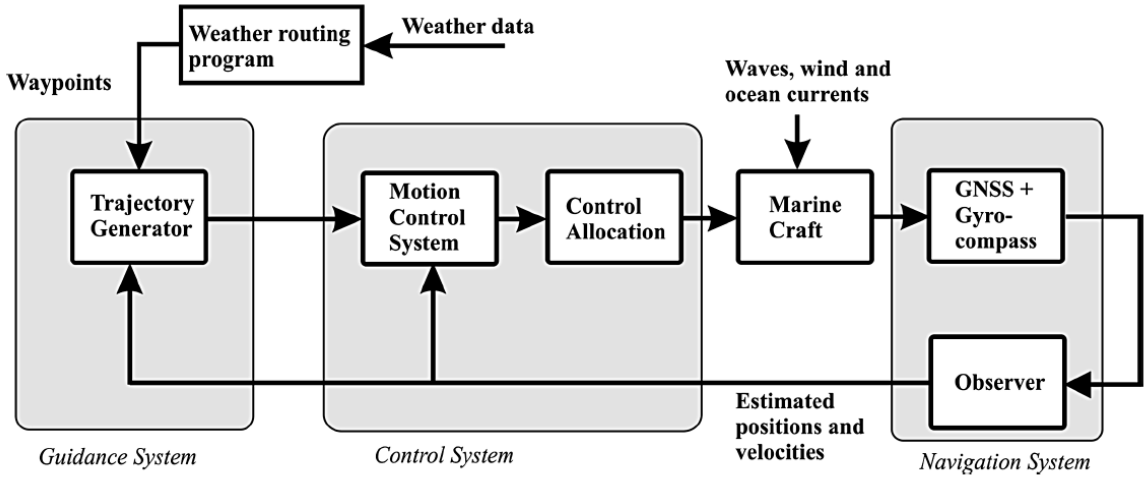

Figure 2.2: GNC Control Flow [18]

Guidance is the action or the system that continuously computes the reference or desired position, velocity and acceleration of a marine craft, which is then used by the motion control system. This data is usually provided by the human operator and the navigation system. Navigation is the science of directing a marine craft by determining the position or altitude, course and distance traveled. This is usually achieved by using a Global Navigation Satellite System (GNSS) and motion sensors (gyros and accelerometers). Lastly, control, or rather motion control, deals with the action of determining the necessary control forces and moments to be applied to the craft in order to satisfy the control objective. This objective is usually followed in combination with the guidance system. Examples of control objectives are trajectory-tracking, path-following and maneuvering control. The control algorithm uses a control loop that takes in outputs from the navigation and guidance system as inputs in order to compute its output (e.g. control forces) [18].

2.1.2. Ship operations

Autonomous operations are improving the safety, efficiency, and environmental performance of modern boats. This involves minimizing collisions and incidents in congested ports, optimizing speed profiles to

save fuel, lowering emissions, and optimizing staff numbers. In practice, however, this is a far-fetched idea with numerous challenges to solve. The key drivers or challenges to solve for autonomy in the maritime industry are the following: overcapacity, increasing safety, reducing the chances of human error, increasing vessel efficiency and decarbonization [26]. To pursue higher levels of autonomy, one first must look at the general current operations of a ship. Currently, the general operations involved in a ship going from point A to point B are the following [27–29].

1. **Unmooring (a ship leaving)**
    - **Before unmooring:** Prepare a berth, safety checks are conducted, communication channels between the relevant parties are established and potential weather conditions are checked to assess potential difficulties.
    - **During unmooring:** Disconnect mooring lines, let the vessel go and communicate with the relevant parties involved to notify the ship's departure.
2. **Transit**
    - **Piloting/navigation:** Execute navigational maneuvers.
    - **Monitoring:** Monitor navigation systems and other relevant instruments. Also, a vigilant watch (personnel) for potential obstacles, traffic, or changes in weather conditions can be required.
3. **Mooring (a ship arriving and potentially staying)**
    - **Before mooring:** Gradually reduce speed as the ship approaches its endpoint of the voyage. Communicate to the port authorities about the ship's arrival and receive potential instructions.
    - **During mooring:** Members of the crew deploy mooring lines and secure them to the shore or terminal bollards. The thrust of the ship needs to be used to maintain the desired position at the mooring location.
    - **Post-mooring:** Potentially shutting down the thrust of the ship. Conduct checks and notify the port authorities.

As can be noted, the current process involves a lot of human controls. In order to move to complete automation the process of mooring and unmooring needs to be automated since it is a vital part of the tasks a ship completes. Going forward, the guidance and control systems will be used going forward with the navigation side being out of the scope of this research.

2.2. Trajectory tracking

Trajectory generation is the process of picking a motion and the related optimal input controls while validating all constraints and minimizing a performance index [30]. The challenge of tracking the trajectory requires the vehicle to reach a specific spot at a predetermined time following a parameterized reference generated [31]. The trajectory to be followed can be defined with point-to-point trajectory tracking. In this case, as the name suggests, only a relatively small number of points are used to create a trajectory. When additional points, known as via points, are added between the beginning and ending positions, a smoother trajectory can be created. This strategy is frequently used to avoid objects and thus prevent collisions, in addition to smoother path following [20].

2.2.1. Trajectory Profiles

To further smooth out the trajectory, the different types of trajectory profiles can be discussed. A polynomial profile leads to a smooth profile with max joint velocity at $t = T/2$ and max joint acceleration and deceleration at $t = 0$ and $t = T$, respectively, as can be seen in figure 2.3 [20].

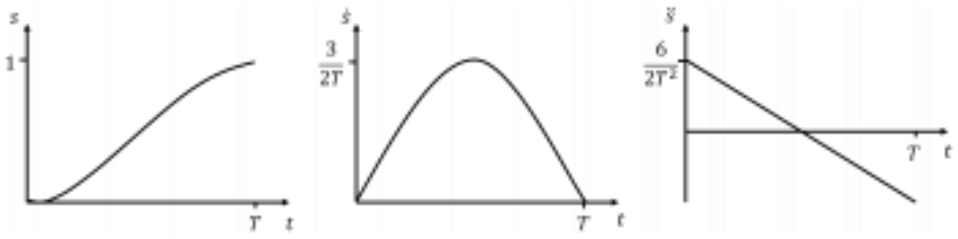

Figure 2.3: Polynomial velocity profile [20]

In addition to the polynomial profile, both the bang-bang acceleration profile (or triangle velocity profile) and the trapezoidal acceleration (or velocity) profile can be introduced. The bang-bang profile consists of a discontinuous acceleration profile that has a constant acceleration until $t = T/2$ which is followed by constant deceleration until $t = T$. The trapezoidal velocity profile maintains a constant velocity phase in addition to following the characteristics of a bang-bang profile. This maximum velocity leads to saturation in the acceleration phase [20].

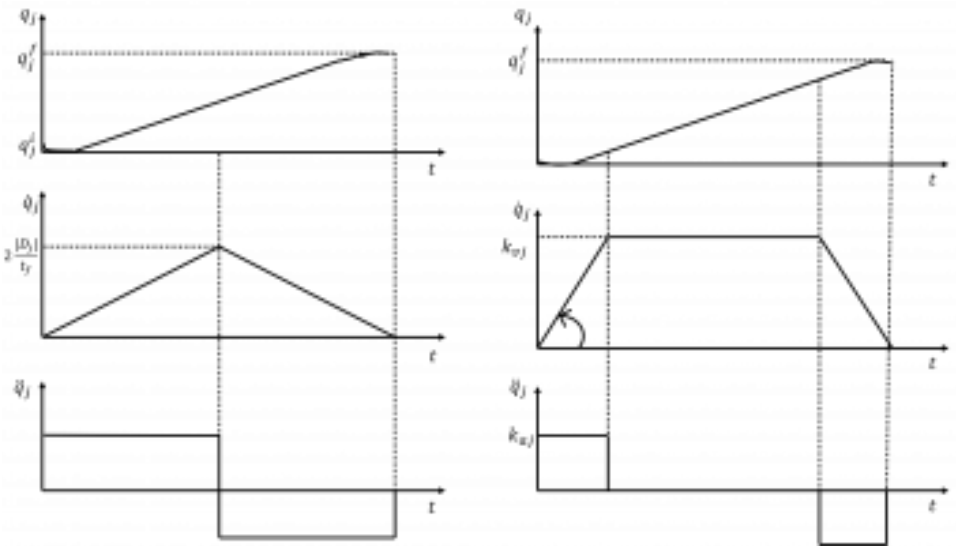

Figure 2.4: Bang-bang velocity profile (left) and trapezoidal velocity profile (right) [20]

The trapezoidal velocity profile trajectory connects waypoints with a motion profile that stops at each waypoint, and the waypoint-to-waypoint motion is guided by a motion profile. The corresponding phases can be seen in figure 2.5. Considering it achieves a compromise between simplicity and efficiency in fulfilling operational constraints, a trapezoidal velocity profile is frequently utilized in a variety of applications.

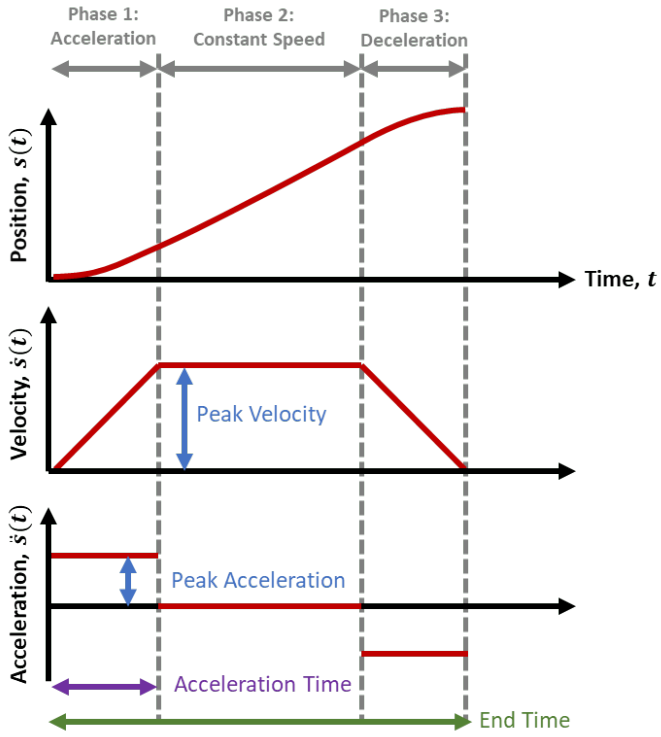

Figure 2.5: Trapezoidal velocity profile phases [32, 33]

As can be observed from figure 2.5, the velocity profile has a total of four parameters. These are the following:

- **End Time:** Duration of each segment between two waypoints
- **Peak Velocity:** The peak velocity of each segment
- **Acceleration Time:** Time spent in the acceleration and deceleration phases
- **Peak Acceleration:** The magnitude of the acceleration during the acceleration and deceleration phases

Mathematically, this profile defines segments on the interval [0, endTime], with acceleration, constant speed, and deceleration phases. The lengths of the acceleration and deceleration phases are equal. Each phase is shown below according to [32, 33].

1. Acceleration Phase: For $t = [0,$ accelTime $]$, $\frac{\mathrm{d}^2}{\mathrm{d}t^2}s(t) = a$, $\frac{d}{\mathrm{d}t}s(t) = at$, $s(t) = a\frac{t^2}{2}$
2. Constant Speed Phase: For $t =$ [accelTime, endTime - accelTime], $\frac{\mathrm{d}^2}{\mathrm{d}t^2}s(t) = 0$, $\frac{d}{\mathrm{d}t}s(t) = v$, $s(t) = vt - \frac{v^2}{2a}$
3. Deceleration Phase: For $t =$ [endTime - accelTime, endTime], $\frac{\mathrm{d}^2}{\mathrm{d}t^2}s(t) = -a$, $\frac{d}{\mathrm{d}t}s(t) = a($endTime $-t)$, $s(t) = \frac{2av*\text{ endTime } -2v^2-a^2(t-\text{endTime})^2}{(2a)}$

2.2.2. Guidance Strategies

In addition to the planning of the trajectory, the guidance system is built on the notions of the Line-Of-Sight (LOS) and the Circle of Acceptance (CoA) around the waypoint. The LOS strategy iteratively uses the current position of the vessel and the next waypoint in order to calculate the reference angle as follows [34]:

$$\psi_{ref} = \text{arctan2}(y_2 - y_1, x_2 - x_1) \tag{2.1}$$

where $(x1, y1)$ and $(x2, y2)$ are the coordinates of the current position and the next waypoint respectively.

To determine the next coordinate for the LOS, a CoA of a prespecified radius is defined around each waypoint. In each time instance, the distance between the vessel's current position and the next waypoint is computed and compared to this radius. Only when the distance is less than the radius, it is determined that the vessel has arrived at the associated waypoint and can receive a new reference angle ψ_{ref} [31]. An example of a trajectory being followed can be seen in figure 2.6.

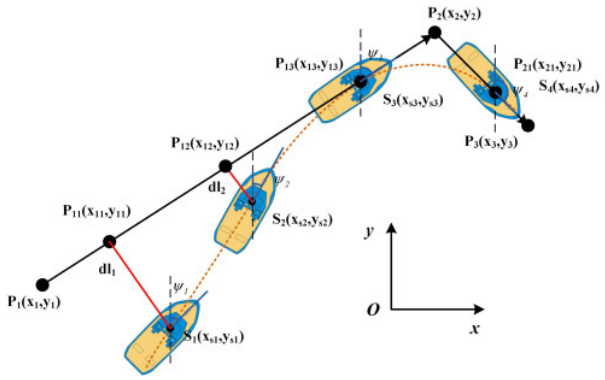

Figure 2.6: Trajectory tracking [35]

From this section the trajectory generation according to a trapezoidal velocity profile will be used going forward. In addition, the LOS and CoA are going to be used as guidance strategies for the research. In the next section, mooring and unmooring operations will be discussed.

2.3. Mooring and unmooring operations

First, it is of importance to define the concept of mooring and unmooring. The terminological definition of mooring is the system that secures a ship to a terminal or multiple terminals. Unmooring deals with releasing a ship from a terminal or multiple terminals [8, 9]. The principle of mooring has changed quite a bit over the years. In the past few decades, a lot of development can be observed in the realm of maritime transportation. These advances include increasing the dimensions of the vessels and increased operations. This means that both ports and vessels have to deal with more challenging conditions. These conditions include disturbances due to waves, wind and also the current [9]. Several improvements have been made in the marine industry in terms of mooring systems, such as automated vacuum mooring systems, magnetic mooring systems, and berthing help systems [36, 37]. However, most vessels continue to use mooring methods that require ropes and windlasses. During this process, the vessel comes close to the mooring point and reduces its speed to, usually between 1 and 2 knots (1.85-3.7 m/s) [38]. These are general numbers, as these values vary depending on specific vessel types, environmental conditions and operating conditions [39].

2.3.1. Conventional methods

An efficient mooring system is crucial for ensuring ship, terminal, and environmental safety. The type and size, as well as other project-related factors of the vessel, affect every component of the mooring system. Mooring systems therefore come in all shapes and sizes. To name a few, conventional solutions include single point mooring (SPM), multi-buoy mooring (MBM), and floating production storage and offloading vessels (FPSO) which can use SPM [40]. This can be seen in figure 2.7 [9].

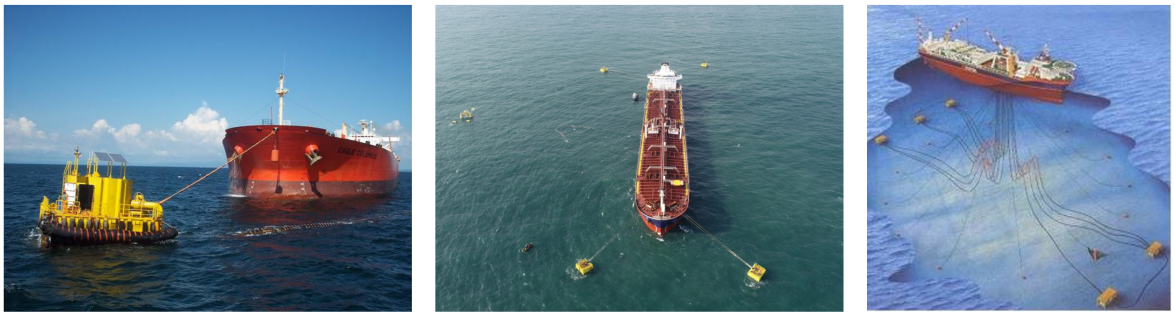

Figure 2.7: SPM, MBM and FPSO [40]

In SPMs, all of the mooring lines are connected to a single connecting point. With the environment loads, the vessel can freely rotate around a single point. Single point moorings come in a variety of forms, usually consisting of turret mooring, single anchor leg mooring (SALM), and catenary anchor leg mooring (CALM) [41]. This can be seen in figure 2.8.

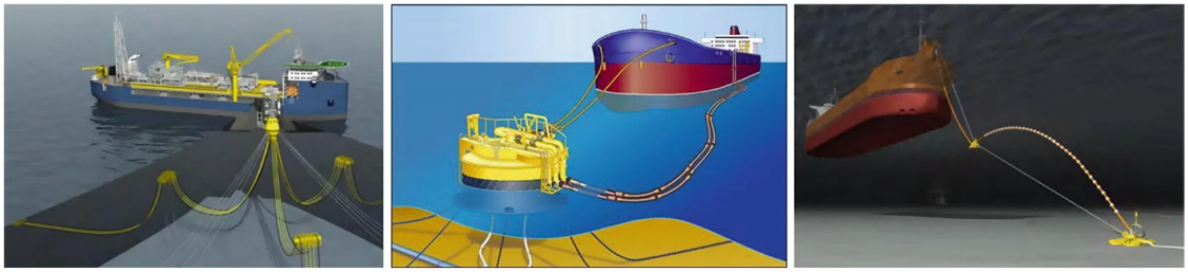

Figure 2.8: Turret mooring, CALM and SALM [41]

Conventional methods used on a larger scale for mooring and unmooring typically use turret systems. The turret systems have a floating structure in order to adapt its heading due to environmental disturbances. There are two categories of these stationkeeping systems: Permanent and non-permanent. In permanent systems, the floating structure remains stationary. In non-permanent systems, the floating structure is temporarily moored for the transfer of for instance cargo. Next, the integration types are the methods by which the mooring system is linked to the floating structure structurally. This can be external or internal (part of the hull structure) as can be seen in figure 2.9. Lastly, there are three types of mooring systems based on their dynamic behavior. Tower systems are permanently attached to seafloor constructions. Column systems are buoyant columns connected to the bottom by a single chain or articulated rigid framework. Mooring Legs are flexible linear elements like chains, polyester ropes, and wire ropes attached to buoys or turrets [41–43].

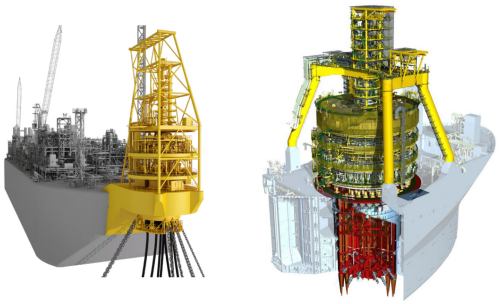

Figure 2.9: External turret (left) and internal turret (right) [42]

2.3.2. Safety in mooring and unmooring

The concept of autonomous mooring is not an entirely new one as several possibilities have been and are currently being explored. This is mainly due to the safety hazards that arrive from mooring and unmooring. Mooring operations aboard ships raise major safety risks for the ship's crew, the ship itself, and the maritime environment. Lack of mooring equipment maintenance, untrained and inexperienced personnel, equipment failures, available weather conditions, poor communication, safety procedure errors, and risk assessment failure are the most frequent causes of mooring accidents involving ropes and windlass [44, 45]. When a ship is tied down to a dock or another vessel, it can be an extremely dangerous process if those involved are not properly taught, have the appropriate equipment and have the proper mindset. An overview of the most common factors is shown in table 2.1 [46, 47].

Table 2.1: Most common risks in mooring [46, 47]

Category	Risk factors
Equipment	Use of old, damaged wires
	Poor equipment
	Poorly designed mooring system
	No overview of mooring area
	Hazard/tripping risk sites not highlighted
	Poor wire/line handling
Work Processes	Lack of communication and planning
	Poor wire/line handling
Crew Qualifications	Unclear instructions
	Lack of information
	Lack of supervision
	Small, untrained deck crew
	Ineffective onboard mooring training
	Crew concentration: stress and fatigue
Ship's Safety Culture	Procedures not followed
	Shortcuts taken
	Standing in the wrong places (snap back zone)
	Walking over a wire
	Quick mooring versus safe mooring
	Lack of risk assessment prior to mooring operations
	Cluttered deck/mooring area
Weather	Icy, slippery deck

2.3.3. Autonomous mooring and unmooring

Studies regarding autonomous mooring have mainly been focused on offshore mooring and coastal observations [16, 17]. These mostly focus on optimizing current mooring processes involving the conventional mooring technologies from section 2.3.1 [36, 37]. Two methods of automatic mooring currently used are magnetic mooring and vacuum mooring. The disadvantages of these systems are potential electrical failures, high purchase costs of the systems and requiring more maintenance [46]. The most notable new method is the MacGregor mooring solution that will allow Yara Birkeland, the world's first autonomous container ship, to moor without human assistance. The system is built on a seven-axis robotic arm that takes looped mooring ropes and wraps them around dock bollards, as can be seen in figure 2.10 [48]. Mooring developments for an autonomous ocean sampling network is also a common topic of interest in research [49, 50].

Figure 2.10: Mooring rope with a robotic arm [48]

Using the information provided on conventional mooring, it can be said that autonomous mooring provides benefits regarding safety and efficiency. Moving towards stationkeeping systems without conventional methods, e.g. using just the ship and its thrusters, will be explored going forward.

2.4. Stationkeeping

Stationkeeping systems use either a mooring system (passive), a dynamic positioning system (active), or a combination of the two. In the past, the bulk of moorings were passively executed. More recently, moorings have been utilized for station-keeping in conjunction with thruster Dynamic Positioning (DP) systems. These help to alleviate loads in the mooring by turning the vessel as needed and protect the vessel from environmental disturbances [43].

2.4.1. Dynamic Positioning (DP)

A DP system is: “An automatic system that maintains the position of a ship or vessel using its thrusters, in the presence of disturbances such as wind, waves, and current” [51]. This is currently commonly used by offshore vessels in deep-water operations. These systems provide a gateway into autonomous mooring, as it only uses a set of thrusters to balance external forces.

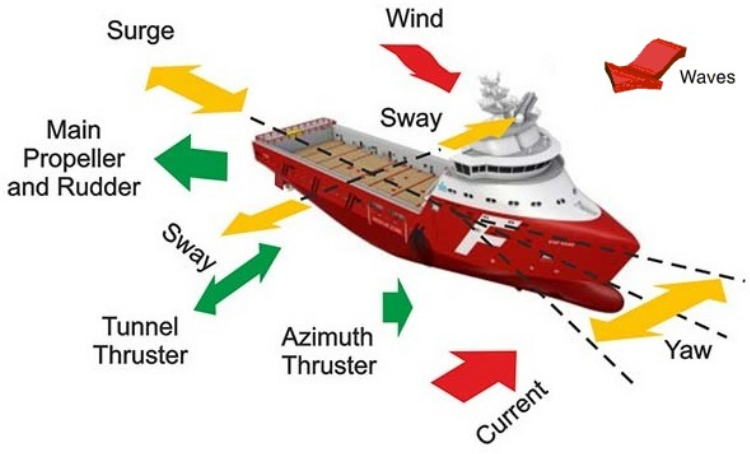

Figure 2.11: DP system using thrusters (green) to balance out forces (red) [11]

When a ship is operating in waterways, waves, wind, and currents are bound to generate disturbances that will cause the ship to drift off course from its intended position and heading. The primary challenge in the design of the DP control system is the suppression of disturbances. With the use of only its own propellers and thrusters, DP technology enables a floating structure, such as a ship or drilling platform, to keep its position and heading at a fixed place or along a predetermined track while being insensitive to the depth of the water [52].

Compared to more conventional vessel positioning techniques like anchor-based systems, dynamic positioning has the following benefits [53]:

- **Accuracy:** Even under difficult circumstances, DP systems are able to retain a vessel's position accurately with outstanding manoeuvrability
- **Flexibility:** Its ability to operate in waters of any depth with rapid responses to changes in the weather or operation's requirements
- **Efficiency:** Quick and easy set-up and able to complete tasks quickly and cost-effectively
- **Safety:** No risk of mooring lines or anchors damaging the seabed

2.4.2. Disturbances

Disturbances are inherently present in the entire system, which are induced by multiple components. These consist of environmental disturbances which are current, wave and wind disturbances. For this research, only the current disturbances will be modeled and looked at. In low-speed applications consisting of DP (up to approximately 2 m/s), ocean currents and damping can be represented using three current coefficients: C_X, C_Y, and C_N. These can be determined experimentally using scale models in wind tunnels. The wind and current coefficients are defined using a counterclockwise rotation γ_c [18].

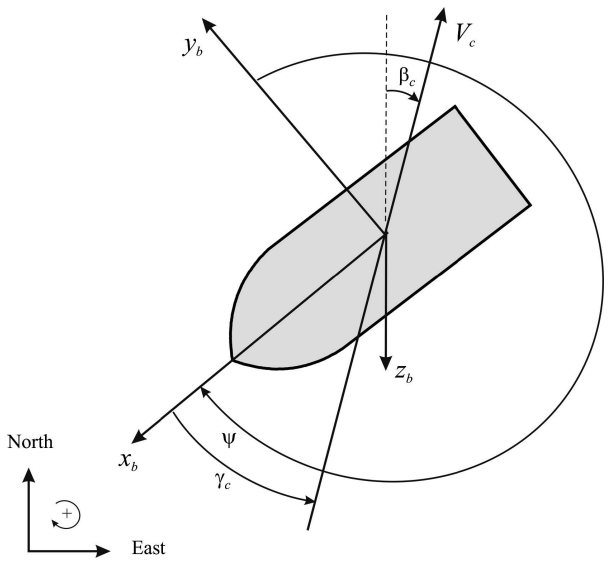

Figure 2.12: The current speed V_c, current direction β_c and current angle of attack, γ_c all relative to the bow [18]

The current forces on a vessel can be expressed in terms of the area-based current coefficients C. The disturbances in the surge, sway and yaw in accordance with figure 2.12 can be seen below.

$$\begin{aligned} X_{current} &= \frac{1}{2}\rho A_{Fc} C_X(\gamma_c) {V_{current}}^2 \\ Y_{current} &= \frac{1}{2}\rho A_{Lc} C_Y(\gamma_c) V_c^2 \\ N_{current} &= \frac{1}{2}\rho A_{Lc} L_{oa} C_N(\gamma_c) V_c^2 \end{aligned} \tag{2.2}$$

Here X_{current} , Y_{current} and N_{current} are the surge damping force in the x-direction, y-direction and about the $z-$axis respectively. C is the current coefficient, which is a function of the angle of attack γ_c relative to the bow. The density of the water is given by ρ. The frontal and lateral projected current areas are given by A_{Fc} and A_{Lc} respectively. L_{oa} is the overall length of the vessel and V_c is the speed of the current.

Since the current is dependent on the direction, the current coefficients are a function of the angle of attack. For a Platform supply vessel (PSV) the current coefficients can be seen in table 2.2. The same current coefficients are used for this research.

Table 2.2: Current coefficients

γ_c	C_X	C_Y	C_N	γ_c	C_X	C_Y	C_N
0	1.01	0	0	180	-0.67	0	0
15	0.75	-9	2	195	-0.53	7.100	1.45
30	0.48	-18	4	210	-0.04	14.85	2.80
45	-0.70	-27.05	5.10	225	0.45	23.05	3.35
60	-1.87	-36.05	6.20	240	0.35	30.40	3
75	-0.58	-38.20	4.20	255	0.54	34.50	0.45
90	0.72	-38.55	2.15	270	0.72	38.55	-2.15
105	0.54	-34.50	-0.45	285	-0.58	37.30	-4.20
120	0.35	-30.40	-3	300	-1.87	36.05	-6.20
135	0.45	-23.05	-3.35	315	-0.70	27.05	-5.10
150	-0.04	-14.85	-2.80	330	0.48	18	-4
165	-0.53	-7.100	-1.45	345	0.75	9	-2

2.5. Conclusion

In this chapter, the following sub-question has been answered: **What are the research gaps and relevant theoretical concepts with respect to trajectory tracking and mooring and unmooring of autonomous marine vessels?** The relevant theoretical concepts have been discussed and going forward, the following concepts will be used. First, it was determined that the control and guidance strategies will be used going forward, with the navigation being kept out of scope. This was followed by the observation of current ship operations, which showed a lot of human controls involved. The current mooring and unmooring processes have a lot of risk and room for improvement. This will entail using the thrusters of the ship in order to moor and unmoor. From the trajectory tracking section, the trapezoidal velocity profile will be used going forward, as well as the CoA and LOS. Going forward, the concept of DP will be used for low speeds and stationkeeping of the ship. In addition, the disturbances from the current will be modeled and used. The next chapter focuses on the mathematical vessel model that will be controlled in this research going forward for unmooring, trajectory tracking and mooring.

3

Mathematical Vessel Model

In this chapter, the following research question will be answered: **What is an applicable mathematical model for the model scale vessel?** The mathematical model of the vessel is introduced to be used in inland waterways at relatively low speeds. To work towards this model, first, in section 3.1 the motion and relevant notation will be provided. Next in sections 3.2 and 3.3 the kinematic model and kinetic model will be shown respectively. Section 3.3 also features the system inertia mass matrix, the Coriolis-Centripetal matrix and the hydrodynamic damping matrix. The next section 3.4 dives into the actuation also Thruster Allocation (TA) for the model scale vessel. Lastly, in section 3.5, a parametrized Tito-Neri model will be shown that will be used in the rest of this research.

3.1. Motion

The dynamics of the ship system can be described using the book of Fossen [18]. A marine craft experiences motion in 6 Degrees Of Freedom (DOFs) while maneuvering, which can be seen in figure 3.1. The DOFs are a collection of independent displacements and rotations that define the craft's location and orientation. Surge (propulsive motion) and sway (sideways motion) are terms used to describe motion in the horizontal plane. Rotation about the vertical axis is described by yaw (the heading of the craft). Roll (rotation about the longitudinal axis), pitch (rotation about the transverse axis), and heave (vertical motion) are the final three DOFs. Often, reduced order models are utilized when constructing control systems for maritime crafts, since most crafts do not actuate in all DOFs [18].

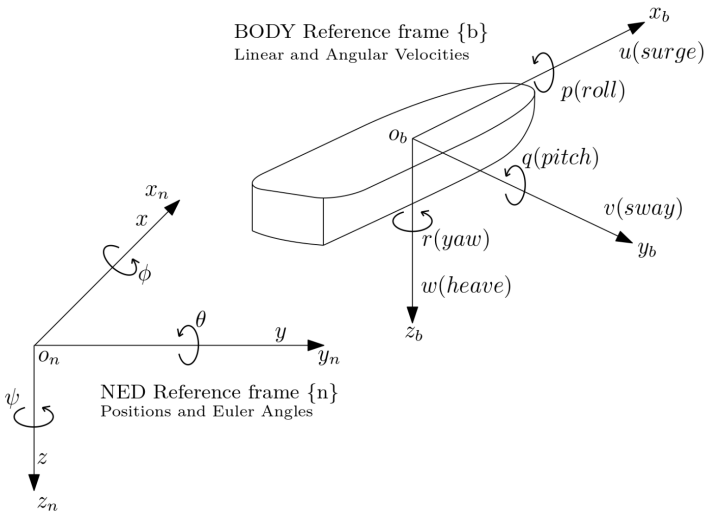

Figure 3.1: DOFs and frames [18]

The vessel's position and orientation are provided using the North-East-Down (NED) coordinate system. Here, the inertial frame is described by $\{n\} = (x_n, y_n, z_n)$ and the body-fixed frame by $\{b\} = (x_b, y_b, z_b)$. The linear and angular velocities of the vessel are described in the body-fixed frame that moves with the vessel. Mooring and unmooring require control of the position and orientation of the vessel, and the vessel is supposed to navigate in inland waterways (calm water). A 3DOF horizontal plane model (Surge, sway and yaw) is best suited for the application. Heave, roll, and pitch motion dynamics are ignored.

Table 3.1: Notation of the Society of Naval Architects and Marine Engineers (SNAME) (1950) for marine vessels [54]

DOF	Forces and moments	Linear and angular velocities	Pos. and Euler angles
Motions in the x-direction (surge)	X	u	x
Motions in the y-direction (sway)	Y	v	y
Motions in the z-direction (heave)	Z	w	z
Rotation about the x-axis (roll, heel)	K	p	ϕ
Rotation about the y-axis (pitch, trim)	M	q	θ
Rotation about the z-axis (yaw)	N	r	ψ

From table 3.1 the following vectors can be defined. Note that here M is the moment about the y-axis and not the mass matrix $\boldsymbol{M}$. Firstly, $\boldsymbol{\nu}= [u, v, w]^\top$ and $\boldsymbol{\omega} = [p, q, r]^\top$ describe the linear velocity and angular velocity respectively of the body fixed origin relative to the inertial origin in $\{n\}$. Lastly, $\boldsymbol{r_g} = [x_g, y_g, z_g]^\top$ is the distance vector from the system origin (CO) to the Center of Gravity (CoG) in $\{b\}$. When CO and CoG coincide with one another, $\boldsymbol{r_g}= 0$. As is the case for the Tito-Neri model. The symbols from table 3.1 will be used in the derivation of the system matrices in the following subsections.

3.2. Kinematic Model

A kinematic model is used in order to treat the geometrical aspects of motion. $\dot{\boldsymbol{\eta}} = [\dot{x}, \dot{y}, \dot{\psi}]^T$ describes the inertial frame velocities and $\boldsymbol{\nu} = [u, v, r]^T$ the body-fixed velocities. The kinematic equation is described in the following manner:

$$\dot{\boldsymbol{\eta}} = \boldsymbol{R}(\psi)\boldsymbol{\nu} \tag{3.1}$$

$\boldsymbol{R}(\psi)$ is the transformation matrix for rotation about the z axis in order to transform from the body-fixed frame to the inertial frame and vice versa.

$$\boldsymbol{R}(\psi) = \begin{bmatrix} \cos(\psi) & -\sin(\psi) & 0 \\ \sin(\psi) & \cos(\psi) & 0 \\ 0 & 0 & 1 \end{bmatrix} \tag{3.2}$$

3.3. Kinetic Model

Kinetics deals with the analysis of the forces that are causing the motion. The rigid body kinetics of marine craft can be expressed in the following vectorial setting.

$$\boldsymbol{M}_{RB}\dot{\boldsymbol{\nu}} + \boldsymbol{C}_{RB}(\boldsymbol{\nu})\boldsymbol{\nu} = \boldsymbol{\tau}_{RB} \tag{3.3}$$

where $\boldsymbol{M}_{RB}$ is the rigid-body mass matrix and $\boldsymbol{C}_{RB}$ is the rigid-body Coriolis and centripetal matrix due to the rotation of the body $\{b\}$ about the inertial frame $\{n\}$. In 3 DOF it gives the following, $\boldsymbol{\nu} = [u, v, r]^\top$ and $\boldsymbol{\tau_{RB}} = [X, Y, N]^\top$. The kinetics provided above can be further elaborated upon by introducing hydrodynamics and hydrostatics. This leads to equation 3.4.

$$\underbrace{\boldsymbol{M_{RB}}\dot{\boldsymbol{\nu}} + \boldsymbol{C_{RB}}(\boldsymbol{\nu})\boldsymbol{\nu}}_{\text{rigid-body forces}} + \underbrace{\boldsymbol{M_A}\dot{\boldsymbol{\nu}}_{\boldsymbol{r}} + \boldsymbol{C_A}\left(\boldsymbol{\nu}_{\boldsymbol{r}}\right)\boldsymbol{\nu}_{\boldsymbol{r}} + \boldsymbol{D}\left(\boldsymbol{\nu}_{\boldsymbol{r}}\right)\boldsymbol{\nu}_{\boldsymbol{r}}}_{\text{hydrodynamic forces}} + \underbrace{\boldsymbol{g}(\boldsymbol{\eta}) + \boldsymbol{g_o}}_{\text{hydrostatic forces}} = \boldsymbol{\tau} \tag{3.4}$$

where $\boldsymbol{M}= \boldsymbol{M}_{RB} +\boldsymbol{M}_A$ is the system inertia matrix, which now also includes added mass $\boldsymbol{M}_A$. The Coriolis-Centripetal matrix including the added mass is $\boldsymbol{C}(\boldsymbol{\nu_r}) = \boldsymbol{C_{RB}}(\boldsymbol{\nu_r}) + \boldsymbol{C_A}(\boldsymbol{\nu_r})$ and $\boldsymbol{D}$ is the hydrodynamic damping matrix. This added mass is induced due to the body accelerating or decelerating, which moves some volume of the surrounding fluid. This is modeled as some additional mass moving along with the body [55]. The relative velocity vector is denoted by $\boldsymbol{\nu_r}$ (without the current velocity).

$\boldsymbol{g(\eta)}$ is the vector of gravitational/buoyancy forces and moments. $\boldsymbol{g_o}$ is the vector that is used for ballast control. Lastly, $\boldsymbol{\tau}$ is the vector of control inputs.

3.3.1. System Inertia Mass Matrix

As stated in the previous section $\boldsymbol{M = M_{RB} + M_A}$. Firstly, the added mass matrix $\boldsymbol{M_A}$ due to fluid displacement is defined, which gives the following according to [18, 56].

$$M_A = -\begin{bmatrix} X_{\dot{u}} & X_{\dot{v}} & X_{\dot{w}} & X_{\dot{p}} & X_{\dot{q}} & X_{\dot{r}} \\ Y_{\dot{u}} & Y_{\dot{v}} & Y_{\dot{w}} & Y_{\dot{p}} & Y_{\dot{q}} & Y_{\dot{r}} \\ Z_{\dot{u}} & Z_{\dot{v}} & Z_{\dot{w}} & Z_{\dot{p}} & Z_{\dot{q}} & Z_{\dot{r}} \\ K_{\dot{u}} & K_{\dot{v}} & K_{\dot{w}} & K_{\dot{p}} & K_{\dot{q}} & K_{\dot{r}} \\ M_{\dot{u}} & M_{\dot{v}} & M_{\dot{w}} & M_{\dot{p}} & M_{\dot{q}} & M_{\dot{r}} \\ N_{\dot{u}} & N_{\dot{v}} & N_{\dot{w}} & N_{\dot{p}} & N_{\dot{q}} & N_{\dot{r}} \end{bmatrix} \tag{3.5}$$

It uses the SNAME (1950) notation for hydrodynamic derivatives. For example, the increased mass force Y along the y axis due to an acceleration $\dot{u}$ in the x direction is expressed as:

$$Y = -Y_{\dot{u}}\dot{u}, \quad Y_{\dot{u}} := \frac{\partial Y}{\partial \dot{u}} \tag{3.6}$$

This then implies $\{M_A\}_{21} = -Y_{\dot{u}}$ in equation 3.5. The 3DOF simplification will be used since only surge, sway and yaw are considered. Thus, only the intersections of the first, second and sixth rows and columns in equation 3.5 will be used. This leads to the following:

$$\boldsymbol{M}_A = \begin{bmatrix} -X_{\dot{u}} & 0 & 0 \\ 0 & -Y_{\dot{v}} & -Y_{\dot{r}} \\ 0 & -N_{\dot{v}} & -N_{\dot{r}} \end{bmatrix} \tag{3.7}$$

Next is the mass matrix that encompasses the rigid body mass. This matrix is denoted as $\boldsymbol{M_{RB}}$ and is shown below.

$$\boldsymbol{M}_{RB} = \begin{bmatrix} m\boldsymbol{I}_{3\times 3} & -m\boldsymbol{S}(\boldsymbol{r}_g) \\ m\boldsymbol{S}(\boldsymbol{r}_g) & \boldsymbol{I_b} \end{bmatrix} \tag{3.8}$$

where $I_{3\times 3}$ is defined as the identity matrix. $\boldsymbol{S}$ is the vector cross product and is also skew-symmetric. $\boldsymbol{I_b}$ is the inertia matrix of the body.

$$\boldsymbol{S}(\boldsymbol{r_g}) = \begin{bmatrix} 0 & -z_g & y_g \\ z_g & 0 & -x_g \\ -y_g & x_g & 0 \end{bmatrix} \tag{3.9}$$

$$\boldsymbol{I}_b := \begin{bmatrix} I_x & -I_{xy} & -I_{xz} \\ -I_{yz} & I_y & -I_{yz} \\ -I_{zx} & -I_{zy} & I_z \end{bmatrix} \tag{3.10}$$

This gives the following 6x6 matrix for the rigid body mass.

$$\boldsymbol{M}_{RB} = \begin{bmatrix} m & 0 & 0 & 0 & mz_g & -my_g \\ 0 & m & 0 & -mz_g & 0 & -mx_g \\ 0 & 0 & m & my_g & mx_g & 0 \\ 0 & -mz_g & my_g & I_x & -I_{xy} & -I_{xz} \\ mz_g & 0 & -mx_g & -I_{xy} & I_y & -I_{yz} \\ -my_g & mx_g & 0 & -I_{xz} & -I_{yz} & I_z \end{bmatrix} \tag{3.11}$$

Again only taking into account surge, sway and yaw will give the following 3x3 matrix.

$$\boldsymbol{M}_{RB} = \begin{bmatrix} m & 0 & 0 \\ 0 & m & mx_g \\ 0 & mx_g & I_z \end{bmatrix} \tag{3.12}$$

For when $CO = COG$, $x_g = 0$ and $\boldsymbol{M}_{RB}$ becomes:

$$M_{RB} = \begin{bmatrix} m & 0 & 0 \\ 0 & m & 0 \\ 0 & 0 & I_z \end{bmatrix} \tag{3.13}$$

The combined mass matrix $\boldsymbol{M} = \boldsymbol{M}_{RB} + \boldsymbol{M}_A$ thus becomes the following.

$$\boldsymbol{M} = \begin{bmatrix} m - X_{\dot{u}} & 0 & 0 \\ 0 & m - Y_{\dot{v}} & mx_g - Y_{\dot{r}} \\ 0 & mx_g - N_{\dot{v}} & I_z - N_{\dot{r}} \end{bmatrix} \tag{3.14}$$

3.3.2. Coriolis-Centripetal Matrix

The Coriolis-Centripetal terms occur due to the rotation of $\{b\}$ with respect to $\{n\}$. Similarly to the inertia mass matrix, rigid body and added mass terms can be found in it according to:

$$\boldsymbol{C}(\boldsymbol{\nu}) = \boldsymbol{C_{RB}}(\boldsymbol{\nu}) + \boldsymbol{C_A}(\boldsymbol{\nu}) \tag{3.15}$$

The Coriolis vector is $\omega \times \nu$ and the centripetal term is $\omega \times (\omega \times \nu)$. The Coriolis-Centripetal matrix will, similarly to the mass matrix, be derived from the 6x6 matrix to a 3x3 matrix [18, 56]. Firstly, the mass matrix is shown with its rigid body mass part.

$$\boldsymbol{M} = \boldsymbol{M}^T = \begin{bmatrix} \boldsymbol{M}_{11} & \boldsymbol{M}_{12} \\ \boldsymbol{M}_{21} & \boldsymbol{M}_{22} \end{bmatrix} \tag{3.16}$$

$$\boldsymbol{C}_{RB}(\boldsymbol{\nu}) = \begin{bmatrix} 0_{3\times 3} & -S\left(M_{11}v^b_{b/n} + M_{12}\omega^b_{b/n}\right) \\ -S\left(M_{11}\boldsymbol{v^b_{b/n}} + M_{12}\boldsymbol{\omega^b_{b/n}}\right) & -S\left(M_{21}v^b_{b/n} + M_{22}\omega^b_{b/n}\right) \end{bmatrix} \tag{3.17}$$

For the rigid body part $\boldsymbol{C_{RB}}$ of the Coriolis-Centripetal matrix it gives the following:

$$\boldsymbol{C}_{RB}(\boldsymbol{\nu}) = \begin{bmatrix} 0 & 0 & 0 \\ 0 & 0 & 0 \\ 0 & 0 & 0 \\ -m(y_g q + z_g r) & m(y_g p + w) & m(z_g p - v) \\ m(x_g q - w) & -m(z_g r + x_G p) & m(z_g q + u) \\ m(x_g r + v) & m(y_g r - u) & -m(x_g p + y_g q) \end{bmatrix} \begin{bmatrix} m(y_g q + z_g r) & -m(x_g q - w) & -m(x_g r + v) \\ -m(y_g p + w) & m(z_g r + x_g p) & -m(y_g r - u) \\ -mz_g p - v & -mz_g q - u & mx_g p + y_g q \\ 0 & -I_{yz}q - I_{xz}p + I_z r & I_{yz}r + I_{xy}p - I_y q \\ I_{yz}q + I_{xz}p - I_z r & 0 & -I_{xz}r - I_{xy}q + I_x p \\ -I_{yz}r - I_{xy}p + I_y q & I_{xz}r + I_{xy}q - I_x p & 0 \end{bmatrix} \tag{3.18}$$

By reducing this matrix to a 3x3 matrix, only taking into account surge, sway and yaw, the following matrix can be obtained.

$$\boldsymbol{C}_{RB}(\boldsymbol{\nu}) = \begin{bmatrix} 0 & 0 & -m\left(x_g r + v\right) \\ 0 & 0 & mu \\ m\left(x_g r + v\right) & -mu & 0 \end{bmatrix} \tag{3.19}$$

Next will be the added mass term $\boldsymbol{C_A}$. Similarly to the previous derivation of C_{RB}, the added mass part of the mass matrix can now be used. This will give the following 6x6 added mass matrix.

$$\boldsymbol{C}_A(\boldsymbol{\nu}) = \begin{bmatrix} 0 & 0 & 0 & 0 & C_A^{15} & C_A^{16} \\ 0 & 0 & 0 & C_A^{24} & 0 & C_A^{26} \\ 0 & 0 & 0 & C_A^{34} & C_A^{35} & 0 \\ 0 & -C_A^{24} & -C_A^{34} & 0 & C_A^{45} & C_A^{46} \\ -C_A^{15} & 0 & -C_A^{35} & -C_A^{45} & 0 & C_A^{56} \\ -C_A^{16} & -C_A^{26} & 0 & -C_A^{46} & -C_A^{56} & 0 \end{bmatrix} \tag{3.20}$$

where

$$
\begin{aligned}
C_A^{15} &= -X_{\dot{w}}u - Y_{\dot{w}}v - Z_{\dot{w}}w - Z_{\dot{p}}p - Z_{\dot{q}}q - Z_{\dot{r}}r \\
C_A^{35} &= X_{\dot{u}}u + X_{\dot{v}}v + X_{\dot{w}}w + X_{\dot{p}}p + X_{\dot{q}}q + X_{\dot{r}}r \\
C_A^{16} &= X_{\dot{v}}u + Y_{\dot{v}}v + Y_{\dot{w}}w + Y_{\dot{p}}p + Y_{\dot{q}}q + Y_{\dot{r}}r \\
C_A^{45} &= -X_{\dot{r}}u - Y_{\dot{r}}v - Z_{\dot{r}}w - K_{\dot{r}}p - M_{\dot{r}}q - N_{\dot{r}}r \\
C_A^{24} &= X_{\dot{w}}u + Y_{\dot{w}}v + Z_{\dot{w}}w + Z_{\dot{p}}p + Z_{\dot{q}}q + Z_{\dot{r}}r \\
C_A^{46} &= X_{\dot{q}}u + Y_{\dot{q}}v + Z_{\dot{q}}w + K_{\dot{q}}p + M_{\dot{q}}q + M_{\dot{r}}r \\
C_A^{26} &= -X_{\dot{u}}u - X_{\dot{v}}v - X_{\dot{w}}w - X_{\dot{p}}p - X_{\dot{q}}q - X_{\dot{r}}r \\
C_A^{56} &= -X_{\dot{p}}u - Y_{\dot{p}}v - Z_{\dot{p}}w - K_{\dot{p}}p - K_{\dot{q}}q - K_{\dot{r}}r \\
C_A^{34} &= -X_{\dot{v}}u - Y_{\dot{v}}v - Y_{\dot{w}}w - Y_{\dot{p}}p - Y_{\dot{q}}q - Y_{\dot{r}}r
\end{aligned}
$$

Again by only taking into account surge, sway and yaw, the 3x3 added mass Coriolis-centripetal matrix becomes the following:

$$
\boldsymbol{C_A}(\boldsymbol{\nu}) = \begin{bmatrix} 0 & 0 & Y_{\dot{v}}v + Y_{\dot{r}}r \\ 0 & 0 & -X_{\dot{u}}u \\ -Y_{\dot{v}}v - Y_{\dot{r}}r & X_{\dot{u}}u & 0 \end{bmatrix} \tag{3.21}
$$

Combined, the Coriolis-Centripetal matrix becomes:

$$
\boldsymbol{C}(\boldsymbol{\nu}) = \begin{bmatrix} 0 & 0 & -m\left(x_g r + v\right) + Y_{\dot{v}}v + Y_{\dot{r}}r \\ 0 & 0 & -X_{\dot{u}}u + mu \\ m\left(x_g r + v\right) - Y_{\dot{v}}v - Y_{\dot{r}}r & -mu + X_{\dot{u}}u & 0 \end{bmatrix} \tag{3.22}
$$

3.3.3. Hydrodynamic Damping

When moving through a fluid, the vessel experiences hydrodynamic damping through drag forces. The hydrodynamic damping consists of a linear and nonlinear part. Both are provided below according to [18]. The total hydrodynamic damping matrix $\boldsymbol{D}(\boldsymbol{\nu_r})$ is the sum of the linear part $\boldsymbol{D_l}$ and the nonlinear part $\boldsymbol{D_n}(\boldsymbol{\nu_r})$ such that:

$$
\boldsymbol{D}\left(\boldsymbol{v}_r\right) := \boldsymbol{D_l} + \boldsymbol{D}_n\left(\boldsymbol{v}_r\right) \tag{3.23}
$$

Figure 3.2 shows the linear and quadratic terms for different speeds of a vessel. To avoid oscillatory behavior at low speeds, models should contain both linear and quadratic damping. The major reason is that linear damping is required for exponential convergence to zero [18].

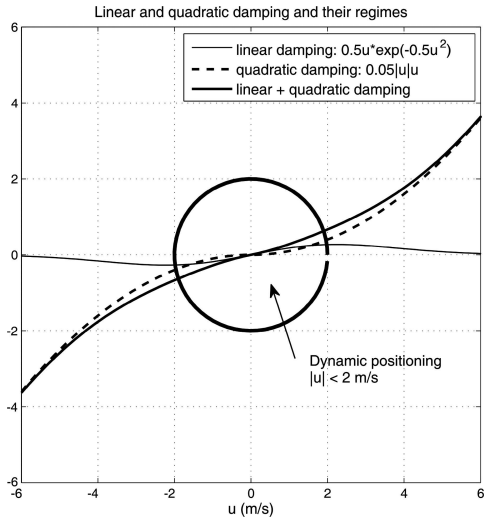

Figure 3.2: Linear and quadratic damping with their speed regimes [18]

The 6x6 matrices for the hydrodynamic damping are given below for the linear and nonlinear parts. The coefficients are called hydrodynamic derivatives.

$$\boldsymbol{D_l} = -\begin{bmatrix} X_u & 0 & 0 & 0 & 0 & 0 \\ 0 & Y_v & 0 & Y_p & 0 & Y_r \\ 0 & 0 & Z_w & 0 & Z_q & 0 \\ 0 & K_v & 0 & K_p & 0 & K_r \\ 0 & 0 & M_w & 0 & M_q & 0 \\ 0 & N_v & 0 & N_p & 0 & N_r \end{bmatrix} \tag{3.24}$$

$$\boldsymbol{D}_n\left(\boldsymbol{v}_r\right) = -\begin{bmatrix} X_{|u|u}\left|u_r\right| & 0 & 0 & 0 & 0 & 0 \\ 0 & Y_{|v|v}\left|v_r\right| + Y_{|r|v}|r| & 0 & 0 & 0 & Y_{|v|r}\left|v_r\right| + Y_{|r|r}|r| \\ 0 & 0 & Z_{|w|w}\left|w_r\right| & 0 & 0 & 0 \\ 0 & 0 & 0 & K_{|p|p}|p| & 0 & 0 \\ 0 & 0 & 0 & 0 & M_{|q|q}|q| & 0 \\ 0 & N_{|v|v}\left|v_r\right| + N_{|r|v}|r| & 0 & 0 & 0 & N_{|v|r}\left|v_r\right| + N_{|r|r}|r| \end{bmatrix} \tag{3.25}$$

Only taking surge sway and yaw into account gives the following 3x3 matrices for the linear and nonlinear damping.

$$\boldsymbol{D}_l = \begin{bmatrix} -X_u & 0 & 0 \\ 0 & -Y_v & -Y_r \\ 0 & -N_v & -N_r \end{bmatrix} \tag{3.26}$$

$$\boldsymbol{D}_n\left(\boldsymbol{v}_r\right) = \begin{bmatrix} -X_{|u|u}\left|u_r\right| & 0 & 0 \\ 0 & -Y_{|v|v}\left|v_r\right| & -Y_{|v|r}\left|v_r\right| \\ 0 & -N_{|v|v}\left|v_r\right| & -N_{|v|r}\left|v_r\right| \end{bmatrix} \tag{3.27}$$

3.4. Actuation and Thruster Allocation (TA)

There are several possible options with regard to actuation, these are given in table 3.2 according to [18].

Table 3.2: Actuators and control variables [18]

Actuator	**u (control input)**	α **(control input)**	$f^\top$ **(force vector)**
Main propellers (longitudinal)	Pitch and rpm	-	[$\boldsymbol{F}$, 0, 0]
Tunnel thrusters (transverse)	Pitch and rpm	-	[0, F, 0]
Azimuth (rotatable) thruster	Pitch and rpm	Angle	[F cos (α), F sin (α), 0]
Aft rudders	Angle	-	[0, F, 0]
Stabilizing fins	Angle	-	[0, 0, F]

The control forces and moments $\boldsymbol{f}$ are expressed as

$$\boldsymbol{f} = \boldsymbol{K}\boldsymbol{u} \tag{3.28}$$

where $\boldsymbol{u}$ is the vector of control inputs and $\boldsymbol{K}$ is a diagonal force coefficient matrix. The actuator forces and moments are related to the control forces and moments with the following:

$$\boldsymbol{\tau} = \boldsymbol{T}(\boldsymbol{\alpha})\boldsymbol{f} = \boldsymbol{T}(\boldsymbol{\alpha})\boldsymbol{K}\boldsymbol{u} \tag{3.29}$$

where $\boldsymbol{\alpha}$ is a vector of the azimuth angles and $\boldsymbol{T}(\boldsymbol{\alpha})$ is the thrust configuration matrix. The following configuration from figure 3.3 will be used going forward.

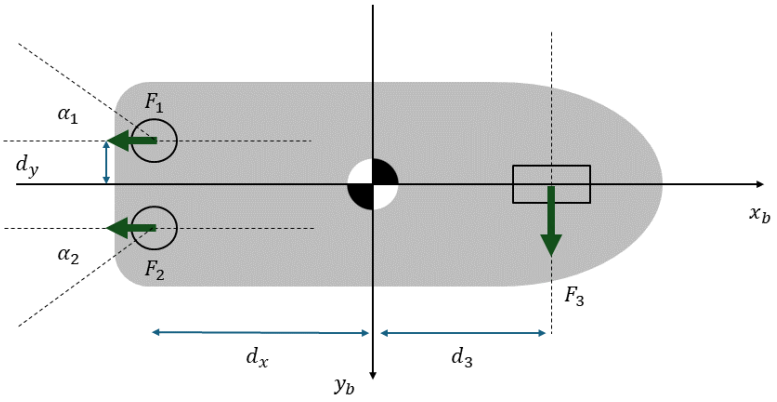

Figure 3.3: Thruster configuration with 2 azimuth and 1 bow thruster

For the 2 azimuth thrusters and a bow thruster the thrust configuration matrix becomes the following.

$$\boldsymbol{\tau} = \boldsymbol{T}(\boldsymbol{\alpha})\boldsymbol{f} = \begin{bmatrix} \cos(\alpha_1) & \cos(\alpha_2) & 0 \\ \sin(\alpha_1) & \sin(\alpha_2) & 1 \\ d_y \cdot \cos(\alpha_1) - d_x \cdot \sin(\alpha_1) & d_y \cdot \cos(\alpha_2) - d_x \cdot \sin(\alpha_2) & d_3 \end{bmatrix} \begin{bmatrix} F_1 \\ F_2 \\ F_3 \end{bmatrix} \tag{3.30}$$

The hydrodynamic interaction of a thruster in the process of propulsion will affect the control of the ship [57]. Determining the orientations and thrust of the provided actuators, given different constraints, is needed. This is commonly known as the TA problem. TA is a vital component of autonomous vessel motion control [58]. In order to achieve this, a thrust allocation algorithm can be used. It is an algorithm that takes an order for the total force and moment that the thrusters should enact on a ship as input and calculates what forces the individual thrusters should produce so that the resultant force and moment on the ship are as instructed [51].

3.5. Parametrized Tito-Neri model

Based on the previous sections, the mathematical model of the ship can now be simplified for the application of trajectory tracking, DP and mooring and unmooring. A linearized model will be used for the Tito-Neri. This simplification is based on the operational condition of the vessel being $u >> v, r$. The kinematic model and simplified kinetic model are shown below.

$$\dot{\boldsymbol{\eta}} = \boldsymbol{R}(\psi)\boldsymbol{\nu} \tag{3.31}$$

$$\boldsymbol{M}\dot{\boldsymbol{\nu}} + \boldsymbol{D}\boldsymbol{\nu} = \boldsymbol{\tau} \tag{3.32}$$

where

$$\boldsymbol{\tau} = \boldsymbol{T}(\boldsymbol{\alpha})\boldsymbol{f} \tag{3.33}$$

The parameters for the Tito-Neri model scale vessel are given according to [59].

Table 3.3: Tito-Neri parameters [59, 60]

Parameters	Value	Unit
m	16.9	kg
$Y_{\dot{v}}$	-49.2	kg
x_g	0.0	m
$Y_{\dot{r}}$	0.0	$kg \cdot m^2$
I_z	0.51	$kg \cdot m^2$
$N_{\dot{v}}$	0.0	kg
$X_{\dot{u}}$	-1.2	kg
$N_{\dot{r}}$	-1.8	$kg \cdot m^2$

This leads to the following system matrices:

$$\boldsymbol{M} = \begin{bmatrix} m - X_{\dot{u}} & 0 & 0 \\ 0 & m - Y_{\dot{v}} & mx_g - Y_{\dot{r}} \\ 0 & mx_g - N_{\dot{r}} & I_z - N_{\dot{r}} \end{bmatrix} = \begin{bmatrix} 18.1 & 0 & 0 \\ 0 & 66.1 & 0 \\ 0 & 0 & 2.31 \end{bmatrix} \tag{3.34}$$

$$\boldsymbol{D}_l = \begin{bmatrix} -X_u & 0 & 0 \\ 0 & -Y_v & -Y_r \\ 0 & -N_v & -N_r \end{bmatrix} = \begin{bmatrix} 0.72253 & 0 & 0 \\ 0 & 0.88965 & 0 \\ 0 & 0 & 1.90 \end{bmatrix} \tag{3.35}$$

For the allocation of the thrust, a fixed configuration is used. The angle for the portside thruster is denoted with ψ_{PS} and the angle for the starboard thruster is denoted as ψ_{SB}. Both angles will be fixed at $-\pi/4$ and $\pi/4$ respectively. This is a middle ground in order to cover simple and relatively complex maneuvers. The length from the origin to each thruster in x is denoted with d. The thrusters can be seen schematically in figure 3.4.

$$\boldsymbol{\tau} = \begin{bmatrix} \cos(\psi_{PS}) & \cos(\psi_{SB}) & 0 \\ \sin(\psi_{PS}) & \sin(\psi_{SB}) & 1 \\ d_y \cdot \cos(\psi_{PS}) - d_x \cdot \sin(\psi_{PS}) & d_y \cdot \cos(\psi_{SB}) - d_x \cdot \sin(\psi_{SB}) & d_{bow} \end{bmatrix} \begin{bmatrix} F_{PS} \\ F_{SB} \\ F_{bow} \end{bmatrix} = \begin{bmatrix} F_x \\ F_y \\ M \end{bmatrix} \tag{3.36}$$

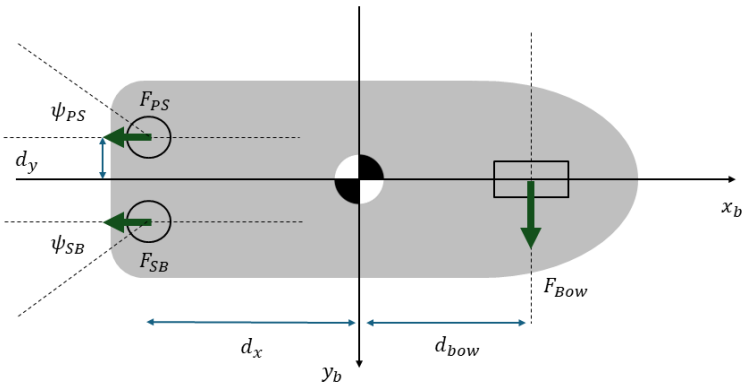

Figure 3.4: Thruster configuration of the Tito-Neri

3.6. Conclusion

In this section, the following sub-question was answered: **What is an applicable mathematical model for the model scale vessel?** The mathematical ship model for control applications was provided in terms of the kinetics and kinematics. The mathematical model used going forward will be a simplification of the model by making use of $u >> v, r$. This study will now move towards selecting and appropriate control strategy that will make use of the mathematical model for the unmooring, trajectory tracking and mooring.

4

Control Strategy

This chapter answers the sub-question: **What is the best control strategy to be selected for the application and how to design it?** First in section 4.1 the requirements and criteria for the application will be explored. Then in section 4.2, the possible control strategies are briefly discussed and a selection will be made in section 4.3. This selection will then be elaborated upon in section 4.4 and onward. This in-depth definition includes the prediction model in section 4.5, the control objective in section 4.6 and the control constraints in section 4.7. Lastly, in section 4.8, the algorithms that will be used in the implementation will be shown.

4.1. Requirements and criteria

To be able to choose the best control strategy for the application, first the requirements for the application need to be specified. The goal of the research is to design a control strategy that is capable of controlling the vessel with the actuator input. This will be used for unmooring, trajectory tracking and mooring for the small-scale vessel (Tito-Neri). A closed-loop control system is a system with one or several feedback control loops, often involving interaction between control loops, as can be seen in figure 4.1 [61]. In this loop, the reference and output will be the position that needs to follow. The system inputs are the forces applied to the system. The system itself will consist of the vessel dynamics which are provided in chapter 3. The sensor dynamics (e.g. navigation) will not be taken into account.

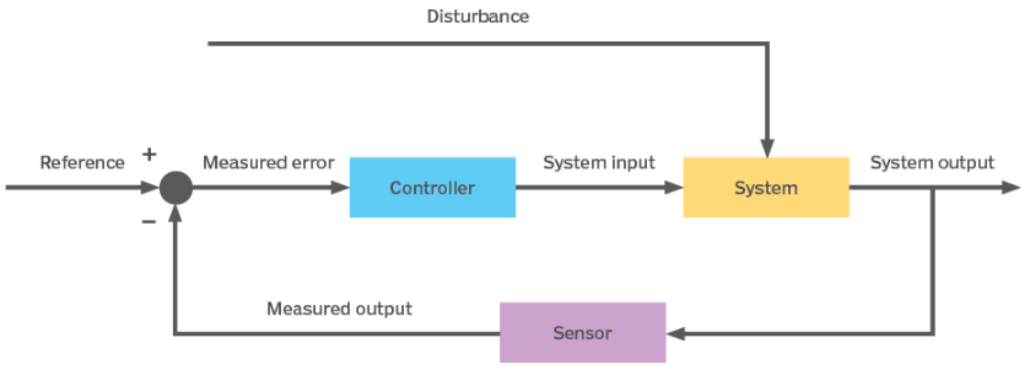

Figure 4.1: General control loop [62]

The initial mathematical model that is derived in chapter 3 is nonlinear. This is due to the Coriolis-Centripetal and nonlinear damping matrix. For the application of mooring and unmooring (low speeds) combined with trajectory tracking, the assumption of linearization will be made. Therefore, the controller does not need to be able to account for non-linearities. For the trajectory tracking and also mooring and unmooring, there are multiple inputs into the system. These consist of the vessel states that describe

the position in x and y and the orientation ψ. The output of the controller consists of the forces or rather actuator inputs into the system. Thus, the system is MIMO [63]. Certain control methods or strategies can handle MIMO systems, whilst others can only handle Single-Input Single-Output (SISO) systems. Every mechanical system also has physical limitations. These limitations are enforced on the system through constraints. Constraints can also be applied in order to avoid excessive wear and tear of the system. The constraints for instance are limitations of the acceleration or maximum forces that can be applied [64]. Not all control strategies will be able to handle (complex) constraints. In addition, from the perspective of logistics, it is beneficial to make predictions regarding disturbances and the arrival time of the vessel. It can therefore be important to be able to simulate the future behavior of the system. This would allow for maneuvers being able to be planned ahead [51] Lastly, control strategies for mooring and trajectory tracking have varying computing complexity depending on the algorithms used, model complexity, real-time needs, and available computer resources [65].

The four criteria to be used in the selection will thus be the controller's ability to handle MIMO systems, control constraints, future behavior and the computational complexity of the strategy.

4.2. Control algorithms

To select a suitable control strategy for mooring and unmooring an overview of each of the relevant ones will be provided. The controllers for trajectory tracking and also DP have evolved during the last three decades. The first innovations can be observed in Proportional Integral Derivative (PID) controllers. A PID controller's three terms satisfy three typical needs of most control issues. In tracking a constant setpoint, the integral term yields zero steady-state error. The proportional term, on the other hand, responds instantly to the present error but often cannot attain the required setpoint precision without an excessively large gain [66].

Optimal control determines the control signals that will cause a process to satisfy constraints and at the same time minimize (or maximize) some performance criterion. The optimal control problem uses a mathematical model of the process to be controlled, physical constraints and a specification of the objective (performance) [67]. Examples of optimal control include Linear Quadratic Regulator (LQR) and Model Predictive Control (MPC) [31].

Next is Nonlinear Time-Invariant Control. Examples of this are Sliding Mode Control (SMC) and Backstepping Control. Since the system used will be linearized, these control strategies will not be taken into account. Introducing nonlinearities into the model only increases the computational burden of the control algorithm, since a linearized system is sufficient for the application [31].

The primary idea behind adaptive control is to estimate unknown parameters live, using known system conditions. The primary goal of robust control is to maintain stability and acceptable performance despite changes in parameters, modeling mistakes, disruptions, and external uncertainties. Combining adaptive control and/or robust control with other control methods will result in better control schemes [31]. According to the operating regimes, hybrid control allows for switching between different controllers. In autonomous shipping, hybrid control refers to the use of both continuous control and discrete control systems to handle various parts of the ship's operations [68].

Intelligent control uses AI and computational intelligence in order to handle complex, nonlinear and also uncertain dynamics. It offers potential, but also presents challenges in the realm of robustness and the need for sufficient data. Examples are Fuzzy Control and Neural Network (NN) Control. Fuzzy Control is based on the operator's manual control strategy or Fuzzy Information that the designer knows about the operation. This can also be combined with other control strategies. A neural network (NN) is a collection of neurons or nodes with configurable connection weights that can achieve great results in trajectory tracking of vessels. It however lacks interpretability since it operates as a black-box model [31].

4.3. Selection of control strategy

Given the information provided on the different control strategies, the best control strategy can be chosen for the application. First, this will be looked at qualitatively in table 4.1.

Table 4.1: Comparison of control strategies

Criteria	PID	LQR	MPC	Hybrid Control	Fuzzy Control	NN Control
MIMO	Yes [1]	Yes	Yes	Yes	Yes	Yes
Constraints	Limited	Limited	Explicit	Flexible	Explicit	Explicit
Comp. complexity	Low	Low	Moderate	Moderate	Moderate	Moderate
Future behavior	No	No	Yes	Limited	Limited	Limited

With the qualitative data, a weighted decision matrix will now be introduced to select the best control strategy for the application (table 4.2). Each of the relevant criteria has weights assigned to them ranging from 1 to 5 based on section 4.1 with 1 being the lowest score and 5 the highest. The control strategies will receive a value ranging from 1 to 5 as well. This will be multiplied by the criteria weight to get a weighted rating. The highest weighted rating becomes the chosen control strategy.

Table 4.2: Weighted decision matrix control strategies

		PID		LQR		MPC		Hybrid		Fuzzy		NN	
Criteria	*Weights*	*Score*	*Total*	*Score*	*Total*	*Score*	*Total*	*Score*	*Total*	*Score*	*Total*	*Score*	*Total*
MIMO	3	3	**9**	5	**15**	5	**15**	5	**15**	5	**15**	5	**15**
Control Constraints	4	2	**8**	2	**8**	3	**12**	3	**12**	5	**20**	5	**20**
Comp. Complexity	2	5	**10**	5	**10**	3	**6**	3	**6**	3	**6**	3	**6**
Future behavior	5	1	**5**	1	**5**	5	**25**	2	**10**	2	**10**	2	**10**
			32		**38**		**66**		**43**		**51**		**51**

The control strategy with the highest score that is best suited for the application of trajectory tracking and autonomous mooring and unmooring will be MPC. The simulation of the future behavior of the system and controlling will provide a control output. This allows for the system to behave optimally [51]. MPC has certain advantages over the other control strategies shown in table 4.2. These advantages are the following [51, 70]:

- **Constraint handling:** Effective handling of constraints by incorporating it directly into the optimization problem. MPC can increase overall system performance by implementing limits that avoid harmful operating conditions.
- **Plan ahead:** Its main advantage and reason for being chosen as the best control strategy for the application is its ability to plan ahead. Accounting for future states and optimizing the control actions over a large time horizon will lead to better tracking. By optimizing control actions based on future predictions, MPC can improve stability, efficiency, and responsiveness.

4.4. Model Predictive Control (MPC)

The chosen control strategy for trajectory tracking and mooring and unmooring will be MPC. The block diagram is shown in figure 4.2. Compared to the standard control loop shown in figure 4.3, the controller in this loop consists of the model and an optimizer.

[1] Decoupling can be employed to make it possible to design separate PID controllers for each decoupled loop [69]

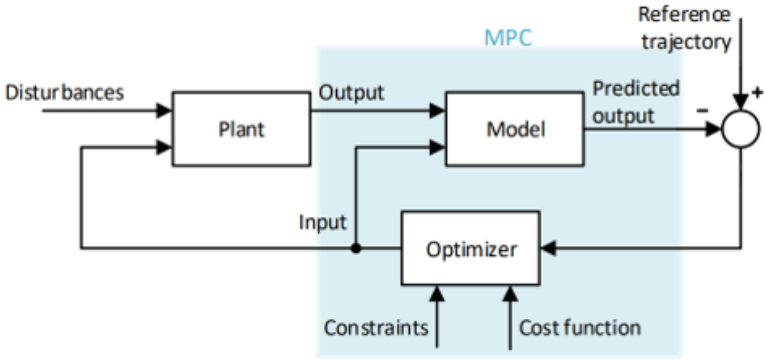

Figure 4.2: MPC block diagram [71]

MPC is also known as receding horizon control or moving horizon control. It is a control method that employs an explicit dynamic plant model to predict the effect of future reactions of the manipulated variables on the output and control signal obtained by minimizing the cost function denoted by J. A receding horizon technique in which the horizon moves forward at each instant by applying the first control signal of the sequence calculated at each step. MPC usually contains the following three points [72]:

- It uses a model to predict the process output along a future time horizon
- Calculating a control sequence to optimize a performance index
- A receding horizon approach, in which the horizon is shifted forward at each moment by applying the first control signal of the sequence calculated at each step.

An overview of the control strategy can be seen in figure 4.3. The measured and predicted output, the reference trajectory and the past and predicted control input can be observed. The controller will take the system's sensed state and create an optimal control plan based on the cost function J defined in the model.

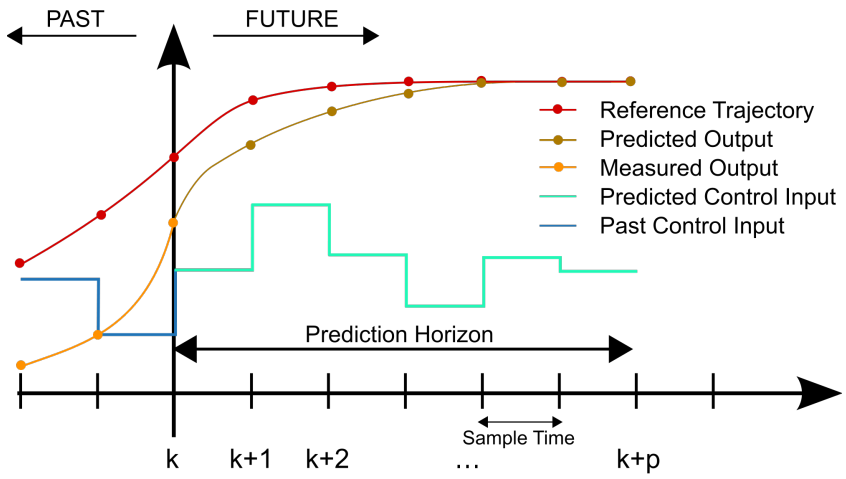

Figure 4.3: MPC overview [73]

The prediction model is shown below in state-space equations. The states of the model will be the position and orientation $\boldsymbol{\eta} = [x, y, \psi]^\top$, and the velocities $\boldsymbol{\nu} = [u, v, r]^\top$. These can both be combined to become the state vector $\boldsymbol{x}(t) = [x, y, \psi, u, v, r]^\top$. The input is described with $\boldsymbol{u}(t)$ which encompasses the thrust. The function $\boldsymbol{f}(\boldsymbol{x}(t), \boldsymbol{u}(t))$ will follow from the kinematics and kinetics. The output will be part of the states (motion in x, y and rotation about z).

$$\dot{\boldsymbol{x}}(t) = \boldsymbol{f}(\boldsymbol{x}(t), \boldsymbol{u}(t)) \tag{4.1}$$

$$\boldsymbol{y}(t) = g(\boldsymbol{x}(t)) \tag{4.2}$$

The equations given are in continuous-time. Continuous-time signals are discretized to perform simulations. This discretization is necessary as computers operate in discrete manners that can only handle finite sequences of inputs. The next step is the performance index J or rather the objective function. This will consist of various terms of the controller that will be optimized. Lastly, constraints are used to achieve feasible results. These follow from for instance physical limitations, e.g. thruster angle or velocity.

An overview of the approach is provided below [74, 75]. First, the control objective is shown. This is to minimize the cost function J. The underlined variables denote the predicted version of that variable.

$$\min \left\{ \sum_{i=0}^{N_p-1} J\left(\underline{y}(k+i+1), \underline{u}(k+i), x_{ref}(k+i+1)\right) \right\} \tag{4.3}$$

with N_p as the prediction horizon. The control objective is subject to the following prediction model

$$\begin{gathered} \underline{x}(k+1) = f(\underline{x}(k), \underline{u}(k), \underline{d}(k)) \\ \underline{y}(k+1) = g(\underline{x}(k+1)) \\ \vdots \\ \underline{x}\left(k+N_p\right) = f\left(\underline{x}\left(k+N_p-1\right), \underline{u}\left(k+N_p-1\right), \underline{d}\left(k+N_p-1\right)\right) \\ \underline{y}\left(k+N_p\right) = g\left(\underline{x}\left(k+N_p\right)\right) \end{gathered} \tag{4.4}$$

The operational constraints are the following

$$\begin{gathered} \boldsymbol{u}_{\text{min}} \leq \underline{u}(k) \leq \boldsymbol{u}_{\text{max}} \\ \boldsymbol{x}_{\text{min}} \leq \underline{x}(k+1) \leq \boldsymbol{x}_{\text{max}} \\ \boldsymbol{y}_{\text{min}} \leq \underline{y}(k+1) \leq \boldsymbol{y}_{\text{max}} \\ \vdots \\ \boldsymbol{u}_{\text{min}} \leq \underline{u}\left(k+N_p-1\right) \leq \boldsymbol{u}_{\text{max}} \\ \boldsymbol{x}_{\text{min}} \leq \underline{x}\left(k+N_p\right) \leq \boldsymbol{x}_{\text{max}} \\ \boldsymbol{y}_{\text{min}} \leq \underline{y}\left(k+N_p\right) \leq \boldsymbol{y}_{\text{max}} \end{gathered} \tag{4.5}$$

Lastly, the initial state and the predictions of disturbances and reference states are shown below

$$\begin{gathered} \underline{x}(k) = \boldsymbol{g^{-1}}(\boldsymbol{y}(k)) \\ \underline{d}(k), \underline{d}(k+1), \ldots, \underline{d}\left(k+N_p-1\right) \\ x_{ref}(k+1), x_{ref}(k+2), \ldots, x_{ref}\left(k+N_p-1\right) \end{gathered} \tag{4.6}$$

For an MPC controller the following steps are followed at each time step k.

1. Receive the measurements $\boldsymbol{y}(k)$
2. Determine the states $\underline{\boldsymbol{x}}(k)$ from the measurements
3. Determine the disturbances $\underline{\boldsymbol{d}}(k), ..., \underline{\boldsymbol{d}}(k+N_p-1)$ and the reference signal $x_{ref}(k+1), ..., x_{ref}(k+N_p)$
4. Solve the MPC problem to get the optimal actions $\underline{\boldsymbol{u}}(k), ..., \underline{\boldsymbol{u}}(k+N_p-1)$
5. Return the optimal actions $\underline{\boldsymbol{u}}(k)$ as $\boldsymbol{u}(k)$ to the system

An overview of the above can be seen in figure 4.4, where the predicted states and outputs are given by $\hat{x}$ and $\hat{y}$.

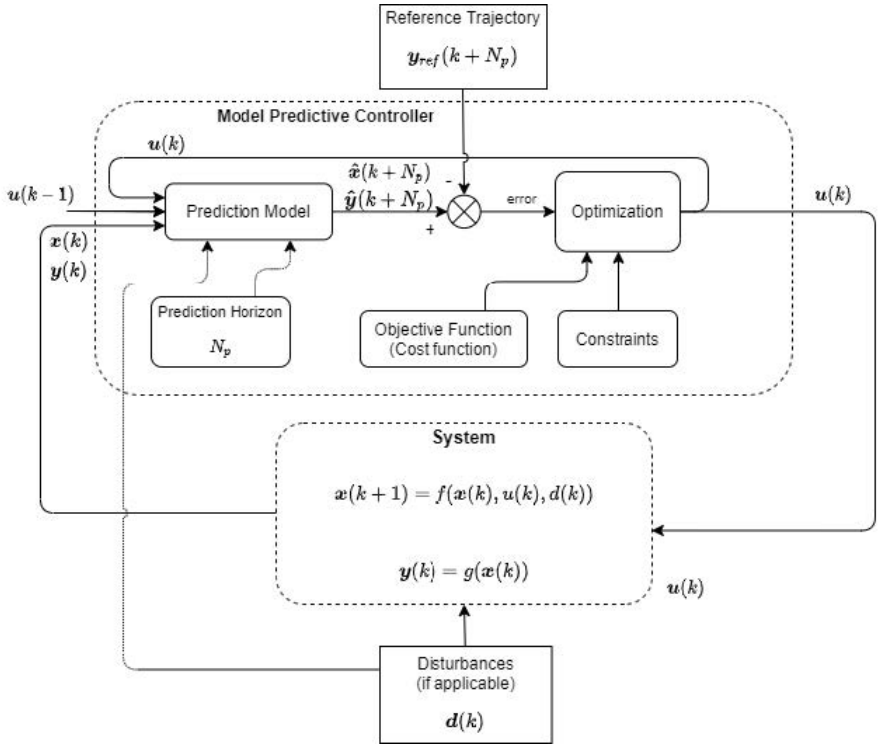

Figure 4.4: MPC structue [75]

4.5. Prediction Model

The previous section showed that the controller uses a prediction model in order to predict the future outputs of the system. In state-space form, it is again the following:

$$\dot{\boldsymbol{x}}(t) = \boldsymbol{f}(\boldsymbol{x}(t), \boldsymbol{u}(t)) \tag{4.7}$$

$$\boldsymbol{y}(t) = g(\boldsymbol{x}(t)) \tag{4.8}$$

The prediction model of the Tito-Neri vessel is derived from the kinetic and kinematic equations provided in chapter 3. The states $\boldsymbol{x}$ are the position x and y and the orientation ψ given as $\boldsymbol{\eta} = [x, y, \psi]^T$ combined with the velocities $\boldsymbol{\nu} = [u, v, r]^T$. The state vector thus becomes $\boldsymbol{x} = [x, y, \psi, u, v, r]^T$. The output vector $\boldsymbol{y}$ will be according to the control objective. This objective is to follow a desired set of coordinates and thus $\boldsymbol{y} = \boldsymbol{\eta} = [x, y, \psi]^T$. Now the continuous time state space model can be defined.

$$\boldsymbol{M}\dot{\boldsymbol{\nu}}(\boldsymbol{t}) + \boldsymbol{D}(\boldsymbol{\nu}(\boldsymbol{t}))\boldsymbol{\nu}(\boldsymbol{t}) = \boldsymbol{\tau}(\boldsymbol{t}) \tag{4.9}$$

This then becomes the following:

$$\dot{\boldsymbol{\nu}}(t) = \boldsymbol{M}^{-1}[-\boldsymbol{D}(\boldsymbol{\nu}(t))\boldsymbol{\nu}(t) + \boldsymbol{\tau}(t)] \tag{4.10}$$

Now the function $\boldsymbol{f}(t)$ can be defined. The rotation matrix from the kinematics will not be used in this prediction model as the system will be controlled locally.

$$\boldsymbol{f}(\boldsymbol{x}(t), \boldsymbol{u}(t)) = \begin{bmatrix} \boldsymbol{I}_{3x3}\boldsymbol{x}_{4:6}(t) \\ \boldsymbol{M}^{-1}\left[-\boldsymbol{D}\left(\boldsymbol{x}_{4:6}(t)\right)\boldsymbol{x}_{4:6}(t) + \boldsymbol{T}\boldsymbol{u}(t)\right] \end{bmatrix} \tag{4.11}$$

As previously mentioned, the output will be the following:

$$g(\boldsymbol{x}(t)) = \boldsymbol{x}(t) = [x(t), y(t), \psi(t), 0, 0, 0]^T \tag{4.12}$$

Simulations require the discretization of continuous-time signals. This discretization is required because computers function in a discrete form and can only process finite sequences of inputs. This will

be achieved through sampling. For staircase inputs, the Zero-Order Hold (ZOH) approach matches continuous- and discrete-time systems exactly in the time domain. The block diagram in figure 4.5 shows the ZOH discretization $H_d(z)$ of a continuous-time linear model $H(s)$ [76].

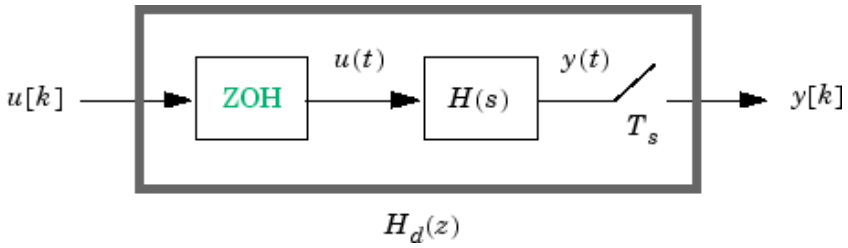

Figure 4.5: Zero-Order Hold discretization [76]

The ZOH block generates the continuous-time input signal $u(t)$ by holding each sample value $u(k)$ constant over a single sample period.

$$u(t) = u[k], \quad kT_s \leq t \leq (k+1)T_s \tag{4.13}$$

The signal $u(t)$ is the input to the continuous system $H(s)$. The output $y[k]$ is the result from sampling $y(t)$ every T_s seconds [76]. The discretized state-space model is given below:

$$\begin{aligned} \boldsymbol{x}(k+1) &= \boldsymbol{f}(\boldsymbol{x}(k), \boldsymbol{u}(k)) \\ \boldsymbol{y}(k) &= \boldsymbol{g}(\boldsymbol{x}(k)) \end{aligned} \tag{4.14}$$

4.6. Control objective

MPC solves an optimization problem, specifically a Quadratic Programming (QP) problem, at each control interval. The purpose of the application is to unmoor, track a desired trajectory and moor by following a reference signal that is defined as $\boldsymbol{y}_{ref}$. The solution of the QP problem defines the Manipulated Variables (MVs) that will be used in the plant until the next control period. The controller will be implemented using MATLAB and MATLAB Simulink. According to the MPC and optimization toolboxes [77], the total cost function is provided below.

$$J\left(z_k\right) = J_y\left(z_k\right) + J_u\left(z_k\right) + J_{\Delta u}\left(z_k\right) + J_c\left(z_k\right) \tag{4.15}$$

Here, z_k is the QP decision variable. This cost function consists of the sum of four terms. These are Output reference tracking, Manipulated Variable (MV) tracking, MV rate suppression and constraint violation.

4.6.1. Output reference tracking

First is the output reference tracking which influences the vessels output with respect to the desired reference positions. The term is given by the scalar $J_y(z_k)$ and consist of the following:

$$J_y\left(z_k\right) = \sum_{j=1}^{n_y} \sum_{i=1}^{N_p} \left\{ \frac{w_{i,j}^y}{s_j^y} \left[r_j(k+i \mid k) - y_j(k+i \mid k) \right] \right\}^2 \tag{4.16}$$

Here,

- k — Current control interval
- N_p — Prediction horizon (number of intervals)
- n_y — Number of plant output variables
- z_k — QP decision variables vector, given by:

$$z_k{}^T = \begin{bmatrix} u(k|k)^T & u(k+1|k)^T & \cdots & u(k+p-1|k)^T & \epsilon_k \end{bmatrix}.$$

- $y_j(k+i|k)$ — Predicted value of the jth plant output at the ith prediction horizon step, in engineering units
- $r_j(k+i|k)$ — Reference value for the jth plant output at the ith prediction horizon step, in engineering units
- s_{yj} — Scale factor for the jth plant output, in engineering units
- $w^y_{i,j}$ — Tuning weight for the jth plant output at the ith prediction horizon step (dimensionless)

4.6.2. MV tracking

In order to keep the MVs near a setpoint or to minimize the amount of energy that is required, MV tracking can be added to the cost function of the controller. An example would be to keep the force of the bow thruster extremely low during the act of trajectory tracking. The MV tracking is given as $J_u(z_k)$ and can be seen below.

$$J_u\left(z_k\right) = \sum_{j=1}^{n_u} \sum_{i=0}^{N_p-1} \left\{ \frac{w^u_{i,j}}{s^u_j} \left[u_j(k+i \mid k) - u_{j,target}(k+i \mid k)\right] \right\}^2 \tag{4.17}$$

Here k, N_p and z_k are the same as above. The additional variables are listed below.

- n_u — Number of manipulated variables
- $u_{j,\text{target}}(k+i|k)$ — Target value for the jth MV at the ith prediction horizon step, in engineering units
- s_{uj} — Scale factor for the jth MV, in engineering units
- $w^u_{i,j}$ — Tuning weight for the jth MV at the ith prediction horizon step (dimensionless)

4.6.3. MV rate suppression

In order to decrease the amount of perturbations of the MV, it is desired to suppress the MV rate. In most mechanical systems it is desired to have small changes. This is also applicable to the thrusters of the Tito-Neri vessel. If the thrust forces were to alternate quickly and constantly it leads to excessive mechanical wear and tear. This in turn decreases the life span of the thrusters. For the MV rate suppression, $J_{\Delta u}$ can be found below.

$$J_{\Delta u}\left(z_k\right) = \sum_{j=1}^{n_u} \sum_{i=0}^{N_p-1} \left\{ \frac{w^{\Delta u}_{i,j}}{s^u_j} \left[u_j(k+i \mid k) - u_j(k+i-1 \mid k)\right] \right\}^2 \tag{4.18}$$

Here the new variable introduced is $w^{\Delta u}_{i,j}$. This is the tuning weight for the jth MV movement at the ith prediction horizon step and is dimensionless.

4.6.4. Constraint Violation

Lastly is the violation of the constraints. It can occur that the feasible solution can only be obtained when the constraints are violated. In order to incorporate this into the QP, a slack variable can be introduced at the control interval k (ε) to make the constraints softer. ρ_ε is the weight of the penalty for constraint violation. This process is also described as Equality Cost Relaxation (ECR). The corresponding performance measure J_c can be seen below.

$$J_c\left(z_k\right) = \rho_c \varepsilon_k^2 \tag{4.19}$$

4.7. Constraints

In order to obtain a feasible solution, it is important to specifiy the constraints that are imposed on the system. The most common MPC constraints are bounds, which are given below [77].

$$\begin{aligned}
&\frac{y_{j,\min}(i)}{s_j^y} - \varepsilon_k V_{j,\min}^y(i) \leq \frac{y_j(k+i \mid k)}{s_j^y} \leq \frac{y_{j,\max}(i)}{s_j^y} + \varepsilon_k V_{j,\max}^y(i), \quad i = 1:p, \quad j = 1:n_y \\
&\frac{u_{j,\min}(i)}{s_j^u} - \varepsilon_k V_{j,\min}^u(i) \leq \frac{u_j(k+i-1 \mid k)}{s_j^u} \leq \frac{u_{j,\max}(i)}{s_j^u} + \varepsilon_k V_{j,\max}^u(i), \quad i = 1:p, \quad j = 1:n_u \\
&\frac{\Delta u_{j,\min}(i)}{s_j^u} - \varepsilon_k V_{j,\min}^{\Delta u}(i) \leq \frac{\Delta u_j(k+i-1 \mid k)}{s_j^u} \leq \frac{\Delta u_{j,\max}(i)}{s_j^u} + \varepsilon_k V_{j,\max}^{\Delta u}(i), \quad i = 1:p, \quad j = 1:n_u
\end{aligned} \tag{4.20}$$

Where,

- V - ECR values which are controller constants analogous to the cost function weights and are used for constraints softeling.
- ε — Scalar QP slack variable (dimensionless) used for constraint softening.
- s_j^y — Scale factor for jth plant output, in engineering units.
- s_j^u — Scale factor for jth MV, in engineering units.
- $y_{j,\min}(i)$, $y_{j,\max}(i)$ — Lower and upper bounds for jth plant output at ith prediction horizon step, in engineering units.
- $u_{j,\min}(i)$, $u_{j,\max}(i)$ — Lower and upper bounds for jth MV at ith prediction horizon step, in engineering units.
- $\Delta u_{j,\min}(i)$, $\Delta u_{j,\max}(i)$ — Lower and upper bounds for jth MV increment at ith prediction horizon step, in engineering units.

The constraints for the Tito-Neri model scale vessel are given according to table 4.3. These constraints consist of the forces that are applied to the vessel.

Table 4.3: Tito-Neri model scale vessel constraints

Operational constraints	**Min**	**Max**	**Rate Min**	**Rate Max**
Force from the starboard thruster F_{SB}	$-1N$	$1N$	$-1N/s$	$1N/s$
Force from the portside thruster F_{PS}	$-1N$	$1N$	$-1N/s$	$1N/s$
Force from the bow thruster F_{bow}	$-0.5N$	$0.5N$	$-1N/s$	$1N/s$

4.8. Algorithms

In order to progress to the simulation stage, the unmooring, trajectory tracking and mooring algorithms need to be shown. These algorithms are identical, with the initial conditions differing. The output of the unmooring algorithm (the final state $\boldsymbol{x}$) is used as input of the trajectory tracking algorithm. The output of the trajectory tracking algorithm is used as the input for the mooring algorithm.

Algorithm 1,2 and 3: Unmooring, trajectory tracking and mooring algorithms

Initial Conditions: $\boldsymbol{x}_0$
MPC Settings:

1. Sample time T_s
2. Prediction horizon N_p
3. Control horizonN_c
4. Set constraints $[y_{min}, y_{max}]$, $[u_{min}, u_{max}]$, $[\Delta u_{min}, \Delta u_{max}]$
5. Set weights $\boldsymbol{w^y}$, $\boldsymbol{w^u}$, $\boldsymbol{w^{\Delta u}}$
6. Set ECR value (constraint violation)

Input initial state $\boldsymbol{x}$

1: **while** $k <$ simDuration$/T_s$ **do**
2: Get vessel states $\boldsymbol{x}(k)$ for the current k-time step
3: Get reference signal $\boldsymbol{y}_{ref}(k+i)$ for $i = 1, 2, 3, \ldots, N_p$
4: Get optimal control sequence for the current time step $u(k+i)$ for $i = 0, 1, \ldots, N_c - 1$
5: Predict the next states $\boldsymbol{x}(k+1)$ based on the optimal control action u
6: Store the predicted states and control actions
7: Apply the first control input of the optimal solution sequence to the actual system as $\boldsymbol{u}(k)$
8: Update the initial state $\boldsymbol{x}_0$ for the next iteration
9: Set $k = k + 1$
10: **end while**
Extract final state $\boldsymbol{x}$

The MATLAB Simulink block schemes which shows each algorithm can be found in appendix B. It also showcases the implementation of the disturbances and guidance strategies.

4.9. Conclusion

In this chapter the following sub-question was answered: **What is the best control strategy to be selected for the application and how to design it?** The control strategy was selected based on weighted decision matrix. MPC is the best strategy for the application due to its ability to predict future behavior. The MPC was explored in-depth and and ultimately the algorithms to be used going forward were provided. These are three algorithms for each phase of the operation which are unmooring, trajectory tracking and mooring. The next chapter will dive into the implementation in MATLAB Simulink.

5

Implementation

This chapter will answer the following sub-question: **How to implement the proposed control strategy in simulation?** First, in section 5.1 the model scale vessel that will be used in simulation will be shown with its specifications. Then in section 5.2, the reference trajectories are shown. This consists of benchmark trajectories that amalgamate into the Delft trajectory. This section also briefly focuses on the trapezoidal velocity profile used to generate the trajectories. Section 5.3 dives into the KPIs that will be used to assess the performance of the vessel. Then 5.4 focuses on the approach of tuning the MPCs and 5.5 dives into the usage of a low-pass filter to smooth out the outputs of the simulation.

5.1. Model scale vessel

The Tito-Neri model scale vessel to be used in simulation has 2 azimuth thrusters and 1 bow thruster. It has a monohull and is equipped with multiple sensors such as accelerometers, encoders, distance measurement sensors, gyro and GPS. It has an ARM Cortex 32-bit CPU hardware and uses a wireless network connection for communication. The Tito-Neri vessel has two Azimuth Stern Drives (ASD) that are capable of rotating 360° in both directions and 1 bow thruster [78]. A picture of the model scale vessel can be seen in figure 5.1.

Figure 5.1: Model scale Tito-Neri [78]

Table 5.1 shows the dimensions of the ship.

Table 5.1: Ship dimensions

	Value
Length overall l_{oa}	$0.97m$
Height h	$0.32m$
Width w	$0.12m$

5.2. Reference Trajectories

To be able to tune the weights and relevant parameters of the controller, different trajectories need to be designed in order to arrive at the Delft trajectory. The vessel navigates an inland waterway system in Delft from the station to the “Nieuwe Haven” as mentioned in the research scope. It is generated using *openseamap* [79]. The path has three distinct phases: unmooring, trajectory tracking and mooring. This final trajectory can be seen in figure 5.2.

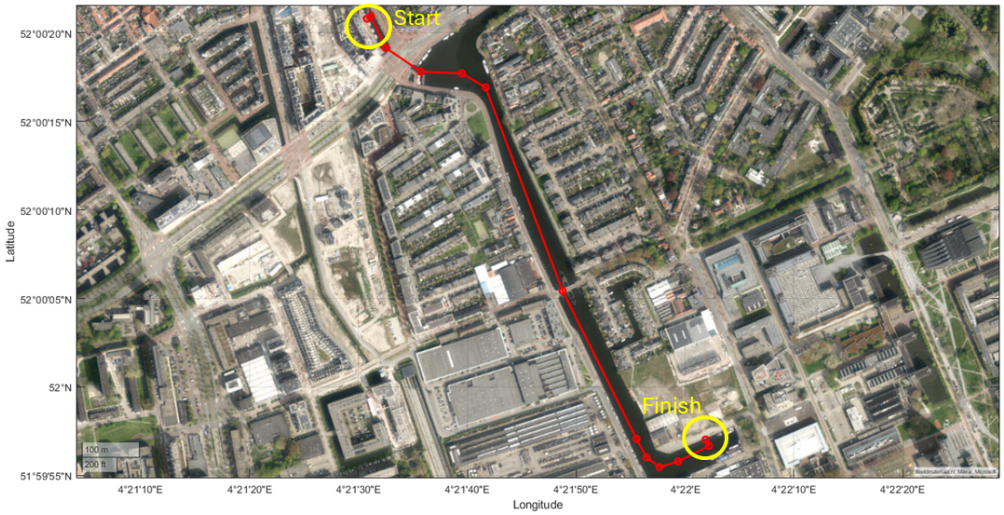

Figure 5.2: Delft trajectory

As can be observed from this trajectory, the trajectory tracking phase consists of a couple of sections. These are an S-shape, a (diagonal) straight line and a 90 degree turn. These can be seen with the unmooring and mooring phases in figure 5.3.

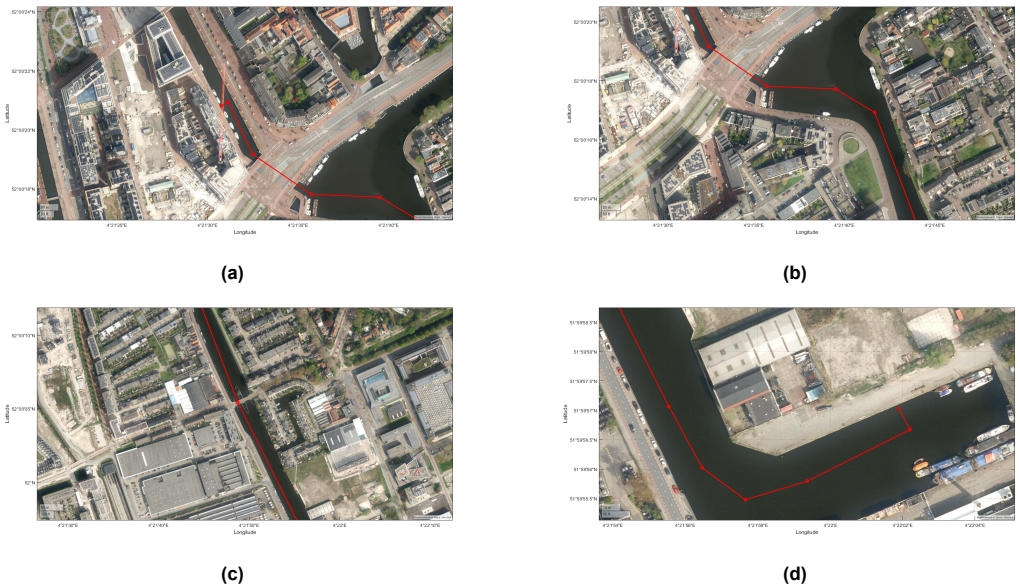

Figure 5.3: Reference trajectory phases: (a) Unmooring, (b) s-curve, (c) straight line, (d) mooring

The preliminary trajectories that will be used in order to work towards the final trajectory are the following three.

- A straight line along the x-axis with a non-changing zero heading for the straight line test
- A diagonal straight line which will encompass the xy-plane
- A path with an S-shape in order to test for the turning capabilities

The trajectories are shown in figure 5.4 below.

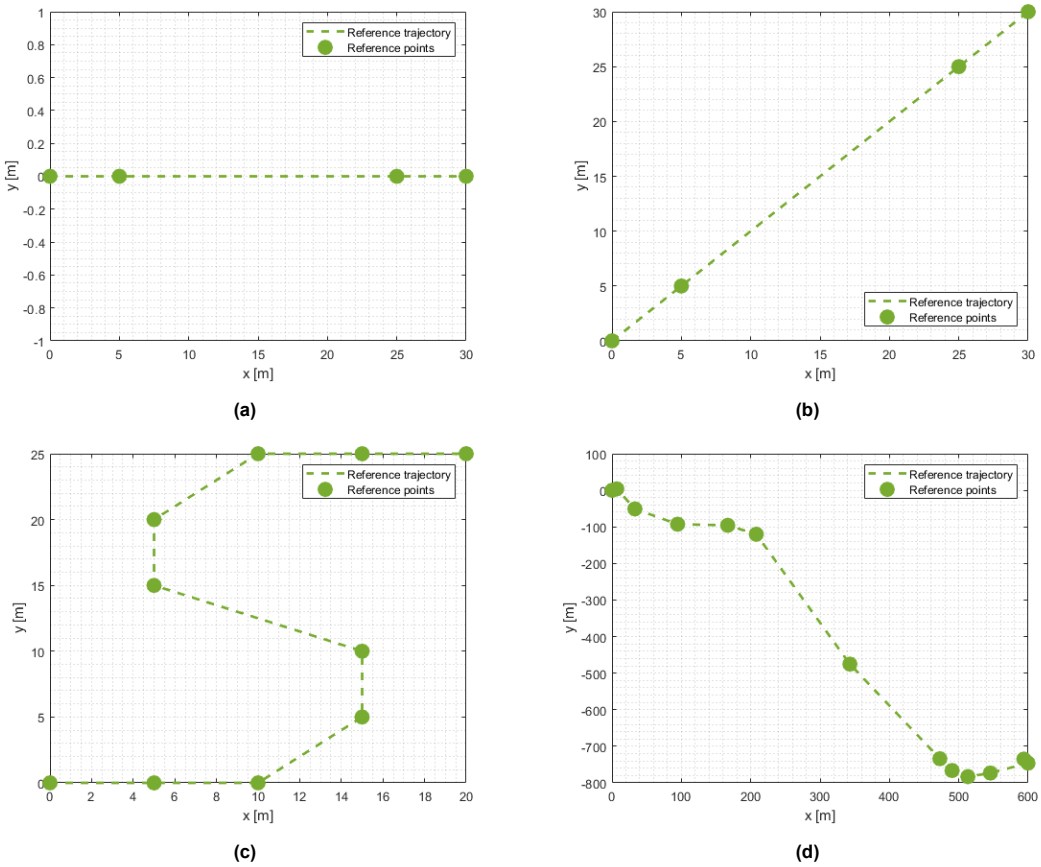

Figure 5.4: Reference trajectories (a) straight line, (b) diagonal line, (c) S-shape, (d) final trajectory

The specific references will follow a trapezoidal trajectory profile. This can be observed in figure 5.5 for the straigh line trajectory in the $x-$direction. A total of $100s$ is used for each phase for more accurate unmooring and mooring. It is generated by using the $trapveltraj$ command in MATLAB [33]. In each of the three phases (unmooring, trajectory tracking, mooring) there is acceleration, a constant velocity and deceleration before the ship reaches the required waypoint. This is achieved by implementing a total of 300 points in between each waypoint for smoother acceleration and deceleration.

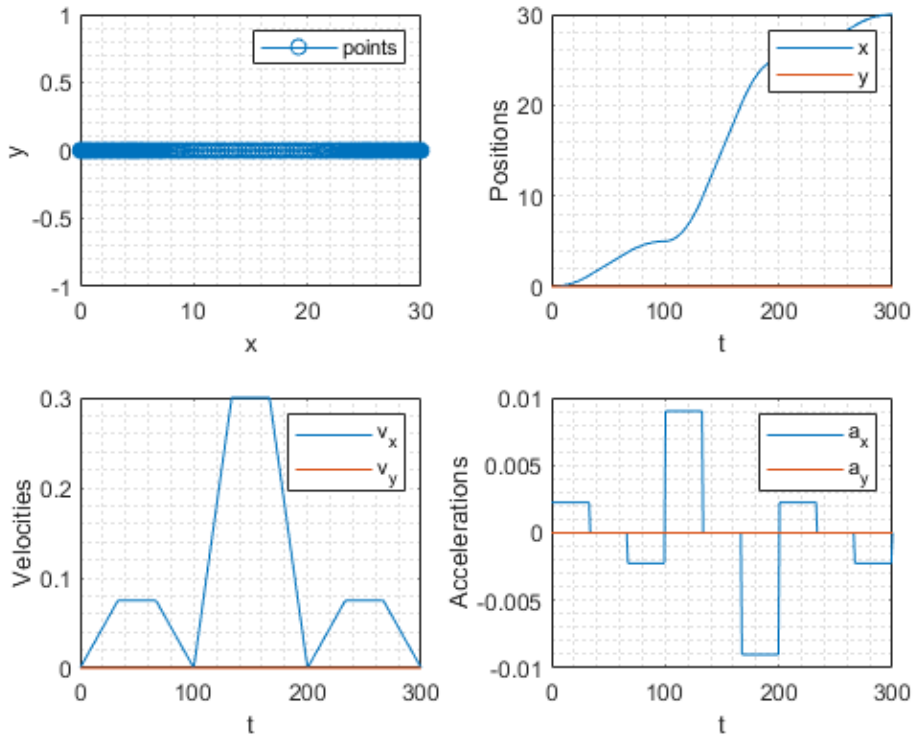

Figure 5.5: Trapezoidal velocity profile (for the straight-line trajectory)

5.3. Key Performance Indicators (KPIs)

In order to be able to assess the control and also the safety performance of the vessel, certain KPIs will be used. These will be split into two categories. The first will be the transient response specifications, which will test the basic control performances. The second will be the course-keeping and mooring abilities, in which the ability of the vessel to follow the predetermined path will be assessed. It should be noted that the overall length of the ship $l_{oa} = 0.97m$. The chosen values are in line with the dimensions of the model scale Tito-Neri model.

5.3.1. Transient Response Specifications

In order to assess the performance of the controllers, the overshoot can be looked at. This is defined as follows according to [80].

$$\text{Overshoot} = \frac{\text{Peak value-Final value}}{\text{Final value}} \cdot 100\% \tag{5.1}$$

In addition, the steady-state error can also be used. The maximum values for each of the three sections can be seen in table 5.2.

Table 5.2: Assessment parameters

	Unmooring	**Trajectory tracking**	**Mooring**
Max. overshoot	20%	20%	0%
Max. steady-state error	1%	1%	1%

5.3.2. Course-keeping abilities

First will be the navigation in a straight line. This will be assessed using the following equation for straight-line stability and course-keeping ability.

$$d_{line}(k) = \frac{|(x_{\text{end}} - x_{\text{start}})(y_{\text{start}} - y_{\text{meas}}(k)) - (x_{\text{start}} - x_{\text{meas}}(k))(y_{\text{end}} - y_{\text{start}})|}{\sqrt{(x_{\text{end}} - x_{\text{start}})^2 + (y_{\text{end}} - y_{\text{start}})^2}} \tag{5.2}$$

where d_{line} is the deviation from the path at a certain time and x_{meas}, y_{meas} is the measured position at said time. The maximum deviation can be assessed and the average deviation over all the points measured.

Table 5.3: Validation criteria for straight line

KPI	Accepted if
Maximum deviation max$\{d_{line}\}$	$d_{line} < 0.1m$
Average deviation avg$\{d_{line}\}$	$d_{line} < 0.05m$

The position and heading error can be defined using the following vector which encompasses the position x and y as well as yaw angle ψ.

$$\eta_{\text{error}}(k) = \begin{bmatrix} x(k) - x_{\text{ref}}(k) \\ y(k) - y_{\text{ref}}(k) \\ \psi(k) - \psi_{\text{ref}}(k) \end{bmatrix} \tag{5.3}$$

Table 5.4: Validation criteria for position/heading error

KPI	Accepted if
Maximum deviation max$\{\eta_x\}$	$\eta_x < 1m$
Average deviation avg$\{\eta_x\}$	$\eta_x < 0.5m$
Maximum deviation max$\{\eta_y\}$	$\eta_y < 1m$
Average deviation avg$\{\eta_y\}$	$\eta_y < 0.5m$
Maximum deviation max$\{\eta_\psi\}$	$\eta_\psi < pi/3$
Average deviation avg$\{\eta_\psi\}$	$\eta_\psi < pi/12$

5.3.3. Mooring abilities

Next is the mooring test which evaluates the vessels ability to come to a precise stop. This is required for mooring as overshoot can lead to collisions and unsafe situations. Here the Euclidian distance towards the mooring point from the vessels position is calculated.

$$d_{moor}(k) = \sqrt{(x_{ref}(k) - x_{meas}(k))^2 + (y_{ref}(k) - y_{meas}(k))^2} \tag{5.4}$$

The distance d_{moor} can not exceed a predetermined value. The test is successful when the d_{moor} is less than that value. This value is 15% of the overall length of the vessel.

Table 5.5: Validation criteria for mooring

KPI	Accepted if
Distance d_{moor}	$d_{moor} < 0.15m$

5.4. MPC Tuning

With the KPIs and the trajectories fully defined, the implementation of the controllers can be realized in MATLAB/Simulink. For each phase, a separate controller will be used. Certain parameters can be adjusted in order to achieve the desired tracking behavior of the controller. These parameters are:

- **Sample time:** T_s

- **Prediction horizon:** N_p
- **Control horizon:** N_c
- **Reference tracking weights:** $\boldsymbol{w^y}$
- **Control inputs weights:** $\boldsymbol{w^u}$
- **Rate of control inputs weights:** $\boldsymbol{w^{\Delta u}}$

The approach for the tuning of the controllers can be quite extensive since there is no official procedure for it. The approach used in this research will consist of the following steps:

- Design of the MPC
  - Define prediction horizon N_p
  - Define control horizon N_c
  - Define constraints
  - Pick sample time T_s
- Tuning of the MPC
  - Reference tracking weights selection $\boldsymbol{w^y}$
  - Control input weights selection $\boldsymbol{w^u}$
  - Rate of control inputs weights selection $\boldsymbol{w^{\Delta u}}$
- Simulation
  - Performance evaluation
  - Adjusting relevant parameters
- Robustness
  - Test the effect of (environmental) disturbances

The process of the evaluation of the performance and adjustments of the relevant parameters is an iterative process.

5.5. Low-pass filter

In order to smooth out the outputs of the position and yaw angle, a low-pass filter is used. There are two types of low-pass filters, Finite Impulse Response (FIR) or Infinite Impulse Response (IIR) filters. IIR filters require less memory since they use fewer coefficients to produce the same filtering function, and they are faster than FIR filters. For this reason, IIR filters are used [81]. In figure 5.6a an example output plot can be seen for the position and orientation of the vessel. Figure 5.6b zooms into a region in order to show the difference between the unfiltered and filtered responses. This filter is used with a normalized passband frequency equal to 0.1. It uses a minimum-order filter with a stopband attenuation of $60db$ and compensates for the delay introduced by the filter [82].

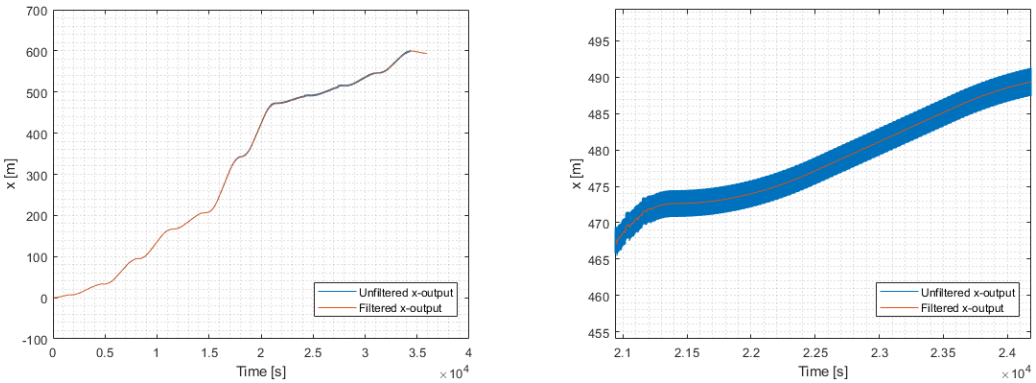

Figure 5.6: Filtered response: (a) output plot, (b) zoomed-in

5.6. Conclusion

This chapter answered the sub-question: **How to implement the proposed control strategy in simulation?** The implementation started by generating the trajectories to be followed in simulation. These were three basic trajectories that combined into the final trajectory. The KPIs were defined for assessment of the performance. A brief overview of the tuning process of the MPCs as well as filtering of the results were also shown. The next chapter will focus on the generated results and assessment of the performance of the MPCs.

6

Results and discussion

This chapter answers the sub-question: **How to evaluate the performance of the control strategy for different trajectories under various operating conditions?** The results of the benchmark trajectories are first shown in section 6.1. These consist of the straight line in x, the diagonal line in x and y and the S-shape. Section 6.2 has the results of the Delft trajectory. Lastly, in section 6.3 the current disturbances will be applied to the vessel in order to mimic various operating conditions.

6.1. Benchmark trajectories and assessment

In this section the results of the benchmark trajectories leading up to the Delft trajectory will be explored. For each of the three phases, a different color will be used. For the unmooring phase, the color blue will be used in the XY-plots. Yellow will be used for the trajectory tracking and red for the mooring phase. In addition to this, the heading of the vessel is visualised with the black line in each triangle.

6.1.1. Straight line in x

First, for the straight line trajectory in the $x-$direction, the XY-plot can be seen in figure 6.1. As can be observed from the graph, the green line is the reference and the triangles represent the vessel. The triangles are plotted every $50s$. The vessel follows the trajectory accurately according to this graph.

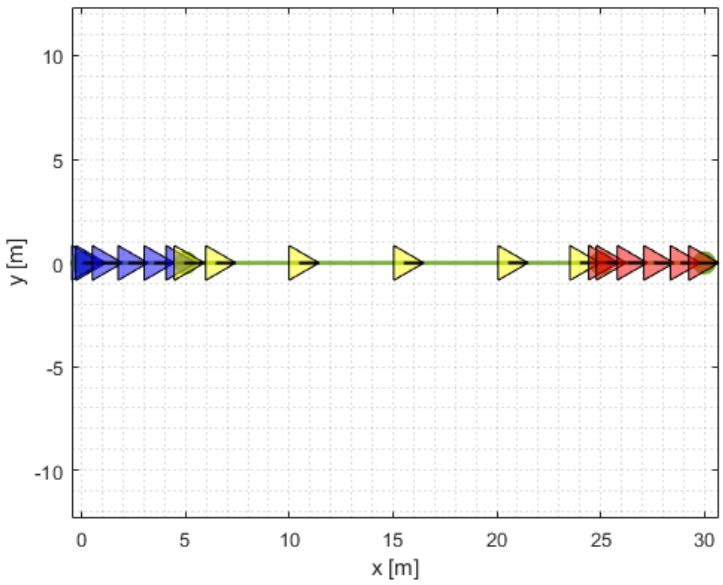

Figure 6.1: XY-plot straight line trajectory in the x-direction

Next, the transient response of each phase for the straight line trajectory can be seen in table 6.1. As can be observed, the maximum overshoot do not exceed the maximum values defined in chapter 5. Mainly for the mooring phase, this is of great importance to be 0% as any overshsoot can cause collisions and unsafe situations.

Table 6.1: Transient response straight line

	Unmooring	**Trajectory tracking**	**Mooring**
Max overshoot	0%	0%	0%
Steady-state error	0.12%	0.05%	0.04%

In figure 6.2 the vessel states or output plots can be seen. The actual output follows the reference well. Near the end of the trajectory tracking phase, some oscillations and a spike of $0.0119m$ seem to appear. This is due to the position being reached and the MPC not knowing what else to do before there is a switch to the next phase. These oscillations however are quite minor. Then in the mooring phase, the largest error can be observed of $0.0673m$ in x and $0.0115m$ in y. These errors are however quite minor as the ship has a length of $0.97m$. In addition at around $t = 600s$ a spike can be observed which causes the reference to change to a negative y to account for this.

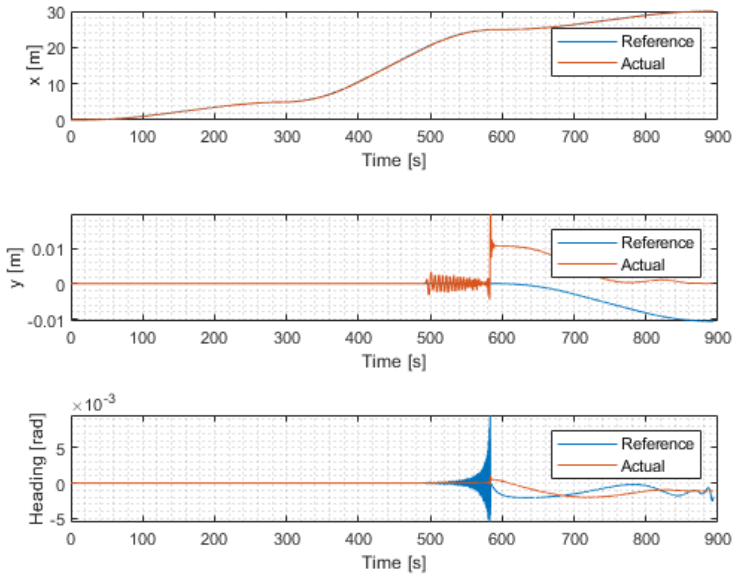

Figure 6.2: Output plots straight line in the x-direction

In table 6.2 in addition to the maximum and mean errors, the results of the straight line and mooring tests can be seen. For the straight line test, a maximum deviation of $0.1m$ is allowed and an average deviation of $0.05m$. Both values are not exceeded and thus the straight-line test is passed. The mooring test result is $0.010m$ (1.0% of the length of the ship), which is really accurate and much less than the maximum value allowed of $0.15m$. All of the values in the table satisfy the criteria mentioned in Chapter 6.

Table 6.2: Results straight line

	Unmooring	Trajectory tracking	Mooring	Total
Maximum deviation straight line	0.0083 m	0.018 m	0.020 m	0.020 m
Mean deviation straight line	0.0042 m	0.0039 m	0.0040 m	0.0047 m
Mooring test	-	-	0.010 m	-
Maximum deviation max$\{\eta_x\}$	0.0255 m	0.118 m	0.0673 m	0.118 m
Maximum deviation max$\{\eta_y\}$	0.0083 m	0.0119 m	0.0115 m	0.0119 m
Maximum deviation max$\{\eta_\psi\}$	0.0299 rad	0.0307 rad	0.0029 rad	0.0307 rad
Average deviation avg$\{\eta_x\}$	0.0158 m	0.0763 m	0.0490 m	0.0476 m
Average deviation avg$\{\eta_y\}$	0.0039 m	-0.0067 m	0.0022 m	0.000253 m
Average deviation avg$\{\eta_\psi\}$	-0.0198 rad	-0.001 rad	0.0001 rad	-0.0066 rad

6.1.2. Diagonal line in x and y

For the diagonal line trajectory in x and y, the XY-plot can be seen in figure 6.3. As can be observed from the graph, again, the green line is the reference and the triangles represent the vessel. The triangles are also plotted every $50s$. It can be observed that the start at the unmooring phase of the heading is $0rad$. The vessel then changes orientation following the reference. A slight bump can also be seen when switching to the trajectory phase. Afterward, the trajectory is followed smoothly.

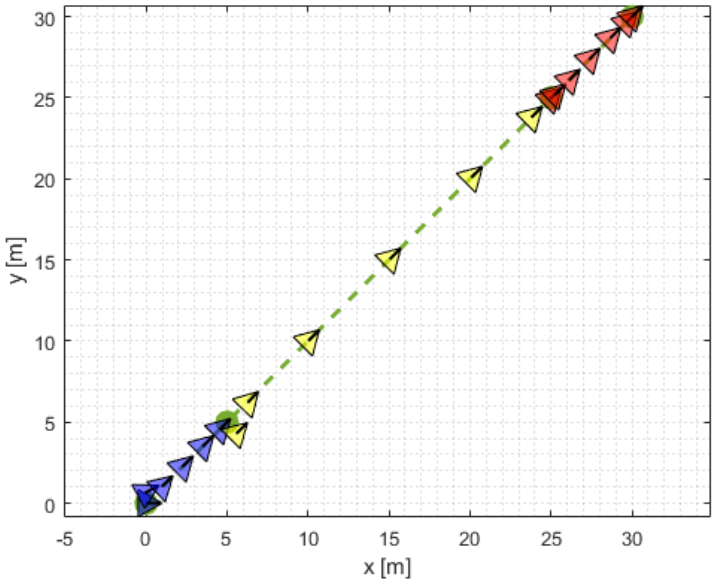

Figure 6.3: XY-plot diagonal line trajectory

Next, the transient response of each phase for the diagonal line trajectory can be seen in table 6.3. As can be observed the maximum overshoot values do not exceed the maximum values defined in chapter 5. The steady-state errors are comparable to that of the straight line only in the $x-$direction except the 0.55% for the trajectory tracking phase here. This value is still less than the 1% that is allowed.

Table 6.3: Transient response diagonal line

	Unmooring	Trajectory tracking	Mooring
Max overshoot	0%	0%	0%
Steady-state error	0.04%	0.55%	0.04%

In figure 6.4 the vessel states or output plots for the diagonal line trajectory can be seen. The actual output follows the reference quite well. During each controller switch an error or small spike can be observed. For the heading or yaw angle, the error is the largest at $0.785rad$. This can be observed

twice at around $t = 300s$ and $t = 600s$. Both are still smaller than the allowed $1.05rad$ or $\pi/3$ and are thus sufficient. Other than this spike a maximum deviation of $0.925m$ can be observed for η_y in the unmooring phase due to the vessel changing orientation first instead of traversing. Again, this value is less than $1m$ and is thus sufficient.

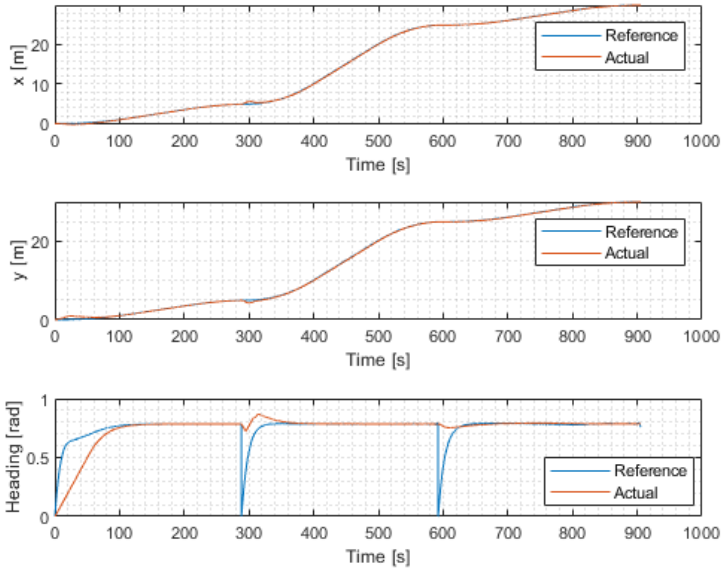

Figure 6.4: Output plots diagonal line trajectory

In table 6.10 in addition to the maximum and mean errors, the results of the mooring test can be seen. The mooring test results are $0.0101m$ (1.0% of the ship length) and is much less than the maximum value allowed of $0.15m$. Furthermore, all of the values in the table satisfy the criteria mentioned in Chapter 5.

Table 6.4: Results diagonal line

	Unmooring	**Trajectory tracking**	**Mooring**	**Total**
Mooring test	-	-	0.0101 m	-
Maximum deviation max$\{\eta_x\}$	0.276 m	0.621 m	0.0674 m	0.621 m
Maximum deviation max$\{\eta_y\}$	0.925 m	0.662 m	0.0811 m	0.925 m
Maximum deviation max$\{\eta_\psi\}$	0.428 rad	0.785 rad	0.785 rad	0.785 rad
Average deviation avg$\{\eta_x\}$	0.0701 m	0.0241 m	0.0321 m	0.0415 m
Average deviation avg$\{\eta_y\}$	-0.114 m	0.119 m	0.0534 m	0.0223 m
Average deviation avg$\{\eta_\psi\}$	0.0694 rad	-0.0317 rad	-0.0221 rad	0.0038 rad

6.1.3. S-shape

For the last benchmark trajectory (the S-shape) the XY-plot can be seen in figure 6.5. As can again be observed from the graph, the green line is the reference and the triangles represent the vessel. The triangles are also plotted every $50s$. The main thing to note is that the vessel now changes its orientation throughout the trajectory. The vessel follows the trajectory quite well as can be observed from the XY-plot.

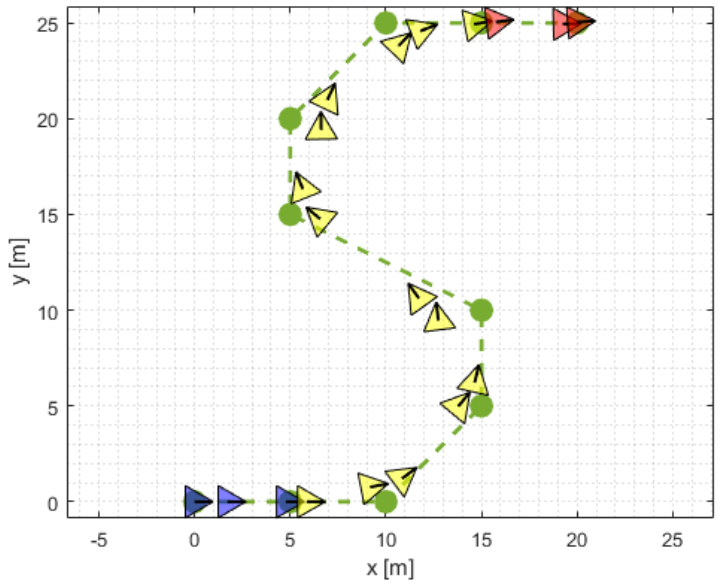

Figure 6.5: XY-plot S-shape trajectory

The transient response of each phase for the diagonal line trajectory can be seen in table 6.5. As can be observed the maximum overshoot values do not exceed the maximum values of 20% for the unmooring and trajectory tracking and 0% for mooring. The steady-state errors are comparable to that of the straight line only in the $x-$direction and the diagonal line. The values of all phases are less than the 1% that is allowed.

Table 6.5: Transient response S-shape

	Unmooring	**Trajectory tracking**	**Mooring**
Max overshoot	0%	0%	0%
Steady-state error	0.2%	0.4%	0.08%

In figure 6.6 the vessel states or output plots for the S-shape trajectory can be seen. The actual output again follows the reference quite well. During each controller switch, an error or small spike can be observed as well as when turning to the left and then right. The largest error observed is at around $t = 400s$ where an error of $2.38m$ can be seen due to the vessel changing direction. For the heading or yaw angle, the error is the largest at $0.728rad$. It is still smaller than the allowed $1.05rad$ and thus is sufficient. Additionally, η_y in the trajectory tracking has a maximum error of $0.891m$. This value is less than $1m$ and is thus sufficient.

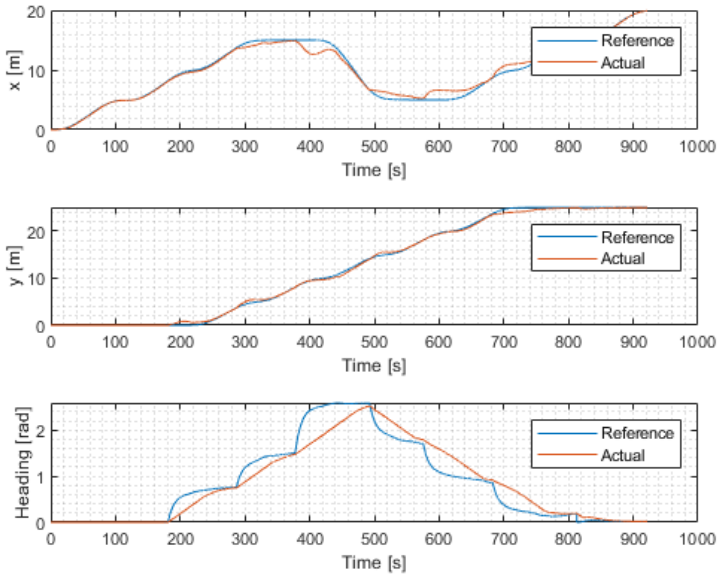

Figure 6.6: Output plots S-shape trajectory

In table 6.10 in addition to the maximum and mean errors, the results of the mooring test can be seen. The mooring test result is $0.0111m$ (1.1% of the ship length) and is much less than the maximum value allowed of $0.15m$. Furthermore, almost all values in the table satisfy the criteria mentioned in Chapter 5. The maximum deviation η_x is $2.38m$ which is larger than what is allowed ($1m$). This fortunately has little consequences on the ultimate purpose which is about the mooring and unmooring accuracies.

Table 6.6: Results S-shape

	Unmooring	**Trajectory tracking**	**Mooring**	**Total**
Mooring test	-	-	0.0111 m	-
Maximum deviation max$\{\eta_x\}$	0.0758 m	2.38 m	0.130 m	2.38 m
Maximum deviation max$\{\eta_y\}$	0 m	0.891 m	0.161 m	0.891 m
Maximum deviation max$\{\eta_\psi\}$	0 rad	0.728 rad	0.527 rad	0.728 rad
Average deviation avg$\{\eta_x\}$	0.0455 m	-0.05 m	0.0526 m	-0.0242 m
Average deviation avg$\{\eta_y\}$	0 m	0.0518 m	0.0222 m	0.0416 m
Average deviation avg$\{\eta_\psi\}$	0 rad	0.0088 rad	-0.0408 rad	0.0006 rad

6.2. Delft trajectory results

For the Delft trajectory the XY-plot can be seen in figure 6.7. The zoomed-in versions of the same trajectory can be seen in figure 6.8.

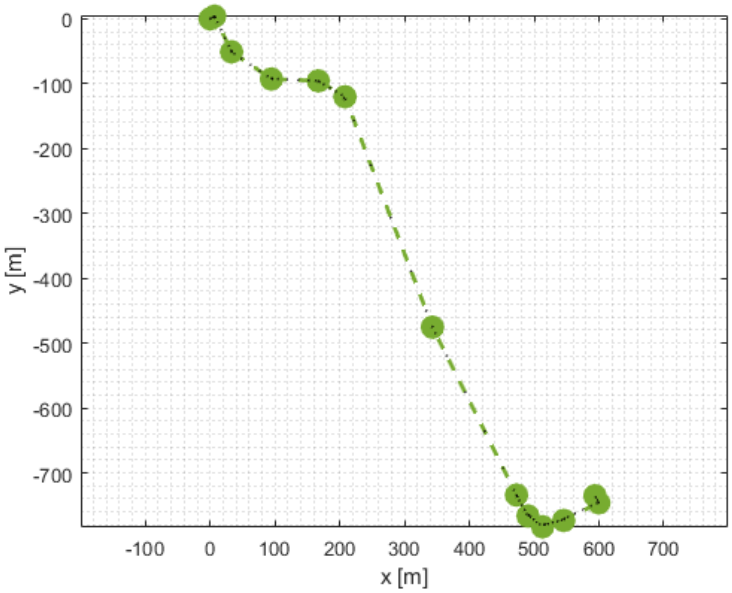

Figure 6.7: XY-plot Delft trajectory

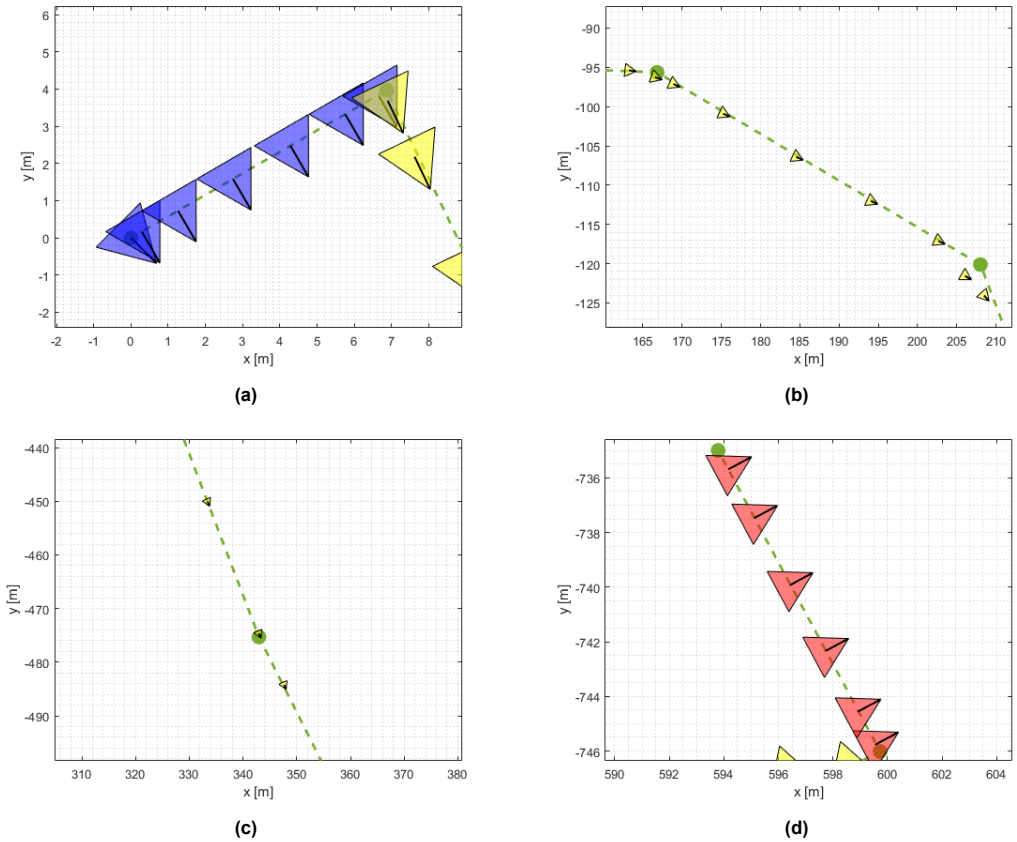

Figure 6.8: XY-plot Delft trajectory (a) unmooring, (b) S-curve, (c) straight line, (d) mooring

As can again be observed from the graphs, the green line is the reference and the triangles represent the vessel. The triangles are plotted every $50s$ in the unmooring and mooring phases and plotted every $500s$ in the trajectory tracking phase. This is done for visualization purposes. The main thing to note is that this trajectory is an amalgamation of the benchmark trajectories, of which the results were shown in the previous section. The vessel appears to follow the trajectory quite well even though this is quite difficult to observe from the plots. It is thus important to look into the quantified results. In table 6.7 the transient responses of this final trajectory can be observed. There is some overshoot in the unmooring phase and trajectory tracking phase of 0.6% and 0.2% respectively. In the mooring phase, it is 0%. For each of the three phases, it is sufficient according to the criteria defined in Chapter 5. The steady-state errors are also quite minor and also satisfy the criteria by all being below 1%.

Table 6.7: Transient response Delft trajectory

	Unmooring	**Trajectory tracking**	**Mooring**
Max overshoot	0.6%	0.2%	0%
Steady-state error	0.2%	0.5%	0.1%

As can be observed from figure 6.9, the reference is being followed quite well. The main inaccuracy in the heading is again due to the switch of the controller from the unmooring to the trajectory tracking phase. This leads to a maximum error of $1.04rad$. During the end of the trajectory tracking phase, there is also a relatively large error due to the turning of the vessel. This results in a mean error of $0.153rad$ for the trajectory tracking phase. These values are both below the maximum allowed values.

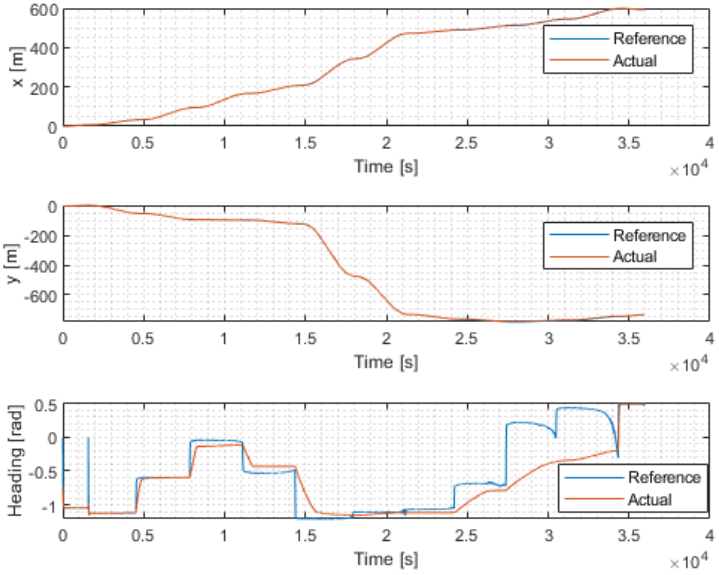

Figure 6.9: Output plots Delft trajectory

In table 6.8 all the relevant KPIs can be seen. First, the mooring test shows a result of $0.0949m$. This is quite larger than the mooring tests of the previous trajectories, which were at roughly $0.01m$. The main difference is due to the vessel in this final trajectory unmooring and also mooring sideways. The $0.0949m$ is still less than the prespecified value of $0.15m$ and 9.8% of the ship length. In addition to this relatively large maximum deviations can be observed during the trajectory tracking phase. For η_x and η_y these values are $3.55m$ and $3.49m$ respectively. The mean deviation η_y is a bit larger than the maximum allowable value of $0.5m$ due to the vessel speeding up and unable to slow down sufficiently. The mean deviation during the mooring phase is also a bit too high at $0.557m$ due to the inaccuracies of the trajectory tracking phase. For the rest of the deviations, the results are sufficient.

Table 6.8: Results Delft trajectory

	Unmooring	Trajectory tracking	Mooring	Total
Mooring test	-	-	0.0949 m	-
Maximum deviation max$\{\eta_x\}$	0.520 m	3.55 m	0.668 m	3.55 m
Maximum deviation max$\{\eta_y\}$	0.510 m	3.49 m	1.40 m	3.49 m
Maximum deviation max$\{\eta_\psi\}$	0.785 rad	1.04 rad	0.450 rad	1.04 rad
Average deviation avg$\{\eta_x\}$	0.0038 m	-0.255 m	-0.557 m	-0.257 m
Average deviation avg$\{\eta_y\}$	0.0007 m	-0.540 m	-0.402 m	-0.510 m
Average deviation avg$\{\eta_\psi\}$	0.0012 rad	0.153 rad	0.0117 rad	0.140 rad

6.3. Disturbances

To further evaluate the robustness of the MPC, disturbances from the current will be introduced. These disturbances are in accordance with the theory of the current disturbances discussed in Chapter 2. There are a total of four cases selected. These are distinguished based on the velocity of the water v_{water} being $0m/s$, $0.1m/s$ and $0.25m/s$. The values chosen are based on the velocity of the ship with the final case of $v_{water} = 0.5m/s$ being an outlier as this value is larger than the maximum velocity of the ship in order to stress the system. The XY-plots as well as the output plots of the vessel states can be found in appendix C.

6.3.1. Straight line in x with disturbances

In figure 6.10 the straight line trajectory with the disturbances added can be observed.

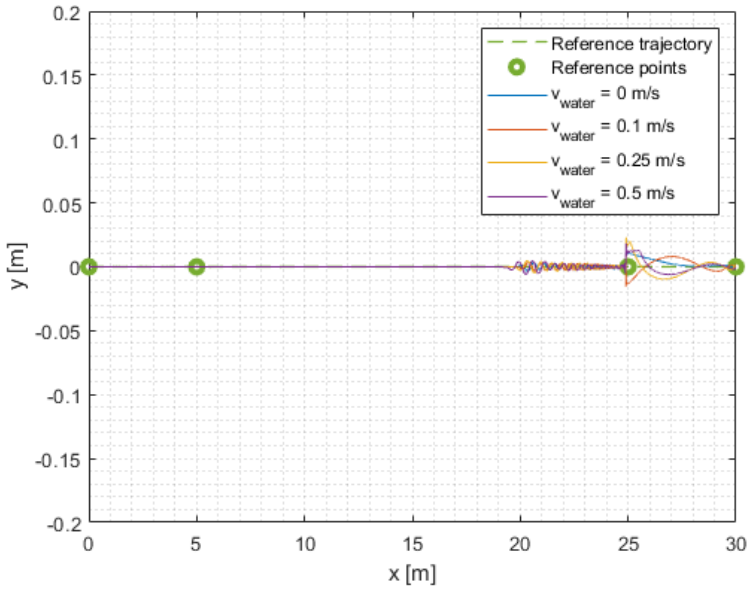

Figure 6.10: Disturbances: Straight line trajectory in the x-direction

As can be observed in this figure, near the end of the trajectory tracking phase some oscillations occur. These then become larger after the switch to the mooring controller. The fluctuations however are quite minor and do not interfere with the vessels ability to accurately follow the trajectory. The maximum and average deviations can be observed in table 6.9. The largest deviations in the most important direction to note (η_y) are relatively minor. The largest value to be observed is at $0.02m$. This is in line with the criteria provided in Chapter 5. The values for maximum and average deviations in x for $v_{water} = 0.5m/s$ do exceed the maximum values of $1m$ and $0.5m$ respectively. This however is not a problem as this solely means that the straight line trajectory is being followed a bit slower and not inaccurately.

Table 6.9: Results disturbances straight line

	$v_{water} = 0m/s$	$v_{water} = 0.1m/s$	$v_{water} = 0.25m/s$	$v_{water} = 0.5m/s$
Maximum deviation max$\{\eta_x\}$	0.118 m	0.0781 m	0.366 m	1.53 m
Maximum deviation max$\{\eta_y\}$	0.0119 m	0.0154 m	0.0230 m	0.0183 m
Maximum deviation max$\{\eta_\psi\}$	0.0307 rad	0.0092 rad	0 rad	0.0165 rad
Average deviation avg$\{\eta_x\}$	0.0476 m	0.0084 m	-0.194 m	-0.9192 m
Average deviation avg$\{\eta_y\}$	0.000253 m	0.0023 m	-0.0029 m	-0.0017 m
Average deviation avg$\{\eta_\psi\}$	-0.0066rad	0 rad	0 rad	0 rad

6.3.2. Diagonal line in x and y with disturbances

Next is the diagonal trajectory in x and y of which the XY-plot can be seen in figure 6.11.

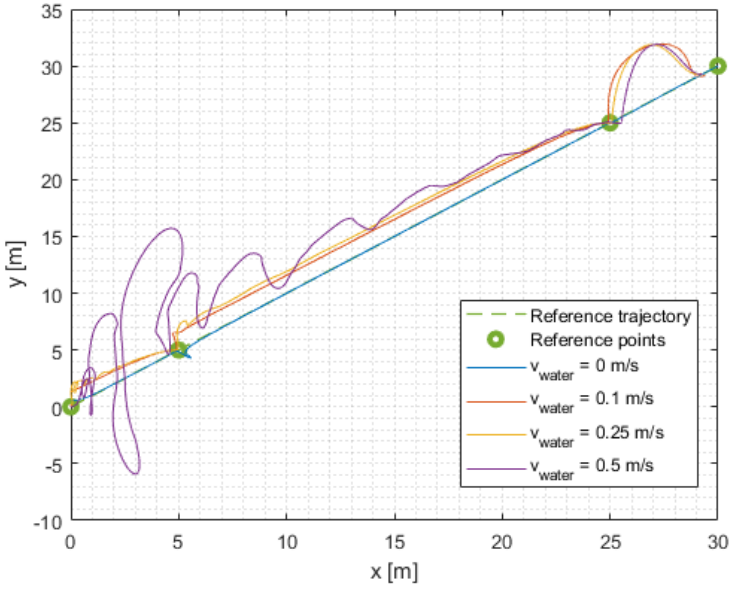

Figure 6.11: Disturbances: Diagonal line trajectory

In table 6.10 the results can be observed. For this case, it becomes more evident that the $v_{water} = 0.5m/s$ is in fact far too large for this system. The maximum deviation observed for this case is $13.3m$. It is worth noting that after the initial oscillations, the vessel does converge to the next coordinate. For the rest of the disturbances the trajectory appears to be followed quite decently except for a steady-state error being introduced. Another thing to note is the jump in position before the final reference point. This is mainly induced due to the tuning of the mooring MPC controller. This is not very fond of the disturbances for this trajectory compared to the trajectory tracking controller for the $v_{water} = 0.1m/s$ and $v_{water} = 0.25m/s$.

Table 6.10: Results disturbances diagonal line

	$v_{water} = 0m/s$	$v_{water} = 0.1m/s$	$v_{water} = 0.25m/s$	$v_{water} = 0.5m/s$
Maximum deviation max$\{\eta_x\}$	0.621 m	0.575 m	0.452 m	2.58 m
Maximum deviation max$\{\eta_y\}$	0.925 m	5.24 m	5.68 m	13.3 m
Maximum deviation max$\{\eta_\psi\}$	0.785 rad	0.712 rad	0.716 rad	1.23 rad
Average deviation avg$\{\eta_x\}$	0.0415 m	0.142 m	-0.151 m	-1.67 m
Average deviation avg$\{\eta_y\}$	0.0223 m	-1.43 m	-1.91 m	-5.11 m
Average deviation avg$\{\eta_\psi\}$	0.0038 rad	0.251 rad	0.358 rad	0.35 rad

6.3.3. S-shape with disturbances

The last trajectory to be tested with disturbances is the S-shape. The trajectory can be seen in figure 6.12.

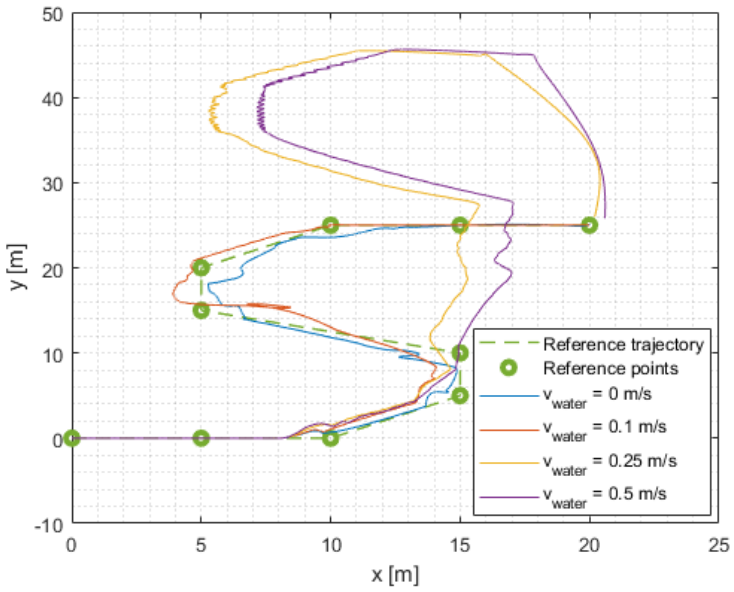

Figure 6.12: Disturbances: S-shape trajectory

From this figure it can be observed that turning is not a motion that is desired by the vessel under the imposed conditions. In table 6.11 the results can be seen. Mainly during the trajectory tracking phase, the maximum deviation η_y for $v_{water} = 0.25m/s$ and $v_{water} = 0.5m/s$ are $26.7m$ and $25.6m$ respectively. The heading of the vessel for these velocities of the current are $2.18rad$ and $2.26rad$ respectively. These values are quite large and do exceed the maximum value allowed of $1.04rad$.

Table 6.11: Disturbances S-shape

	$v_{water} = 0m/s$	$v_{water} = 0.1m/s$	$v_{water} = 0.25m/s$	$v_{water} = 0.5m/s$
Maximum deviation max$\{\eta_x\}$	2.38 m	7.56 m	1.59 m	3.46 m
Maximum deviation max$\{\eta_y\}$	0.891 m	5.41 m	26.7 m	25.6 m
Maximum deviation max$\{\eta_\psi\}$	0.728 rad	2.33 rad	4.62 rad	4.61 rad
Average deviation avg$\{\eta_x\}$	-0.0242 m	0.844 m	-0.535 m	-2.09 m
Average deviation avg$\{\eta_y\}$	0.0416 m	-0.940 m	-13.5 m	-13.8 m
Average deviation avg$\{\eta_\psi\}$	0.0006 rad	0.398 rad	2.18 rad	2.26 rad

6.4. Conclusion

This chapter answered the sub-question: **How to evaluate the performance of the control strategy for different trajectories under various operating conditions?** The accuracy of the results is the highest when not having or with low disturbances of the current. In addition, for each of the benchmark trajectories the results were quite solid with a small outlier for the trajectory tracking phase of the S-shape. The Delft trajectory saw larger errors in this trajectory tracking phase. For the other two phases, the unmooring and mooring, the results were quite accurate and relatively small errors were observed. For the mooring test of the final trajectory, a maximum distance of 9.8% of the ship length was recorded. For the benchmark trajectories, this value was 1.0%. These results mean that using an MPC for the mooring and unmooring is a solid strategy.

7

Conclusion and recommendations

7.1. Conclusion

The research aimed to develop and implement an appropriate strategy for trajectory tracking, unmooring and mooring in simulation. The main research question answered during this study is “How to realize trajectory tracking and autonomous mooring and unmooring capabilities of an autonomous model scale vessel? This research question is answered by means of multiple subquestions/objectives.

Objective 1: Identifying research gaps and relevant theoretical concepts in trajectory tracking and mooring and unmooring of autonomous marine vessels. This was addressed in Chapter 2 which looked at the theoretical foundations of autonomous ships, such as trajectory tracking, mooring and unmooring, stationkeeping and disturbances.

Objective 2: Developing a mathematical model of the model scale vessel. In Chapter 3, a mathematical model was proposed. It provided the relevant concepts for the mathematical model and narrowed it down to the specific application. It included the kinematic and kinetic models, which were followed up by looking into the actuation and thruster allocation. This model provides the necessary foundation for designing a control strategy tailored to the specific behavior of the vessel.

Objective 3: Selecting the best control strategy for the application. Chapter 4 compared various control strategies based on the relevant requirements. Different potential control algorithms were briefly explored. Both qualitatively and quantitatively through a weighted decision matrix, it was noted that MPC is the most suitable due to its capability to predict future states. The flexibility and robustness of the MPC make it ideal for this application of trajectory tracking, mooring and unmooring. Chapter 4 also includes turning the mathematical vessel model into a prediction model as well as defining the control objective and its relevant parameters. This was followed by defining the operational constraints of the Tito-Neri model scale vessel. The chapter also showed the three controllers used and how these operate.

Objective 4: Implementing the proposed control strategy in simulation. Chapter 5 focused on the trajectory generation and an overview of the tuning of the MPC. The relevant KPIs that were used to assess the performance of the model scale vessel were also shown. Lastly, the concept of a low-pass filter was explored for the processing of the data.

Objective 5: Evaluating the performance of the control strategy on multiple trajectories under various operating conditions. Chapter 6 documented the implementation of the MPC strategy in MATLAB/Simulink. Performance evaluation of the various trajectories demonstrated the effectiveness of the MPC in achieving accurate trajectory tracking and robust mooring/unmooring capabilities. For the mooring test of the Delft trajectory, a maximum distance of 9.8% of the ship length was recorded. For the simpler benchmark trajectories, this value was 1.0%. These results mean that using the MPC for the mooring and unmooring is accurate.

This study has filled the gap between theoretical principles and the practical application of control systems for the autonomous mooring and unmooring of autonomous model scale vessels. It paints a complete picture of the operations of an autonomous vessel using an MPC, ranging from unmooring to trajectory tracking to mooring. It also establishes a strong foundation for future advancements in autonomous maritime vessel operations by paving a way for increased efficiency and safety.

7.2. Future work and recommendations

To better understand the implications of the results, future research should address some key points. These include a more complex and realistic mathematical model and thruster configuration, live testing and scaling up the system for real-world applications.

- **More complex and realistic mathematical model:** The proposed mathematical model for this study included several simplifications. Though justified, to create a more realistic implementation, a more complex mathematical model should be explored. This consists of nonlinearities which are the Coriolis-Centripetal term as well as nonlinear damping. These mathematical models should also incorporate environmental variables such as varying weather conditions, complex marine traffic, and differing water currents. This enhancement could improve the robustness and reliability of the control strategy in real-world scenarios.
- **More realistic thruster allocation:** Enhancing the precision and effectiveness of the control approach will require the implementation of a more realistic thruster allocation system that more closely resembles the real operational capabilities and constraints of marine thrusters. This entails taking the variable thruster configuration into account as opposed to a fixed configuration.
- **Live testing with the actual model scale vessel:** Live testing on an actual model scale vessel would offer real-time feedback and validation of the control approach. This approach would ensure that the strategy operates successfully in real-world settings, allowing for appropriate tweaks and enhancements.
- **Scaling up for real-world applications:** Extending the testing and implementation to full-scale vessels is crucial for capturing the complexities and challenges that are not evident in a scaled-down model. Full-scale tests would provide a comprehensive understanding of the control strategy's effectiveness and adaptability in real-world maritime operations.

By addressing these areas, future research can build on the foundation laid by this study, further advancing the capabilities of autonomous marine vessels.

References

[1] M. Shahbakhsh, G. R. Emad, and S. Cahoon, "Industrial revolutions and transition of the maritime industry: The case of seafarer's role in autonomous shipping," *The Asian Journal of Shipping and Logistics*, vol. 38, no. 1, pp. 10–18, 2022.

[2] B. V. Marine & Offshore, *The autonomous shipping research projects reshaping society*, Jul. 2019. [Online]. Available: https://marine-offshore.bureauveritas.com/autonomous-shipping-research-projects-reshaping-society (Retrieved 05/31/2023).

[3] P. of Rotterdam, *Portvision rotterdam*. [Online]. Available: https://www.portofrotterdam.com/sites/default/files/2021-06/port%20vision.pdf (Retrieved 06/11/2023).

[4] Consultancy.eu, *Europe inland shipping market set for growth and consolidation*, Jan. 2024. [Online]. Available: https://www.consultancy.eu/news/9601/europe-inland-shipping-market-set-for-growth-and-consolidation#:~:text=Inland%20waterway%20shipping%20revenue%20in,it%20an%20uncontested%20regional%20leader..

[5] D. Stanisic, M. Efthymiou, M. Kimiaei, and W. Zhao, "Evaluation of conventional methods of establishing extreme mooring design loads," in *International Conference on Offshore Mechanics and Arctic Engineering*, American Society of Mechanical Engineers, vol. 57656, 2017, V03AT02A017.

[6] S. Ahvenjärvi, "Unmanned ships and the maritime education and training," in *Global perspectives in MET: Towards Sustainable, Green and Integrated Maritime Transport*, 2017, pp. 245–254.

[7] B. Sluiskes, "Safety in mooring," *Terra et Aqua*, no. 143, pp. 14–19, 2016.

[8] Y. E. Nazligul and D. Yazir, "Comparison of automated mooring systems against existing mooring systems by using the if-topsis method," *Ocean Engineering*, vol. 285, p. 115 269, 2023.

[9] R. Villa-Caro, J. C. Carral, J. Á. Fraguela, M. López, and L. Carral, "A review of ship mooring systems," *Brodogradnja: Teorija i praksa brodogradnje i pomorske tehnike*, vol. 69, no. 1, pp. 123–149, 2018.

[10] Z.-H. Hu, "Low-emission berth allocation by optimizing sailing speed and mooring time," *Transport*, vol. 35, no. 5, pp. 486–499, 2020.

[11] offshore123, *Introduction to dp systems - what is a dynamic positioning*, Dec. 2021. [Online]. Available: https://www.offshoreengineering.com/dp-dynamic-positioning/what-is-dynamic-positioning/ (Retrieved 06/11/2023).

[12] T. Hahn, R. Damerius, C. Rethfeldt, A. U. Schubert, M. Kurowski, and T. Jeinsch, "Automated maneuvering using model-based control as key to autonomous shipping," *at-Automatisierungstechnik*, vol. 70, no. 5, pp. 456–468, 2022.

[13] T. Trym, E. F. Brekke, and T. A. Johansen, "On collision risk assessment for autonomous ships using scenario-based mpc," *IFAC-PapersOnLine*, vol. 53, no. 2, pp. 14 509–14 516, 2020.

[14] H. Zheng, R. R. Negenborn, and G. Lodewijks, "Trajectory tracking of autonomous vessels using model predictive control," *IFAC Proceedings Volumes*, vol. 47, no. 3, pp. 8812–8818, 2014.

[15] A. Haseltalab and R. R. Negenborn, "Model predictive maneuvering control and energy management for all-electric autonomous ships," *Applied Energy*, vol. 251, p. 113 308, 2019.

[16] S. Wood, M. Rees, and Z. Pfeiffer, "An autonomous self-mooring vehicle for littoral & coastal observations," in *OCEANS 2007-Europe*, IEEE, 2007, pp. 1–6.

[17] G. S. Ramos, D. B. Haddad, A. L. Barros, L. de Melo Honorio, and M. F. Pinto, "Ekf-based vision-assisted target tracking and approaching for autonomous uav in offshore mooring tasks," *IEEE Journal on Miniaturization for Air and Space Systems*, vol. 3, no. 2, pp. 53–66, 2022.

[18] T. I. Fossen, *Handbook of marine craft hydrodynamics and motion control*. John Wiley & Sons, 2011.

[19] Ø. L. Aakre, "Development of a dynamic positioning system for merlin wr200 rov," M.S. thesis, NTNU, 2016.

[20] A. Lunia *et al.*, *Modeling, Motion Planning, and Control of Manipulators and Mobile Robots*. Clemson University, 2021.

[21] V. Bertram, *Unmanned surface vehicles – a survey*, 2008. [Online]. Available: https://citeseerx.ist.psu.edu/document?repid=rep1&type=pdf&doi=461789955de8ddb5c6195b9c95c0ff985caccf7c (Retrieved 06/13/2023).

[22] Z. Liu, Y. Zhang, X. Yu, and C. Yuan, "Unmanned surface vehicles: An overview of developments and challenges," *Annual Reviews in Control*, vol. 41, pp. 71–93, 2016.

[23] S. Ahvenjärvi, "The human element and autonomous ships," *TransNav: International Journal on Marine Navigation and Safety of Sea Transportation*, vol. 10, no. 3, pp. 517–521, 2016.

[24] X. Hong, C. Harris, and P. Wilson, "Autonomous ship collision free trajectory navigation and control algorithms," in *1999 7th IEEE International Conference on Emerging Technologies and Factory Automation. Proceedings ETFA'99 (Cat. No. 99TH8467)*, IEEE, vol. 2, 1999, pp. 923–929.

[25] F. Youd, *Crewless cargo: The world's first autonomous electric cargo ship*, 2022. [Online]. Available: https://www.ship-technology.com/features/crewless-cargo-the-worlds-first-autonomous-electric-cargo-ship/#catfish (Retrieved 06/13/2023).

[26] Wärtsilä, *The future of smart autonomy is here*, Dec. 2021. [Online]. Available: https://www.wartsila.com/insights/whitepaper/the-future-of-smart-autonomy-is-here (Retrieved 02/04/2024).

[27] P. O. T. London, *Mooring operations manual*. [Online]. Available: https://www.forthports.co.uk/wp-content/uploads/2018/11/POTLLMooringManual.pdf (Retrieved 08/07/2023).

[28] *Marc022 perform mooring and unmooring activities*, 2021. [Online]. Available: https://training.gov.au/TrainingComponentFiles/MAR/MARC022_R1.pdf (Retrieved 08/07/2023).

[29] BardexCorporation, *Mooring system manual*. [Online]. Available: https://www.mapsoffshore.com.sg/wp-content/uploads/2016/08/Mooring-System-Manual.pdf (Retrieved 08/07/2023).

[30] T. Chettibi and P. Lemoine, "Generation of point to point trajectories for robotic manipulators under electro-mechanical constraints," *International Review of Mechanical Engineering, IREME, ISSN 1970-8734*, vol. 1, no. 2, pp–131, 2007.

[31] D. Li and L. Du, "Auv trajectory tracking models and control strategies: A review," *Journal of Marine Science and Engineering*, vol. 9, no. 9, p. 1020, 2021.

[32] K. M. Lynch and F. C. Park, *Modern robotics*. Cambridge University Press, 2017.

[33] MathWorks, *Design trajectory with velocity limits using trapezoidal velocity profile*. [Online]. Available: https://www.mathworks.com/help/robotics/ug/design-a-trajectory-with-velocity-limits-using-a-trapezoidal-velocity-profile.html (Retrieved 02/04/2024).

[34] A. M. Lekkas and T. I. Fossen, "Line-of-sight guidance for path following of marine vehicles," *Advanced in marine robotics*, vol. 5, pp. 63–92, 2013.

[35] L. Wang, S. Li, J. Liu, Q. Wu, and R. R. Negenborn, "Ship docking and undocking control with adaptive-mutation beetle swarm prediction algorithm," *Ocean Engineering*, vol. 251, p. 111 021, 2022.

[36] K. Yan, S. Zhang, J. Oh, and D.-W. Seo, "A review of progress and applications of automated vacuum mooring systems," *Journal of Marine Science and Engineering*, vol. 10, no. 8, p. 1085, 2022.

[37] Z. Zhang, Y. Zong, and X. Zhao, "Design and research of port automatic magnetic mooring device based on electromagnetic technology," in *Journal of Physics: Conference Series*, IOP Publishing, vol. 2131, 2021, p. 032 118.

[38] PI, *Pi loss prevention bulletin - preventing an anchor from dragging*. [Online]. Available: https://www.piclub.or.jp/wp-content/uploads/2018/04/Loss-Prevention-Bulletin-Vol.25-Light.pdf.

[39] Standard-Club, *A master's guide to berthing*. [Online]. Available: https://www.standard-club.com/fileadmin/uploads/standardclub/Documents/Import/publications/masters-guides/3391962-sc-mg-berthing-20210203-final.pdf (Retrieved 08/13/2023).

[40] G. Rutkowski, "A comparison between conventional buoy mooring cbm, single point mooring spm and single anchor loading sal systems considering the hydro-meteorological condition limits for safe ship's operation offshore," *TransNav: International Journal on Marine Navigation and Safety of Sea Transportation*, vol. 13, no. 1, pp. 187–195, 2019.

[41] W. Cui, S. Fu, and Z. Hu, *Encyclopedia of Ocean Engineering*. Springer, 2022.

[42] S. offshore, *Turret mooring systems supply record*. [Online]. Available: https://www.sbmoffshore.com/sites/sbm-offshore/files/sbm-offshore/newsroom/press-kit/pdf/turret-mooring-systems-2020-08.pdf (Retrieved 08/13/2023).

[43] S. Chakrabarti, *Handbook of Offshore Engineering (2-volume set)*. Elsevier, 2005.

[44] A. C. Kuzu and Ö. Arslan, "Analytic comparison of different mooring systems," in *Global Perspectives in MET: Towards Sustainable, Green and Integrated Maritime Transport*, 2017, pp. 265–274.

[45] A. C. Kuzu, E. Akyuz, and O. Arslan, "Application of fuzzy fault tree analysis (ffta) to maritime industry: A risk analysing of ship mooring operation," *Ocean Engineering*, vol. 179, pp. 128–134, 2019.

[46] M. F. de Jong, "The ecological effects of deep sand extraction on the dutch continental shelf: Implications for future sand extraction," Ph.D. dissertation, Wageningen University and Research, 2016.

[47] S. Denmark, *Mooring - Do It Safely*. Seahealth Denmark, 2013. [Online]. Available: https://seatracker.ru/viewtopic.php?t=52449 (Retrieved 04/04/2024).

[48] *Automated mooring system*. [Online]. Available: https://www.macgregor.com/intelligent-solutions/automated-mooring-system/ (Retrieved 08/11/2023).

[49] H. Singh *et al.*, "Docking for an autonomous ocean sampling network," *IEEE Journal of Oceanic Engineering*, vol. 26, no. 4, pp. 498–514, 2001.

[50] D. E. Frye, J. Kemp, W. Paul, and D. Peters, "Mooring developments for autonomous ocean-sampling networks," *IEEE Journal of Oceanic Engineering*, vol. 26, no. 4, pp. 477–486, 2001.

[51] A. Veksler, T. A. Johansen, F. Borrelli, and B. Realfsen, "Dynamic positioning with model predictive control," *IEEE Transactions on Control Systems Technology*, vol. 24, no. 4, pp. 1340–1353, 2016.

[52] J. Du, X. Hu, M. Krstić, and Y. Sun, "Dynamic positioning of ships with unknown parameters and disturbances," *Control Engineering Practice*, vol. 76, pp. 22–30, 2018.

[53] S. H. Lift, *Dynamic positioning*. [Online]. Available: https://sal-heavylift.com/fleet/183/dynamic-positioning#:~:text=Main%20advantages%20of%20dynamic%20positioning,in%20the%20weather%20(weather%20vane) (Retrieved 05/02/2024).

[54] T. SNAME, "Nomenclature for treating the motion of a submerged body through a fluid," *The Society of Naval Architects and Marine Engineers, Technical and Research Bulletin*, no. 1950, pp. 1–5, 1950.

[55] A. I. Korotkin, *Added masses of ship structures*. Springer Science & Business Media, 2008, vol. 88.

[56] S. I. Sagatun and T. I. Fossen, "Lagrangian formulation of underwater vehicles' dynamics," in *Conference Proceedings 1991 IEEE International Conference on Systems, Man, and Cybernetics*, IEEE, 1991, pp. 1029–1034.

[57] C. Yao and W. Dong, "Numerical study on local steady flow effects on hydrodynamic interaction between two parallel ships advancing in waves," *Engineering Analysis with Boundary Elements*, vol. 66, pp. 129–144, 2016.

[58] J. Billet, P. Pilozzi, R. Louw, T. Schamp, and P. Slaets, "Model predictive and decoupled thrust allocation for overactuated inland surface vessels," in *2023 European Control Conference (ECC)*, IEEE, 2023, pp. 1–6.

[59] D. Bruggink, Q. Cremer, R. Groenewegen, and A. Klokgieters, “Differentiation of maneuvering coefficients for scaled model vessels,” Technical report, Delft University of Technology, Tech. Rep., 2018.

[60] Z. Du, “Cooperative control of autonomous multi-vessel systems for floating object manipulation,” 2022.

[61] R. Burns, “Closed-loop control systems,” pp. 63–109, 2001. DOI: 10.1016/B978-075065100-4/50005-X.

[62] R. Awati, *What is proportional control?: Definition from techtarget*, Jul. 2023. [Online]. Available: https://www.techtarget.com/whatis/definition/proportional-control (Retrieved 05/20/2024).

[63] H.-X. Li and S. Tong, “A hybrid adaptive fuzzy control for a class of nonlinear mimo systems,” *IEEE Transactions on Fuzzy Systems*, vol. 11, no. 1, pp. 24–34, 2003.

[64] G. Li, H. P. Hildre, and H. Zhang, “Toward time-optimal trajectory planning for autonomous ship maneuvering in close-range encounters,” *IEEE Journal of Oceanic Engineering*, vol. 45, no. 4, pp. 1219–1234, 2019.

[65] V. Blondel and J. Tsitsiklis, “A survey of computational complexity results in systems and control,” *Autom.*, vol. 36, pp. 1249–1274, 2000. DOI: 10.1016/S0005-1098(00)00050-9.

[66] C. Knospe, “Pid control,” *IEEE Control Systems Magazine*, vol. 26, no. 1, pp. 30–31, 2006.

[67] D. E. Kirk, *Optimal control theory: an introduction*. Courier Corporation, 2004.

[68] A. J. Sørensen, “A survey of dynamic positioning control systems,” *Annual reviews in control*, vol. 35, no. 1, pp. 123–136, 2011.

[69] K. J. Astrom, K. H. Johansson, and Q.-G. Wang, “Design of decoupled pid controllers for mimo systems,” in *Proceedings of the 2001 American Control Conference.(Cat. No. 01CH37148)*, IEEE, vol. 3, 2001, pp. 2015–2020.

[70] Š. Kozák, “From pid to mpc: Control engineering methods development and applications,” in *2016 cybernetics & informatics (K&I)*, IEEE, 2016, pp. 1–7.

[71] M. Michalczuk, B. Ufnalski, and L. M. Grzesiak, “Imposing constraints in a full state feedback system using multithreaded controller,” *IEEE Transactions on Industrial Electronics*, vol. 68, no. 12, pp. 12 543–12 553, 2021. DOI: 10.1109/TIE.2020.3044778.

[72] K. Holkar and L. M. Waghmare, “An overview of model predictive control,” *International Journal of control and automation*, vol. 3, no. 4, pp. 47–63, 2010.

[73] L. Wang, *Model predictive control system design and implementation using MATLAB®*. Springer Science & Business Media, 2009.

[74] S. J. Qin and T. A. Badgwell, “An overview of industrial model predictive control technology,” in *AIche symposium series*, New York, NY: American Institute of Chemical Engineers, 1971-c2002., vol. 93, 1997, pp. 232–256.

[75] M. Morari and J. H. Lee, “Model predictive control: Past, present and future,” *Computers & chemical engineering*, vol. 23, no. 4-5, pp. 667–682, 1999.

[76] MathWorks, *Continuous-discrete conversion methods*. [Online]. Available: https://nl.mathworks.com/help/control/ug/continuous-discrete-conversion-methods.html (Retrieved 06/13/2024).

[77] MathWorks, *Optimization problem*. [Online]. Available: https://nl.mathworks.com/help/mpc/ug/optimization-problem.html#bujxw9t (Retrieved 05/13/2024).

[78] *Tito neri*. [Online]. Available: https://rasdelft.nl/facilities-2/tito-neri-1/ (Retrieved 05/20/2024).

[79] O. Hannemann, *The free nautical chart*, Jun. 2012. [Online]. Available: https://map.openseamap.org/.

[80] M. S. Fadali and A. Visioli, “Chapter 5 - analog control system design,” in *Digital Control Engineering (Third Edition)*, M. S. Fadali and A. Visioli, Eds., Third Edition, Academic Press, 2020, pp. 141–179.

[81] S. R. Sutradhar, N. Sayadat, A. Rahman, S. Munira, A. F. Haque, and S. N. Sakib, “Iir based digital filter design and performance analysis,” in *2017 2nd International Conference on Telecommunication and Networks (TEL-NET)*, IEEE, 2017, pp. 1–6.

[82] MathWorks, *Lowpass-filter signals*. [Online]. Available: `https://www.mathworks.com/help/signal/ref/lowpass.html#d126e126714` (Retrieved 06/20/2024).

A

Scientific Research Paper

This appendix consists of the Scientific Research Paper, starting on the next page.

Autonomous Mooring and Unmooring with use of a Model Predictive Control Strategy

R. W. Jagernath V. Garofano Y. Pang

***Abstract*— Mooring and unmooring are vital processes in the operation of ships as it is the system that secures and releases a ship to a terminal or multiple terminals. The process has remained relatively the same over the years whereas autonomous shipping has been researched over time. The purpose of this study is to provide an alternative to this by making use of a control strategy in order to achieve autonomous mooring and unmooring. A mathematical vessel model is proposed to be used by the control strategy that is selected. The implementation includes multiple controllers on multiple trajectories for each phase of the operation (unmooring, trajectory tracking and mooring). For the mooring test of the final trajectory, a maximum distance of 9.8% of the ship length was recorded. For the simpler trajectories, this value was 1.0%. These results mean that using this control strategy for the mooring and unmooring is quite accurate.**

***Keywords* – Autonomous Shipping, Mooring, Unmooring, Trajectory Tracking, Ship Dynamics, Model Predictive Control (MPC).**

I. Introduction

A. Background

Autonomous systems have gained significant interest in the maritime industry due to their potential to increase efficiency, safety, and sustainability [1], [2]. The Port of Rotterdam, the largest in Europe, handled 469 million tonnes in 2018 and is crucial for global trade and the European market. It generated €15 billion in 2017, with projections of €19 billion by 2030 [3]. Inland waterway shipping revenue in the Netherlands rose by 43% in 2022, accounting for over a third of EU27 transport activity [4]. One area of particular importance in inland waterways is vessel mooring and unmooring, which is crucial for port operations and maritime logistics.

Mooring and unmooring of vessels entail securing or releasing a ship to or from a berth with ropes, lines, and other equipment [5], [6]. Mooring and unmooring are the start and the finish in the process of a ship involving transit from point A to point B. This typically requires trained crew members to be able to maneuver the vessel safely and efficiently whilst taking into account external factors such as the wind, waves and current [7]. Advancements in the autonomous shipping industry (regarding control strategies, sensors and actuators) allow for this process to be developed into autonomous mooring and unmooring.

B. Problem

Mooring and unmooring vessels, essential for port operations, have traditionally been labor-intensive, time-consuming, and prone to human error [8], [9]. These processes involve securing or releasing a ship at a berth using ropes and other equipment [5], [6], requiring skilled crew members to handle external factors like wind and currents [7].

Advances in control strategies, sensors, and actuators in autonomous shipping enable the development of autonomous mooring and unmooring. Current automatic mooring methods, such as magnetic and vacuum, are costly and have maintenance challenges [7]. An alternative is to use thrusters on the vessels managed by a control strategy.

Autonomous mooring and unmooring can streamline port operations, reduce manual labor, increase efficiency, and minimize accidents [7]. These systems, combined with other autonomous technologies, can enable 24/7 port operations, reduce fuel consumption, and lower environmental impact [10]. The challenge of developing reliable control systems that manage uncertainties such as weather, vessel characteristics, and berth configurations [11].

This research aims to develop a control strategy for autonomous mooring and unmooring, combined with trajectory tracking for an autonomous vessel in inland waterways. Although extensive research on autonomous shipping has been conducted focusing on collision risk [12], trajectory tracking [13], and energy management [14], the specific application of autonomous mooring/unmooring with trajectory tracking remains largely unexplored [15], [16]. This study will address this gap, aiming to enhance the efficiency and safety of current marine processes through autonomous operations [1], [2].

C. Goal

The main research question is: **How to realise trajectory tracking and autonomous mooring and unmooring capabilities of an autonomous model scale vessel?** To address this, the study will begin with a literature review to gather information on theoretical concepts and identify gaps in current knowledge. Following this, a mathematical model of the model scale vessel will be shown. An appropriate control strategy will be chosen. The trajectory will be created and assessed using predefined Key Performance Indicators (KPIs). The implementation will contain benchmark trajectories and a final combination of these trajectories. Lastly, it will be concluded whether or not the strategy implemented was effective.

II. Literature review

A. Autonomous ship systems

Autonomous vessels have been under investigation since World War II, when early experiments with Unmanned Surface Vehicles (USVs) began, such as torpedoes used to

lay smoke screens. From 1950-1980, the focus shifted to Remote Operated Vehicles (ROVs) for underwater tasks, especially minesweeping. The development of modern USVs gained momentum from 1990-2000 due to technological advancements, with a focus on reconnaissance and surveillance missions [17]. In recent decades, numerous institutions and militaries have been developing USVs for diverse applications, with fully autonomous vessels in dynamic maritime environments remaining a key challenge. Notable advancements include the MV Yara Birkeland, the first fully autonomous cargo ship, which completed its maiden voyage in 2022 [18].

Autonomous operations aim to enhance safety, efficiency, and environmental performance in maritime operations. Key challenges include managing overcapacity, improving safety, reducing human error, increasing efficiency, and decarbonization. Typical ship operations involve unmooring, transit, and mooring, all of which currently require substantial human intervention. Automating these processes, especially mooring and unmooring, is crucial for achieving full autonomy [19].

B. Guidance, Navigation and Control

The development of Guidance, Navigation, and Control (GNC) systems has been critical for (semi-)autonomous vessel operation. Guidance systems continuously compute the desired position, velocity, and acceleration based on inputs from human operators and navigation systems. Guidance strategies such as Line-Of-Sight (LOS) and the Circle of Acceptance (CoA) are employed to navigate vessels. LOS calculates the reference angles between the current position and the next waypoint, while CoA determines the waypoint arrival based on proximity. These strategies will be used for trajectory planning and can be seen in figure 1 [20], [21]. Navigation involves determining the vessel's position and course using Global Navigation Satellite Systems (GNSS) and motion sensors. Control systems apply the necessary forces to achieve objectives such as trajectory-tracking or path-following, using a control loop that integrates outputs from guidance and navigation systems [22].

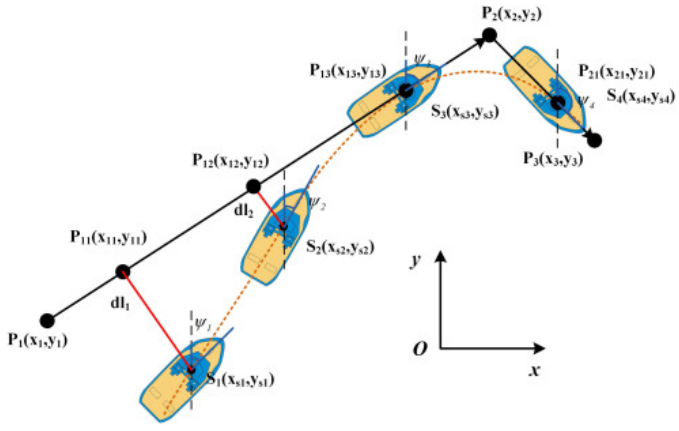

Fig. 1. Guidance strategy [21]

Trajectory tracking entails guiding a vessel down a predefined path while adhering to limitations and optimizing performance metrics. Trajectories can be created using a variety of profiles, including polynomial, bang-bang, and trapezoidal profiles. The trapezoidal profile is very good for regulating acceleration and deceleration phases. It contains four main parameters: end time, peak velocity, acceleration time, and peak acceleration as can be seen in figure 2. The trapezoidal profile includes the continuous acceleration, velocity, and deceleration phases [23], [24], [25], [26].

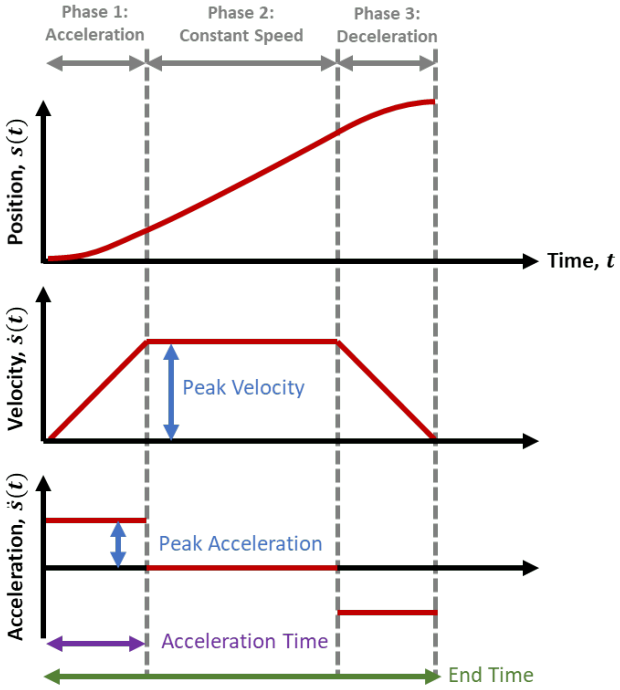

Fig. 2. Trapezoidal velocity profile phases [25], [26]

C. Mooring and unmooring

The terminological definition of mooring is the system that secures a ship to a terminal or multiple terminals. Unmooring deals with the opposite of mooring [5], [9]. During this process, the vessel gets near the mooring point and reduces its speed to typically around 1 to 2 knots (1.85-3.7 m/s) [27]. Mooring and unmooring involve significant safety risks. Mooring operations aboard ships raise major safety risks for the ship's crew, the ship itself, and the maritime environment. Lack of mooring equipment maintenance, untrained and inexperienced personnel, equipment failures, available weather conditions, poor communication, safety procedure errors, and risk assessment failure are the primary causes of mooring accidents involving ropes and windlass. Effective risk management is critical to prevent accidents [28], [29], [30], [31]. Autonomous mooring is being investigated using technologies like as magnetic and vacuum mooring systems, although they present issues such as high costs and maintenance requirements. Innovations such as the robotic arm for the Yara Birkeland fully autonomous ship provide potential breakthroughs, highlighting advantages in safety and efficiency [32], [33], [34].

D. Stationkeeping

Dynamic Positioning (DP) systems use thrusters to keep a vessel's location and heading stable in regardless of environmental changes. DP technology provides accurate, versatile, efficient, and safe vessel positioning when compared to traditional anchor-based methods [35], [36]. These systems provide a gateway into autonomous mooring as it only uses the set of thrusters to balance external forces as can be seen in figure 3.

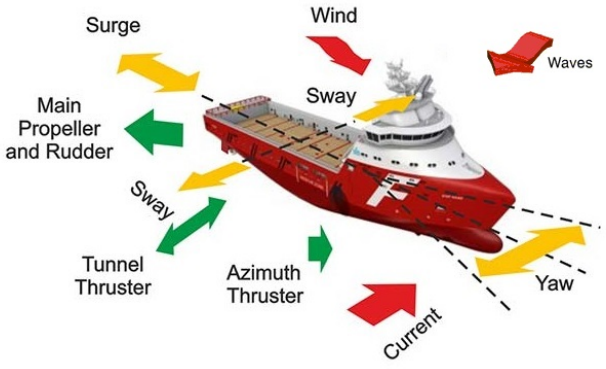

Fig. 3. DP system using thrusters (green) to balance out forces (red) [11]

III. Mathematical Vessel Model

The dynamics of the ship system can be described using Fossen's [22] framework. When moving, a marine craft experiences motion in six Degrees of Freedom (DOFs). The position and orientation of the craft are defined by a set of independent displacements and rotations that are collectively referred to as the DOFs. Motion in the horizontal plane is described by surge (propulsive motion) and sway (sideways motion), while rotation about the vertical axis is represented by yaw. Reduced-order models are frequently used for the building of control systems, focusing on the DOFs most pertinent to the particular application.

The ship's motion is controlled by a 6 DOF model, although a 3 DOF model is employed for horizontal plane analysis in calm inland waterways. The kinematic model defines the relationship between the vessel's body-fixed and inertial frame velocities, whereas the kinetic model considers the forces and moments operating on the vessel, such as rigid-body, additional mass, hydrodynamic damping, and hydrostatic forces. The kinematic equation is described in the following manner:

$$\dot{\boldsymbol{\eta}} = \boldsymbol{R}(\psi)\boldsymbol{\nu} \tag{1}$$

$R(\psi)$ is the transformation matrix for rotation about the z axis in order to transform from the body-fixed frame to the inertial frame and vice versa.

$$\boldsymbol{R}(\psi) = \begin{bmatrix} \cos(\psi) & -\sin(\psi) & 0 \\ \sin(\psi) & \cos(\psi) & 0 \\ 0 & 0 & 1 \end{bmatrix} \tag{2}$$

A linearized model will be used for the Tito-Neri. This simplification is based on the operational condition of the vessel being $u >> v, r$. The kinematic model is shown below.

$$\boldsymbol{M}\dot{\boldsymbol{\nu}} + \boldsymbol{D}\boldsymbol{\nu} = \boldsymbol{\tau} \tag{3}$$

where $\boldsymbol{M}$ is the mass inertia matrix, $\boldsymbol{\nu}$ is the velocity vector, $\boldsymbol{D}$ the damping matrix, and where

$$\boldsymbol{\tau} = \boldsymbol{T}(\boldsymbol{\alpha})\boldsymbol{f} \tag{4}$$

where $\boldsymbol{\alpha}$ is a vector of the azimuth angles and $\boldsymbol{T}(\boldsymbol{\alpha})$ is the thrust configuration matrix. The Tito-Neri model scale vessel has 2 azimuth thrusters and 1 bow thruster. It has a mono hull and it is equipped with multiple sensors such as accelerometers, encoders, distance measurement sensors, gyro and GPS. A schematic overview can be seen in figure 4.

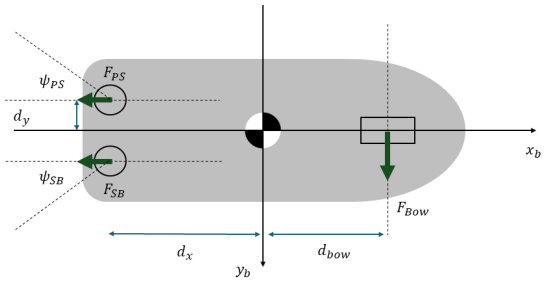

Fig. 4. Thruster configuration of the Tito-Neri

For the 2 azimuth thrusters and a bow thruster the thrust configuration matrix becomes the following.

$$\begin{bmatrix} \cos(\psi_{PS}) & \cos(\psi_{SB}) & 0 \\ \sin(\psi_{PS}) & \sin(\psi_{SB}) & 1 \\ d_y \cdot \cos(\psi_{PS}) - d_x \cdot \sin(\psi_{PS}) & d_y \cdot \cos(\psi_{SB}) - d_x \cdot \sin(\psi_{SB}) & d_{bow} \end{bmatrix} \tag{5}$$

IV. Control Strategy

A. Selection

To select the most suitable control strategy for the application, it is essential to define the requirements. The primary goal of this research is to develop a control strategy capable of maneuvering the vessel using actuator inputs. These inputs will be utilized for unmooring, trajectory tracking, and mooring of a small-scale vessel, the Tito-Neri. The controller has to account for Multi-Input Multi-Output (MIMO), be able to handle constraints and not be computationally complex. In addition, it is also beneficial for the controller to be able to predict future behavior due to its requirement to track the position accurately. MPC is preferred due to its ability to handle constraints effectively, integrate environmental uncertainties, and plan ahead by optimizing control actions over a prediction horizon [37].

B. Model Predictive Control (MPC)

MPC is also known as receding horizon control or moving horizon control. It is a control method that employs an explicit dynamic plant model to predict the effect of future

reactions of the manipulated variables on the output and control signal obtained by minimizing the cost function denoted by J. A receding horizon technique in which the horizon moves forward at each instant by applying the first control signal of the sequence calculated at each step. An overview of the control strategy can be seen in figure 5. A discrete input, along with the trajectory (both reference and predicted) can be observed at the top.

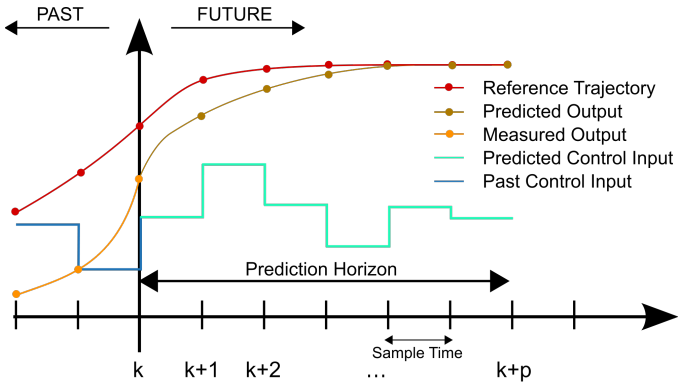

Fig. 5. Model Predictive Control [38]

An overview of the approach is provided below [39], [40]. First, the control objective is shown. This is to minimize the cost function J. The underlined variables denote the predicted version of that variable.

$$\min \left\{ \sum_{i=0}^{N_p-1} J\left(\underline{y}(k+i+1), \underline{u}(k+i), x_{ref}(k+i+1)\right) \right\} \tag{6}$$

with N_p as the prediction horizon. For an MPC controller the following steps are followed at each time step k.

1) Receive the measurements $\boldsymbol{y}(k)$
2) Determine the states $\underline{\boldsymbol{x}}(k)$ from the measurements
3) Determine the disturbances $\underline{\boldsymbol{d}}(k), ..., \underline{\boldsymbol{d}}(k+N_p-1)$ and the reference signal $x_{ref}(k+1), ..., x_{ref}(k+N_p)$
4) Solve the MPC problem to get the optimal actions $\underline{\boldsymbol{u}}(k), ..., \underline{\boldsymbol{u}}(k+N_p-1)$
5) Return the optimal actions $\underline{\boldsymbol{u}}(k)$ as $\boldsymbol{u}(k)$ to the system

C. Prediction model

The prediction model of the Tito-Neri vessel is derived from the kinetic and kinematic equations provided in section III. In state-space form, it becomes the following:

$$\dot{\boldsymbol{x}}(t) = \boldsymbol{f}(\boldsymbol{x}(t), \boldsymbol{u}(t)) \tag{7}$$

$$\boldsymbol{y}(t) = g(\boldsymbol{x}(t)) \tag{8}$$

The states $\boldsymbol{x}$ are the position x and y and the orientation ψ given as $\boldsymbol{\eta} = [x, y, \psi]^T$ combined with the velocities $\boldsymbol{\nu} = [u, v, r]^T$. The state vector thus becomes $\boldsymbol{x} = [x, y, \psi, u, v, r]^T$. The output vector $\boldsymbol{y}$ will be according to the control objective. This objective is to follow a desired set of coordinates and thus $\boldsymbol{y} = \boldsymbol{\eta} = [x, y, \psi]^T$. Now the continuous time state space model can be defined.

$$\boldsymbol{M}\dot{\boldsymbol{\nu}}(\boldsymbol{t}) + \boldsymbol{D}(\boldsymbol{\nu}(\boldsymbol{t}))\boldsymbol{\nu}(\boldsymbol{t}) = \boldsymbol{\tau}(\boldsymbol{t}) \tag{9}$$

This then becomes the following:

$$\dot{\boldsymbol{\nu}}(t) = \boldsymbol{M}^{-1}[-\boldsymbol{D}(\boldsymbol{\nu}(t))\boldsymbol{\nu}(t) + \boldsymbol{\tau}(t)] \tag{10}$$

Now the function $\boldsymbol{f}(t)$ can be defined. The rotation matrix will not be used in this prediction model as the system will be controlled locally. The transformation to the global position is not required.

$$\boldsymbol{f}(\boldsymbol{x}(t), \boldsymbol{u}(t)) = \begin{bmatrix} \boldsymbol{I}_{3x3}\boldsymbol{x}_{4:6}(t) \\ \boldsymbol{M}^{-1}\left[-\boldsymbol{D}\left(\boldsymbol{x}_{4:6}(t)\right)\boldsymbol{x}_{4:6}(t) + \boldsymbol{T}\boldsymbol{u}(t)\right] \end{bmatrix} \tag{11}$$

The output will be the following:

$$g(\boldsymbol{x}(t) = \boldsymbol{x}(t) = [x(t), y(t), \psi(t), 0, 0, 0]^T \tag{12}$$

D. Objective and constraints

MPC solves an optimization problem, specifically a Quadratic Programming (QP) problem, at each control interval. The purpose of the application is to unmoor, track a desired trajectory, and moor following a reference signal defined as $\boldsymbol{y}_{ref}$. The solution to the QP problem defines the Manipulated Variables (MVs) that will be used in the plant until the next control period. The controller will be implemented using MATLAB and MATLAB Simulink. According to the MPC and optimization toolboxes [41], the total cost function is provided below.

$$J\left(z_k\right) = J_y\left(z_k\right) + J_u\left(z_k\right) + J_{\Delta u}\left(z_k\right) + J_c\left(z_k\right) \tag{13}$$

Here, z_k is the QP decision variable. This cost function consists of the sum of four terms. These are Output reference tracking, Manipulated Variable (MV) tracking, MV rate suppression and constraint violation.

The constraints for the Tito-Neri model scale vessel are given according to table I. These constraints consist of the forces that are applied to the vessel.

TABLE I
TITO-NERI MODEL SCALE VESSEL CONSTRAINTS

	Min	Max	Rate Min	Rate Max
F_{SB}	$-1N$	$1N$	$-1N/s$	$1N/s$
F_{PS}	$-1N$	$1N$	$-1N/s$	$1N/s$
F_{bow}	$-0.5N$	$0.5N$	$-1N/s$	$1N/s$

V. Implementation

A. Reference trajectories

To be able to adjust the weights and assess the performance of the controllers, different trajectories need to be designed. The trajectories are based on a trapezoidal velocity profile as mentioned in section II. The vessel navigates an inland waterway system in Delft and has three distinct

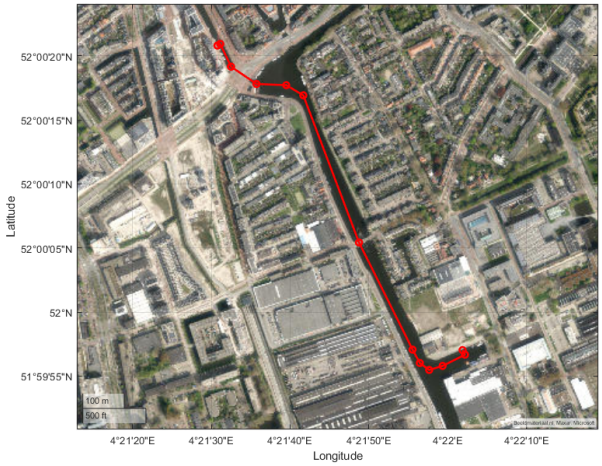

Fig. 6. Reference trajectory

phases. These will be unmooring, trajectory tracking and mooring. The final trajectory can be seen in figure 6.

The preliminary trajectories that will be used in order to work towards the final trajectory are the following three. These trajectories are all individually used as a stepping stone towards the final trajectory and can be seen in figure 7.

- A straight line along the x-axis
- A diagonal straight line which is on the XY-plane
- A path with an S-shape in order to test for turning

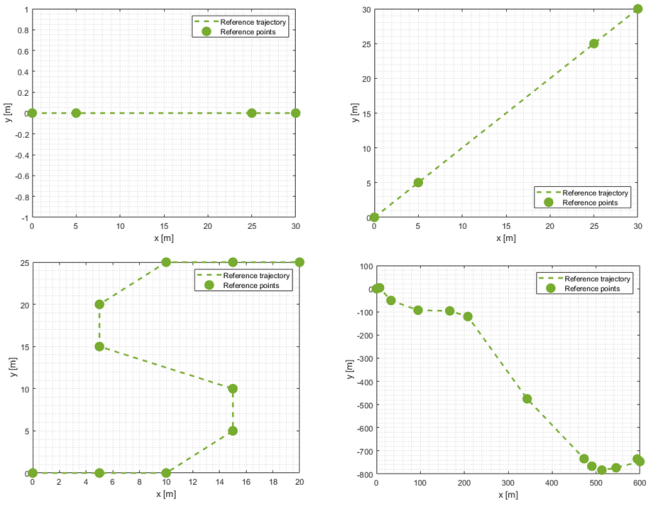

Fig. 7. Reference trajectories (straight line, diagonal line, S-shape, final)

B. KPIs

Table II shows the dimensions of the ship. It should be noted that the overall length of the ship $l_{oa} = 0.97m$. The chosen values are in line with the dimensions of the model scale Tito-Neri model. To evaluate the performance and safety of the vessel control system, several Key Performance Indicators (KPIs) are defined. These KPIs are divided into two primary categories: transient response specifications and course-keeping and mooring abilities.

TABLE II
SHIP DIMENSIONS

	Value
Length overall l_{oa}	$0.97m$
Height h	$0.32m$
Width w	$0.12m$

For the transient response, there are the maximum overshoot and steady-state (SS) errors. The overshoot evaluates how much the system exceeds its desired final value during transient response. Steady-state error is a metric that measures the difference between the desired final value and the actual steady-state value of the system.

TABLE III
ASSESSMENT PARAMETERS

	Unmooring	**Trajectory tracking**	**Mooring**
Max. overshoot	20%	20%	0%
Max. SS error	1%	1%	1%

For course-keeping abilities and mooring abilities, certain tests will be performed. First will be the straight line test.

$$d_{line}(k) = \frac{|(x_{\text{end}} - x_{\text{start}})(y_{\text{start}} - y_{\text{meas}}(k)) - (x_{\text{start}} - x_{\text{meas}}(k))(y_{\text{end}} - y_{\text{start}})|}{\sqrt{(x_{\text{end}} - x_{\text{start}})^2 + (y_{\text{end}} - y_{\text{start}})^2}} \quad (14)$$

This criterion is passed when it is in accordance with table IV below.

TABLE IV
VALIDATION CRITERIA FOR STRAIGHT LINE

KPI	**Accepted if**
Maximum deviation max$\{d_{line}\}$	$d_{line} < 0.1m$
Average deviation avg$\{d_{line}\}$	$d_{line} < 0.05m$

Next is the mooring test which evaluates the vessels ability to come to a precise stop. This is required for mooring as overshoot can lead to collisions and unsafe situations. Here the Euclidian distance towards the mooring point from the vessels position is calculated.

$$d_{mooring}(k) = \sqrt{(x_{ref}(k) - x_{meas}(k))^2 + (y_{ref}(k) - y_{meas}(k))^2} \quad (15)$$

The distance $d_{mooring}$ can not exceed a predetermined value. The test is successful when the $d_{mooring}$ is less than the value from table V. In addition, position and heading errors can be defined using table VI.

TABLE V
VALIDATION CRITERIA FOR MOORING

KPI	**Accepted if**
Distance d_{moor}	$d_{moor} < 0.15m$

$$\eta_{\text{error}}(k) = \begin{bmatrix} x(k) - x_{ref}(k) \\ y(k) - y_{\text{ref}}(k) \\ \psi(k) - \psi_{\text{ref}}(k) \end{bmatrix} \quad (16)$$

TABLE VI

VALIDATION CRITERIA FOR POSITION/HEADING ERROR

KPI	Accepted if
Maximum deviation max$\{\eta_x\}$	$\eta_x < 1m$
Average deviation avg$\{\eta_x\}$	$\eta_x < 0.5m$
Maximum deviation max$\{\eta_y\}$	$\eta_y < 1m$
Average deviation avg$\{\eta_y\}$	$\eta_y < 0.5m$
Maximum deviation max$\{\eta_\psi\}$	$\eta_\psi < pi/3$
Average deviation avg$\{\eta_\psi\}$	$\eta_\psi < pi/12$

VI. RESULTS

A. Benchmark trajectories

First, the results of the benchmark trajectories leading up to the final trajectory will be explored. For each of the three phases, a different color will be used. For the unmooring phase, the color blue will be used in the XY-plots. Yellow will be used for the trajectory tracking and red for the mooring phase. In addition to this, the heading of the vessel is visualised with the black line in each triangle.

For the straight line trajectory in the $x-$direction, the XY-plot can be seen in figure 8. As can be observed from the graph, the green line is the reference and the triangles represent the vessel. The triangles are plotted every $50s$. The mooring test showed a value of $0.010m$ which is 1.0% of the length of the ship. The straight-line test showed a maximum deviation of $0.02m$ and a mean of $0.0047m$.

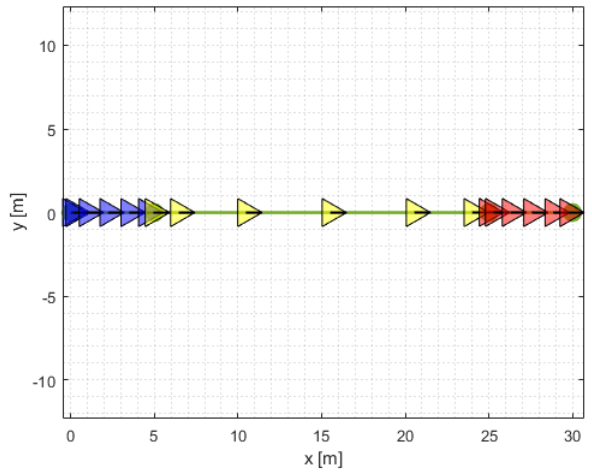

Fig. 8. XY-plot straight line trajectory in the x-direction

The transient response of the straight line trajectory can be seen in table VII. This does not exceed the maximum KPI values.

TABLE VII

TRANSIENT RESPONSE STRAIGHT LINE

	Unmooring	Trajectory tracking	Mooring
Max overshoot	0%	0%	0%
Steady-state error	0.12%	0.05%	0.04%

For the diagonal line, it can be observed that the starting heading at the unmooring phase is $0rad$. The vessel then changes orientation in accordance with the reference. A slight bump can also be seen when switching to the trajectory phase. For this trajectory the mooring test results in a value of $0.0101m$ which is about 1.0% of the length of the vessel model.

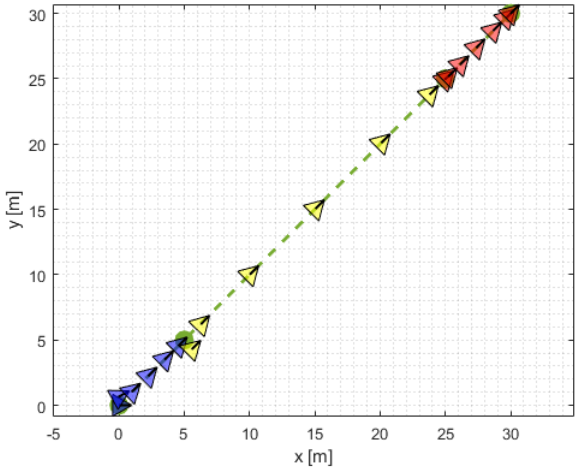

Fig. 9. XY-plot diagonal line trajectory

The transient response of the straight line trajectory can be seen in table VIII. This does not exceed the maximum KPI values.

TABLE VIII

TRANSIENT RESPONSE DIAGONAL LINE

	Unmooring	Trajectory tracking	Mooring
Max overshoot	0%	0%	0%
Steady-state error	0.04%	0.55%	0.04%

For the last benchmark trajectory (the S-shape) the XY-plot can be seen in figure 10. The main thing to note is that the vessel now changes its orientation throughout the trajectory. The vessel follows the trajectory quite well as can be observed from the XY-plot. The mooring test is $0.0111m$ which is also 1.0% of the overall length of the ship. The transient response of the straight line trajectory can be seen in table IX. This does again not exceed the maximum KPI values.

TABLE IX

TRANSIENT RESPONSE S-SHAPE

	Unmooring	Trajectory tracking	Mooring
Max overshoot	0%	0%	0%
Steady-state error	0.2%	0.4%	0.08%

B. Final trajectory

The final trajectory can be seen in parts in figure 11. The triangles are plotted every $50s$ in the unmooring and mooring phases and plotted every $500s$ in the trajectory tracking phase. This is done for visualization purposes.

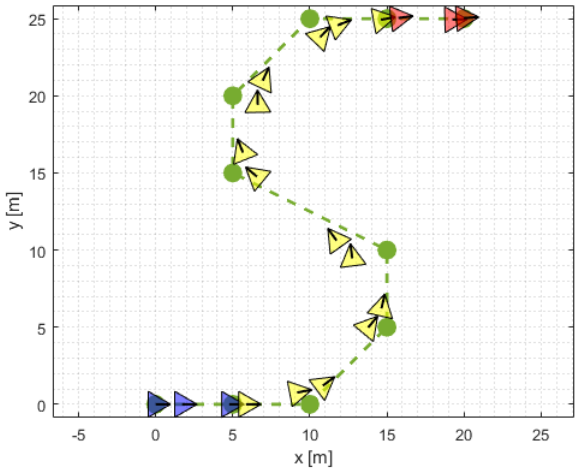

Fig. 10. XY-plot S-shape trajectory

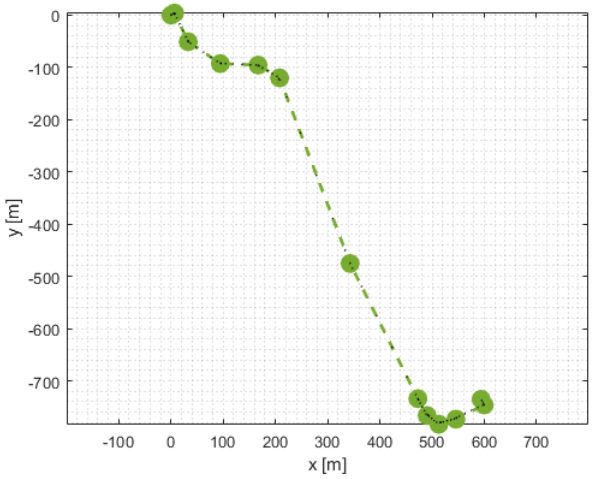

Fig. 11. XY-plot final trajectory

In figure 12 a zoomed-in version of each phase can be seen. The main thing to note is that this trajectory is an amalgamation of the benchmark trajectories of which the results were shown in the previous section. The vessel appears to follow the trajectory quite well even though this is quite difficult to observe from the plots.

In table X the transient responses of this final trajectory can be observed. There is some overshoot in the unmooring phase and trajectory tracking phase of 0.6% and 0.2% respectively. In the mooring phase, it is 0%. For each of the three phases, it is sufficient according to the criteria defined in section V. The steady-state errors are also quite minor and also satisfy the criteria by all being below 1%. The mooring test shows a maximum deviation of $0.0949m$ (9.8% of ship length) which is less than the maximum allowed value of $0.15m$.

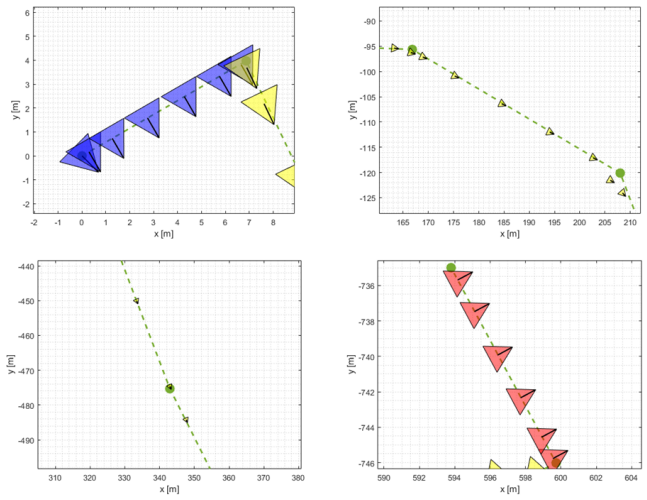

Fig. 12. XY-plot final trajectory: unmooring, S-shape, straight-line and mooring

TABLE X

TRANSIENT RESPONSE FINAL TRAJECTORY

	Unmooring	Trajectory tracking	Mooring
Max overshoot	0.6%	0.2%	0%
SS error	0.2%	0.5%	0.1%

VII. CONCLUSION AND FUTURE WORK

A. Conclusion

This research developed a strategy for trajectory tracking, unmooring, and mooring of an autonomous model scale vessel, addressing the primary question: ”How to achieve trajectory tracking and autonomous mooring/unmooring?”

The literature research and mathematical modeling of this study demonstrate the advances and difficulties in the field of autonomous ship systems, with a special emphasis on mooring operations, stationkeeping, and GNC systems. MPC is a good option for the autonomous operation of the Tito-Neri model vessel because of its capacity to manage constraints and predict future behavior. To conclude, the performance evaluation of the various trajectories demonstrated the effectiveness of the MPC in achieving accurate trajectory tracking and mooring/unmooring capabilities.

B. Future work

For future works, it would be beneficial to make use of a more complex and realistic mathematical model. The proposed mathematical model for this study included several simplifications. The thruster allocation also needs to be more realistic. Enhancing the precision and effectiveness of the control approach will require the implementation of a more realistic thruster allocation system that more closely resembles the real operational capabilities and constraints of marine thrusters. Lastly, the model has to be scaled up and also tested live for real-world application. This would allow for the complexities and challenges that are not evident in a simulation environment to come to light.

REFERENCES

[1] M. Shahbakhsh, G. R. Emad, and S. Cahoon, "Industrial revolutions and transition of the maritime industry: The case of seafarer's role in autonomous shipping," *The Asian Journal of Shipping and Logistics*, vol. 38, no. 1, pp. 10–18, 2022.

[2] B. V. Marine & Offshore, "The autonomous shipping research projects reshaping society," July 2019, https://marine-offshore.bureauveritas.com/autonomous-shipping-research-projects-reshaping-society (Retrieved 31/05/2023).

[3] P. of Rotterdam, "Portvision rotterdam," https://www.portofrotterdam.com/sites/default/files/2021-06/port

[4] Consultancy.eu, "Europe inland shipping market set for growth and consolidation," Jan 2024. [Online]. Available: https://www.consultancy.eu/news/9601/europe-inland-shipping-market-set-for-growth-and-consolidation#:~:text=Inland%20waterway%20shipping%20revenue%20in,it%20an%20uncontested%20regional%20leader.

[5] Y. E. Nazligul and D. Yazir, "Comparison of automated mooring systems against existing mooring systems by using the if-topsis method," *Ocean Engineering*, vol. 285, p. 115269, 2023.

[6] R. Villa-Caro, J. C. Carral, J. Á. Fraguela, M. López, and L. Carral, "A review of ship mooring systems," *Brodogradnja: Teorija i praksa brodogradnje i pomorske tehnike*, vol. 69, no. 1, pp. 123–149, 2018.

[7] B. Sluiskes, "Safety in mooring," *Terra et Aqua*, no. 143, pp. 14–19, 2016.

[8] D. Stanisic, M. Efthymiou, M. Kimiaei, and W. Zhao, "Evaluation of conventional methods of establishing extreme mooring design loads," in *International Conference on Offshore Mechanics and Arctic Engineering*, vol. 57656. American Society of Mechanical Engineers, 2017, p. V03AT02A017.

[9] S. Ahvenjärvi, "Unmanned ships and the maritime education and training," in *Global perspectives in MET: Towards Sustainable, Green and Integrated Maritime Transport*, 2017, pp. 245–254.

[10] Z.-H. Hu, "Low-emission berth allocation by optimizing sailing speed and mooring time," *Transport*, vol. 35, no. 5, pp. 486–499, 2020.

[11] offshore123, "Introduction to dp systems - what is a dynamic positioning," Dec 2021, https://www.offshoreengineering.com/dp-dynamic-positioning/what-is-dynamic-positioning/ (Retrieved 11/06/2023).

[12] T. Trym, E. F. Brekke, and T. A. Johansen, "On collision risk assessment for autonomous ships using scenario-based mpc," *IFAC-PapersOnLine*, vol. 53, no. 2, pp. 14 509–14 516, 2020.

[13] H. Zheng, R. R. Negenborn, and G. Lodewijks, "Trajectory tracking of autonomous vessels using model predictive control," *IFAC Proceedings Volumes*, vol. 47, no. 3, pp. 8812–8818, 2014.

[14] A. Haseltalab and R. R. Negenborn, "Model predictive maneuvering control and energy management for all-electric autonomous ships," *Applied Energy*, vol. 251, p. 113308, 2019.

[15] S. Wood, M. Rees, and Z. Pfeiffer, "An autonomous self-mooring vehicle for littoral & coastal observations," in *OCEANS 2007-Europe*. IEEE, 2007, pp. 1–6.

[16] G. S. Ramos, D. B. Haddad, A. L. Barros, L. de Melo Honorio, and M. F. Pinto, "Ekf-based vision-assisted target tracking and approaching for autonomous uav in offshore mooring tasks," *IEEE Journal on Miniaturization for Air and Space Systems*, vol. 3, no. 2, pp. 53–66, 2022.

[17] V. Bertram, "Unmanned surface vehicles – a survey," 2008, https://citeseerx.ist.psu.edu/document?repid=rep1type=pdfdoi=461789955de8ddb5c6195b9c95c0ff985caccf7c (Retrieved 13/06/2023).

[18] F. Youd, "Crewless cargo: The world's first autonomous electric cargo ship," 2022, https://www.ship-technology.com/features/crewless-cargo-the-worlds-first-autonomous-electric-cargo-ship/catfish (Retrieved 12/06/2023).

[19] P. O. T. London, "Mooring operations manual," https://www.forthports.co.uk/wp-content/uploads/2018/11/POTLLMooringManual.pdf (Retrieved 07/08/2024).

[20] A. M. Lekkas and T. I. Fossen, "Line-of-sight guidance for path following of marine vehicles," *Advanced in marine robotics*, vol. 5, pp. 63–92, 2013.

[21] L. Wang, S. Li, J. Liu, Q. Wu, and R. R. Negenborn, "Ship docking and undocking control with adaptive-mutation beetle swarm prediction algorithm," *Ocean Engineering*, vol. 251, p. 111021, 2022.

[22] T. I. Fossen, *Handbook of marine craft hydrodynamics and motion control*. John Wiley & Sons, 2011.

[23] T. Chettibi and P. Lemoine, "Generation of point to point trajectories for robotic manipulators under electro-mechanical constraints," *International Review of Mechanical Engineering, IREME, ISSN 1970-8734*, vol. 1, no. 2, pp. pp–131, 2007.

[24] D. Li and L. Du, "Auv trajectory tracking models and control strategies: A review," *Journal of Marine Science and Engineering*, vol. 9, no. 9, p. 1020, 2021.

[25] K. M. Lynch and F. C. Park, *Modern robotics*. Cambridge University Press, 2017.

[26] MathWorks, "Design trajectory with velocity limits using trapezoidal velocity profile."

[27] PI, "Pi loss prevention bulletin - preventing an anchor from dragging." [Online]. Available: https://www.piclub.or.jp/wp-content/uploads/2018/04/Loss-Prevention-Bulletin-Vol.25-Light.pdf

[28] A. C. Kuzu and Ö. Arslan, "Analytic comparison of different mooring systems," in *Global Perspectives in MET: Towards Sustainable, Green and Integrated Maritime Transport*, 2017, pp. 265–274.

[29] A. C. Kuzu, E. Akyuz, and O. Arslan, "Application of fuzzy fault tree analysis (ffta) to maritime industry: a risk analysing of ship mooring operation," *Ocean Engineering*, vol. 179, pp. 128–134, 2019.

[30] M. F. de Jong, "The ecological effects of deep sand extraction on the dutch continental shelf: Implications for future sand extraction," Ph.D. dissertation, Wageningen University and Research, 2016.

[31] S. Denmark, *Mooring - Do It Safely*. Seahealth Denmark, 2013, https://seatracker.ru/viewtopic.php?t=52449 (Retrieved 04/04/2024).

[32] "Automated mooring system," https://www.macgregor.com/intelligent-solutions/automated-mooring-system/ (Retrieved 11/08/2023).

[33] H. Singh, J. G. Bellingham, F. Hover, S. Lemer, B. A. Moran, K. Von der Heydt, and D. Yoerger, "Docking for an autonomous ocean sampling network," *IEEE Journal of Oceanic Engineering*, vol. 26, no. 4, pp. 498–514, 2001.

[34] D. E. Frye, J. Kemp, W. Paul, and D. Peters, "Mooring developments for autonomous ocean-sampling networks," *IEEE Journal of Oceanic Engineering*, vol. 26, no. 4, pp. 477–486, 2001.

[35] A. Veksler, T. A. Johansen, F. Borrelli, and B. Realfsen, "Dynamic positioning with model predictive control," *IEEE Transactions on Control Systems Technology*, vol. 24, no. 4, pp. 1340–1353, 2016.

[36] J. Du, X. Hu, M. Krstić, and Y. Sun, "Dynamic positioning of ships with unknown parameters and disturbances," *Control Engineering Practice*, vol. 76, pp. 22–30, 2018.

[37] Š. Kozák, "From pid to mpc: Control engineering methods development and applications," in *2016 cybernetics & informatics (K&I)*. IEEE, 2016, pp. 1–7.

[38] L. Wang, *Model predictive control system design and implementation using MATLAB®*. Springer Science & Business Media, 2009.

[39] S. J. Qin and T. A. Badgwell, "An overview of industrial model predictive control technology," in *AIche symposium series*, vol. 93, no. 316. New York, NY: American Institute of Chemical Engineers, 1971-c2002., 1997, pp. 232–256.

[40] M. Morari and J. H. Lee, "Model predictive control: past, present and future," *Computers & chemical engineering*, vol. 23, no. 4-5, pp. 667–682, 1999.

[41] MathWorks, "Optimization problem," https://nl.mathworks.com/help/mpc/ug/optimization-problem.htmlbujxw9t (Retrieved 13/05/2024).

B

MATLAB code and Simulink schemes

In this appendix the relevant Simulink schemes and MATLAB code will be shown. First the overall Simulink scheme for the unmooring part is given in figure B.1. This is followed by the trajectory tracking scheme in figure B.2. Lastly, the mooring scheme in figure B.3. All of these schemes from left to right consist of the following:

- Generation of the reference and guidance strategy (figure B.4)
- Smoothing of the reference
- Rotation matrix converting the global refernce to local for the controller
- The MPC that performs the optimization and outputs the forces
- The disturbances modelled after the current (figure B.5)
- Allocation of the thrust according to the TA Matrix
- The dynamics of the vessel
- Rotation matrix to convert the local position to a global position
- Outputting the data/generating results and graphs

The trajectory tracking scheme and mooring scheme both have an additional block for the initial condition. The global initial condition has to be converted to the local frame to be used by the vessel. In the next pages, figure B.1 shows the unmooring scheme with a blue background in order to be in line with the XY-plot visualization. Figure B.2 shows the trajectory tracking scheme with a yellow background and figure B.3 shows the mooring Simulink scheme with a red background.

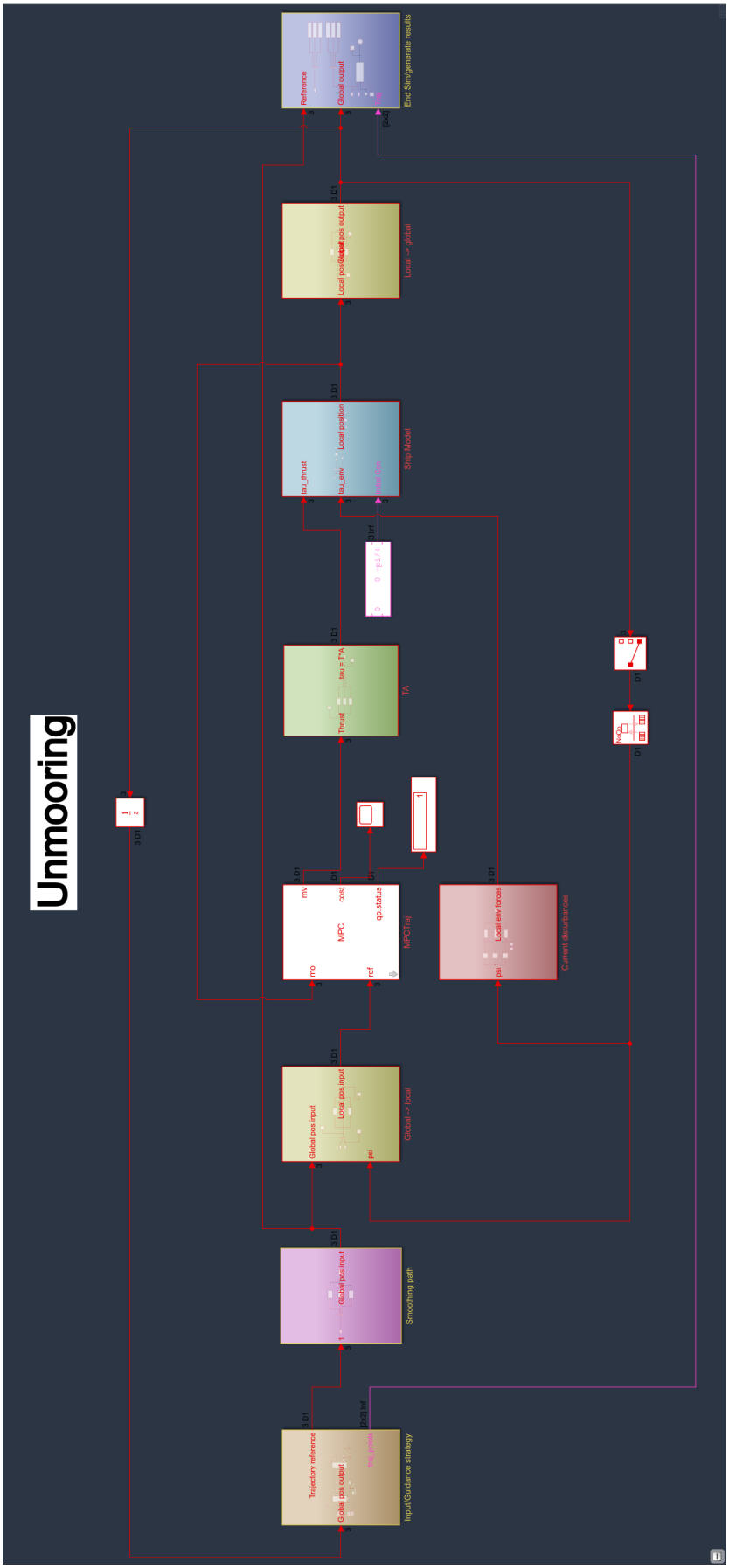

Figure B.1: Unmooring Simulink scheme

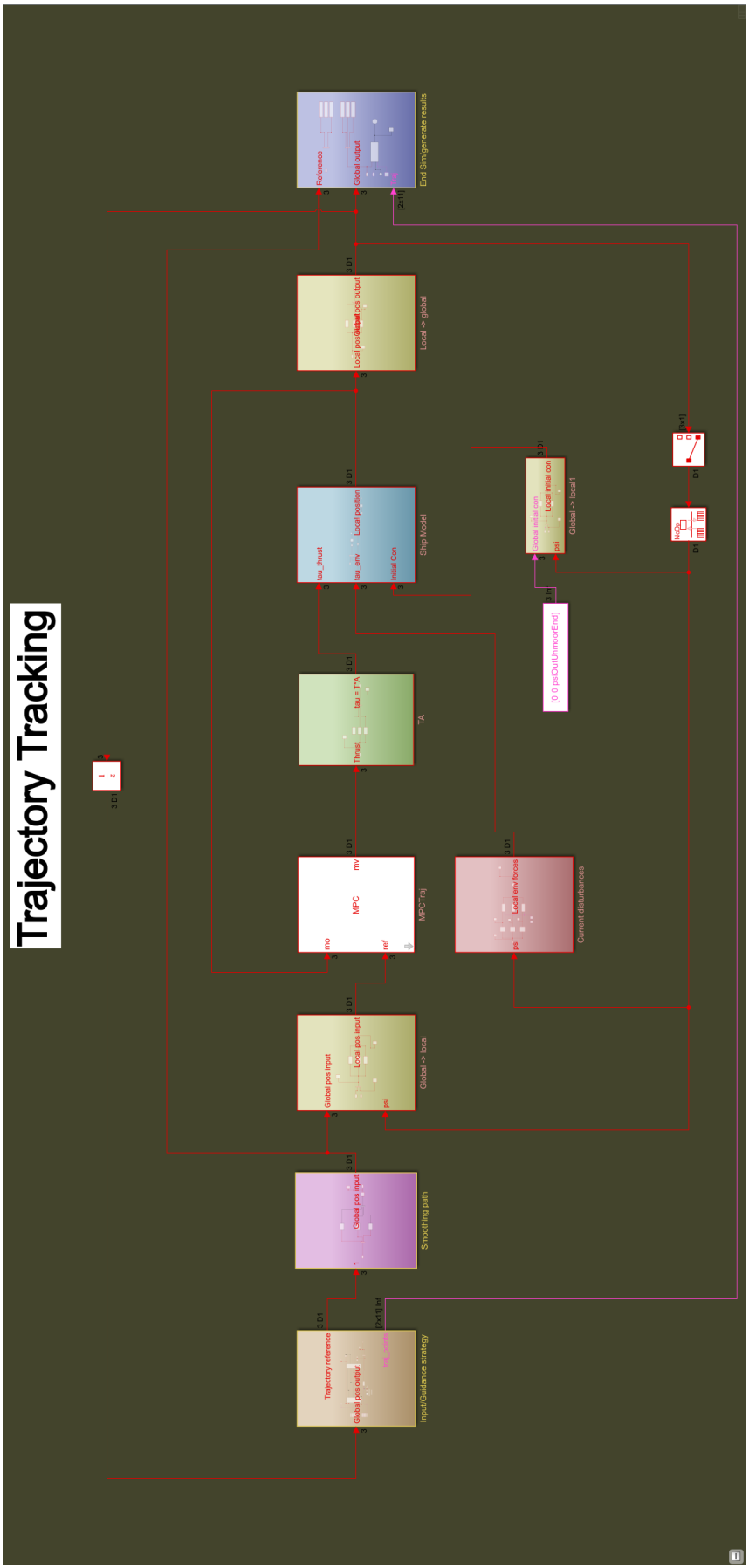

Figure B.2: Trajectory tracking Simulink scheme

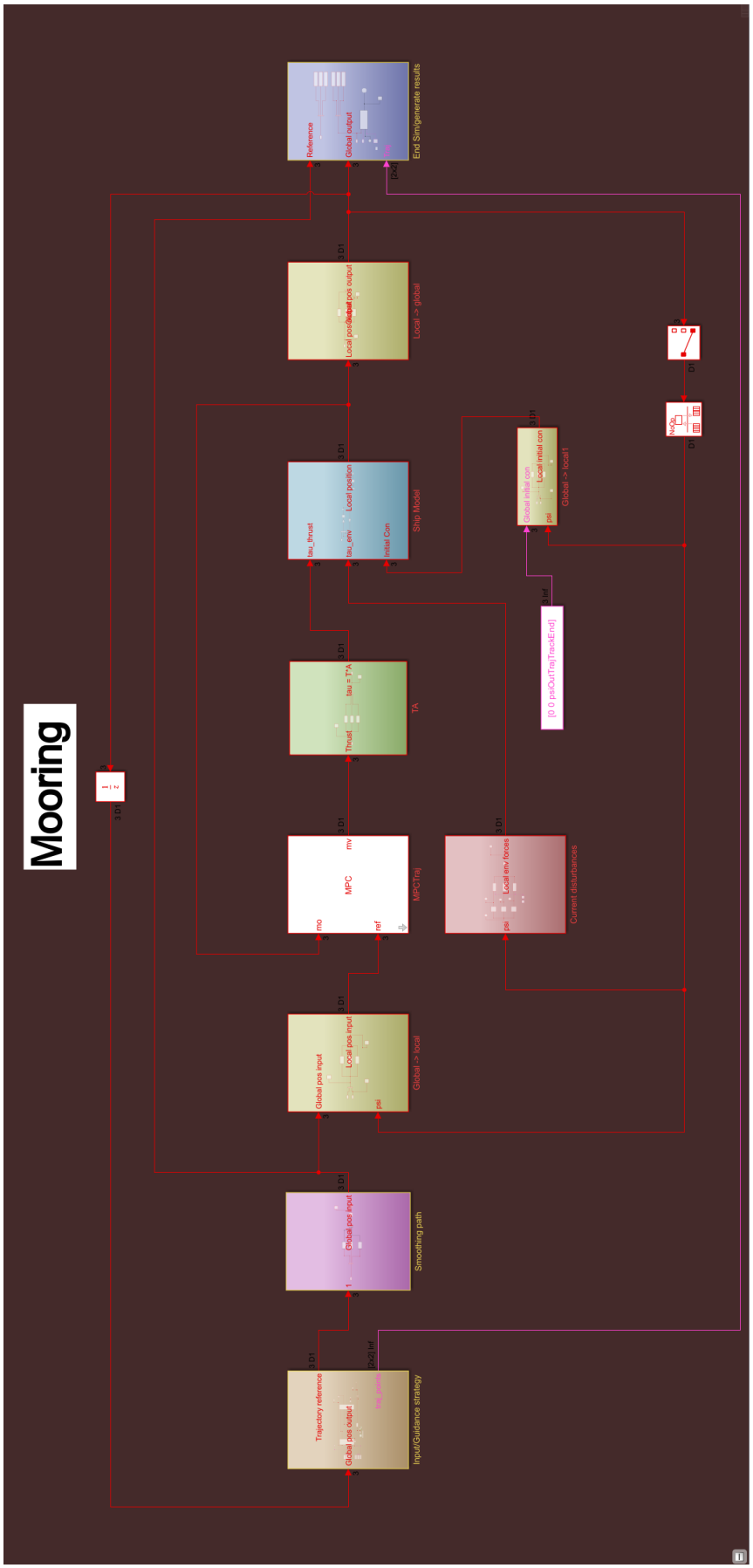

Figure B.3: Mooring Simulink scheme

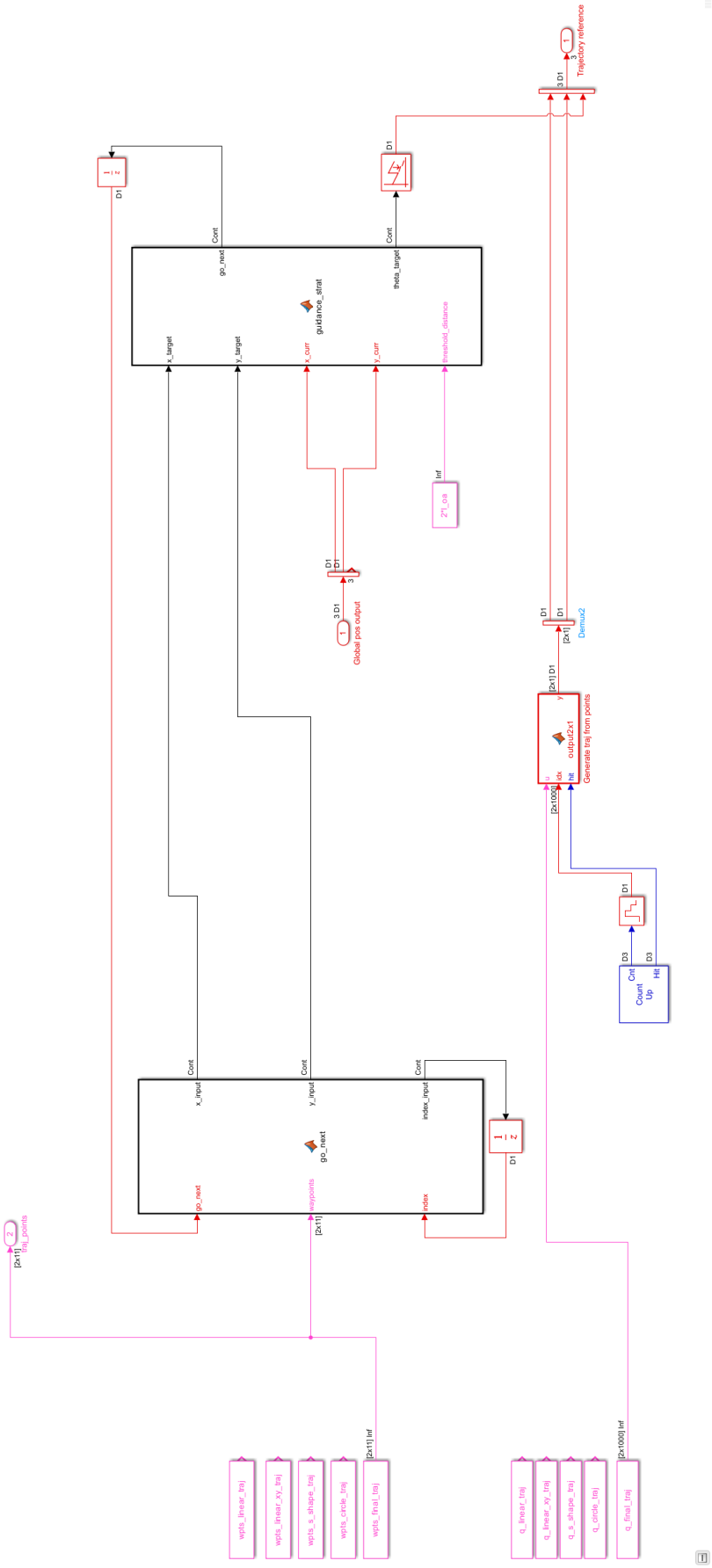

Figure B.4: Guidance strategy Simulink scheme

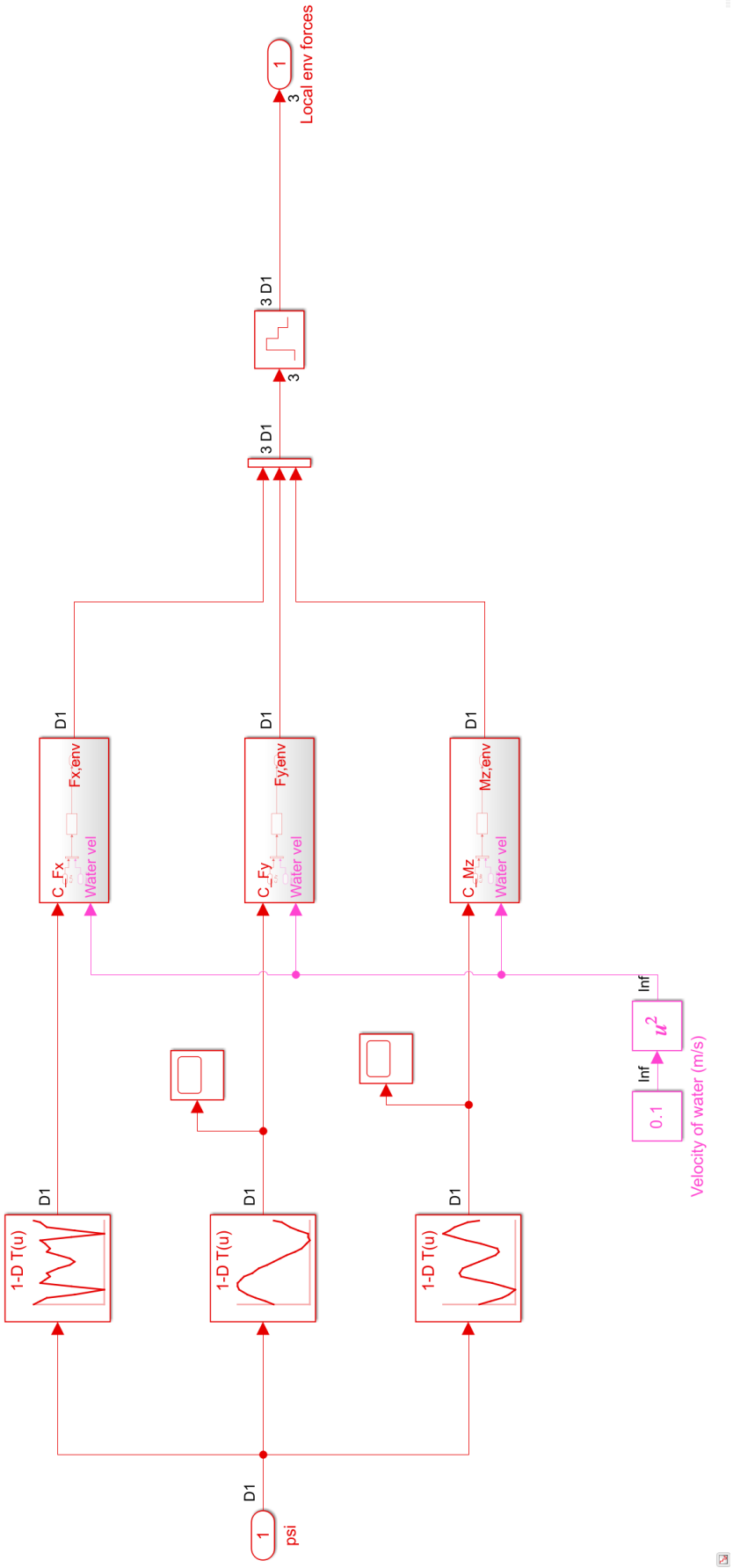

Figure B.5: Current disturbances Simulink scheme

In the guidance strategy, for the CoA and LOS, the following code is used.

```
function [go_next,theta_target] = guidance_strat(x_target, y_target, x_curr, y_curr,
    threshold_distance)

    delta_x = x_target - x_curr;
    delta_y = y_target - y_curr;


    %Angle between the vessels orientation and the vector to next
    %coordinate
    theta_target = atan2(delta_y, delta_x);

    % Euclidian distance check
    distance_to_target = sqrt(delta_x^2 + delta_y^2);
    within_threshold = distance_to_target <= threshold_distance;

    % Input next coordinate
    if  within_threshold
        go_next = 1;
    else
        go_next = 0;
    end
end
```

Listing B.1: CoA and LOS

C

Current disturbances results

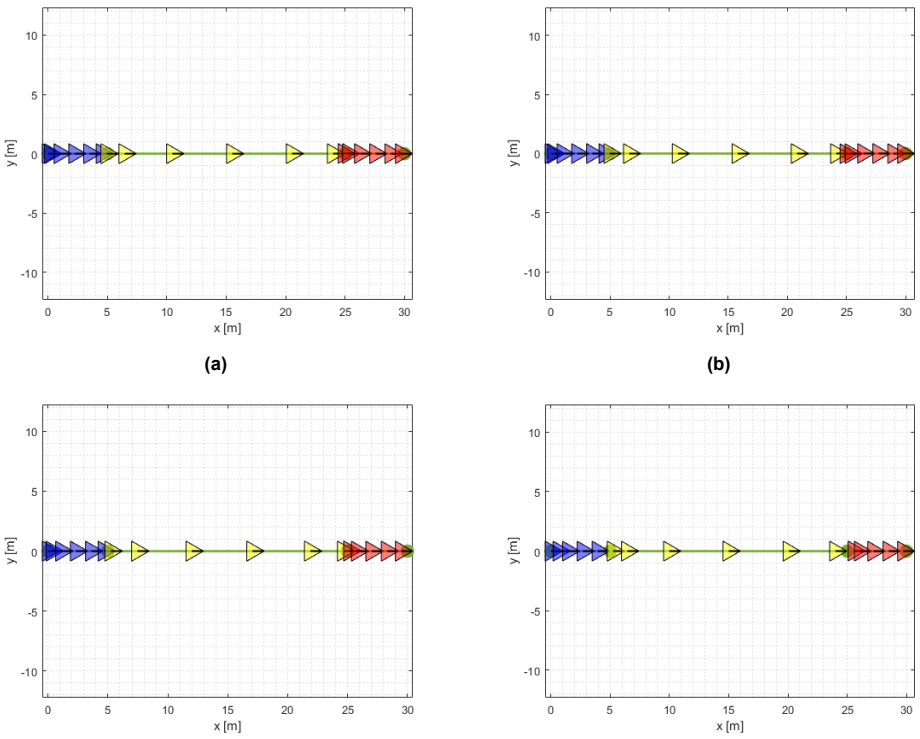

Figure C.1: Straight line trajectory with current velocity of (a) $0m/s$, (b) $0.1m/s$, (c) $0.25m/s$, (d) $0.5m/s$

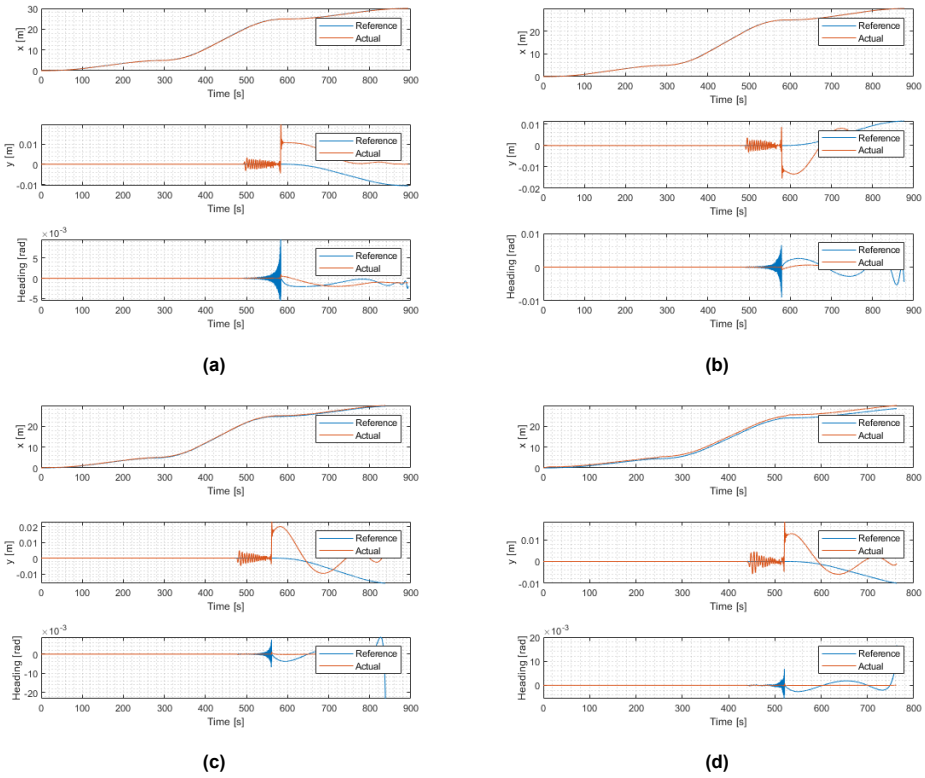

Figure C.2: Output plots straight line trajectory with current velocity of (a) $0m/s$, (b) $0.1m/s$, (c) $0.25m/s$, (d) $0.5m/s$

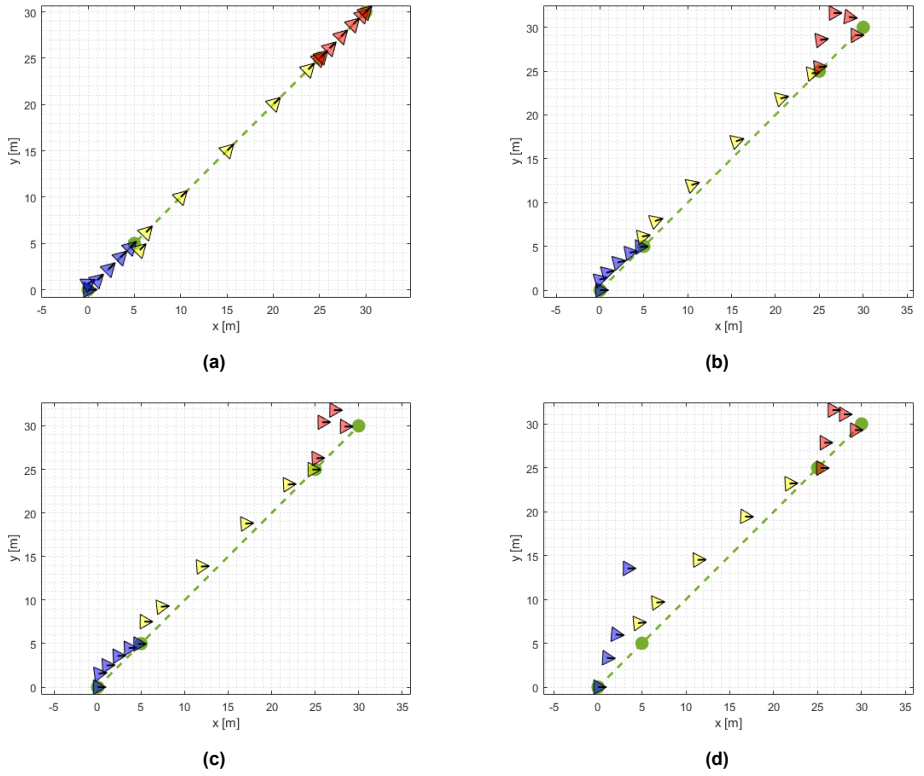

Figure C.3: Diagonal line trajectory with current velocity of (a) $0m/s$, (b) $0.1m/s$, (c) $0.25m/s$, (d) $0.5m/s$

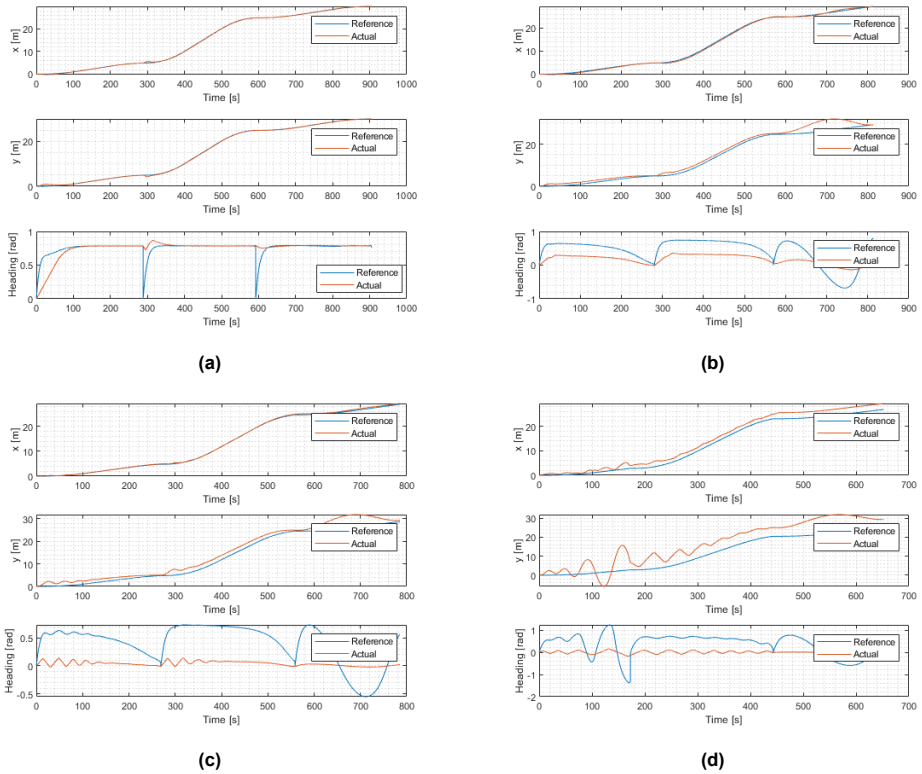

Figure C.4: Output plots diagonal line trajectory with current velocity of (a) $0m/s$, (b) $0.1m/s$, (c) $0.25m/s$, (d) $0.5m/s$

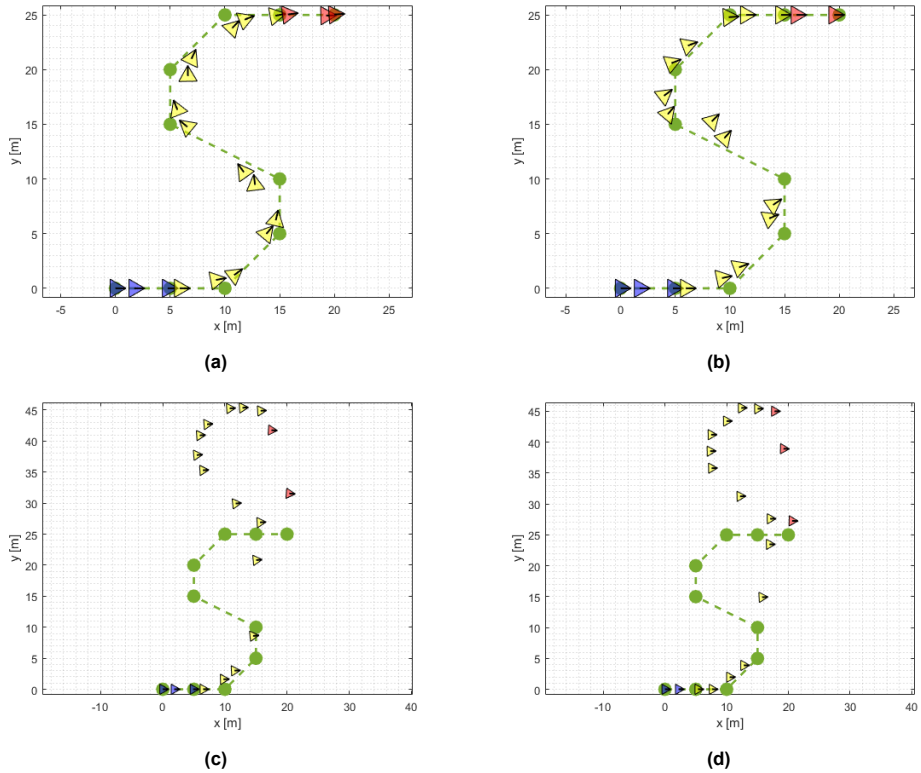

Figure C.5: S-shape trajectory with current velocity of (a) $0m/s$, (b) $0.1m/s$, (c) $0.25m/s$, (d) $0.5m/s$

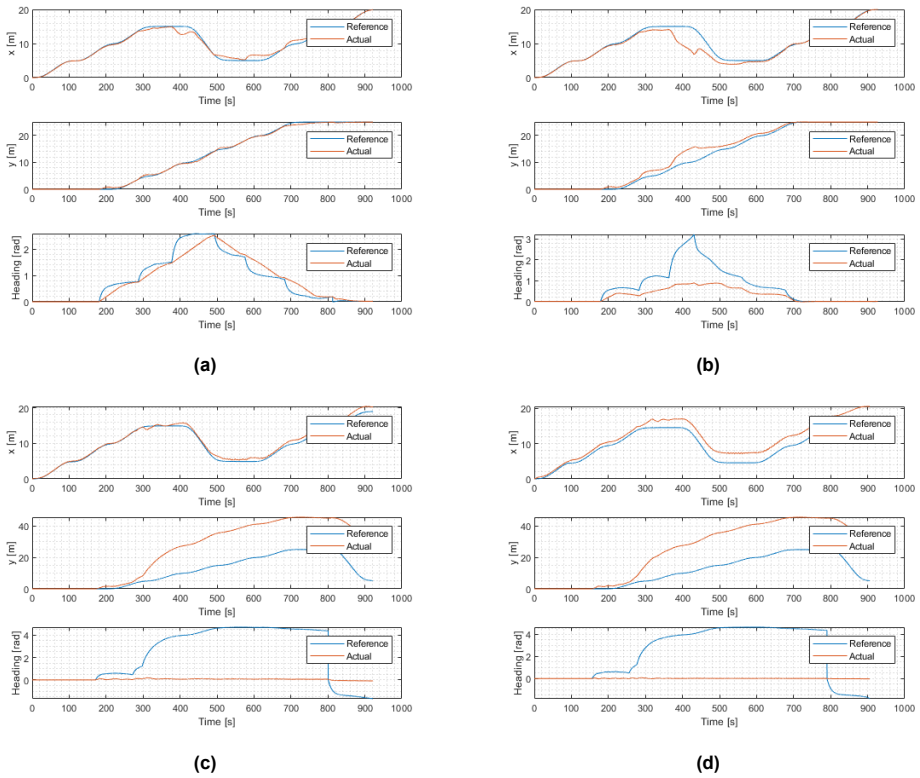

Figure C.6: Output plots s-shape trajectory with current velocity of (a) $0m/s$, (b) $0.1m/s$, (c) $0.25m/s$, (d) $0.5m/s$